CHALMERS UNIVERSITY OF TECHNOLOGY
Division of Concrete Structures

Publication 96:1

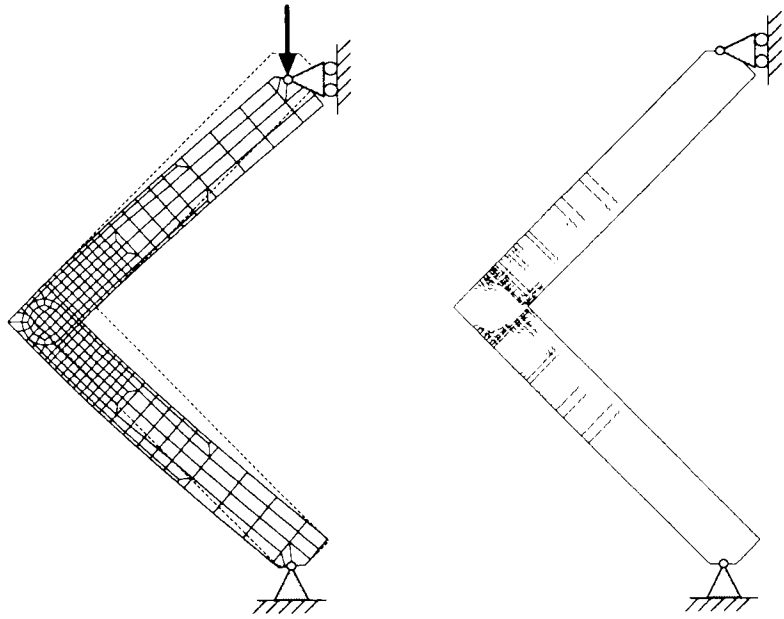

New Reinforcement Detailing in Concrete Frame Corners of Civil Defence Shelters

Non-linear Finite Element Analyses and Experiments

Morgan Johansson

Licentiate thesis

Göteborg November 1996

CHALMERS UNIVERSITY OF TECHNOLOGY
DEPARTMENT OF STRUCTURAL ENGINEERING
DIVISION OF CONCRETE STRUCTURES

ARB NR: 1106

Publication 96:1

New Reinforcement Detailing in Concrete Frame Corners of Civil Defence Shelters: Non-linear Finite Element Analyses and Experiments

Morgan Johansson

Göteborg November 1996

Adress: Chalmers University of Technology
Division of Concrete Structures
S-412 96 Göteborg, Sweden
Telephone: 031 - 772 10 00 Telefax: 031 - 772 22 60

ISSN 0349-8581

PREFACE

This study deals with the reinforcement detailing of frame corners in civil defence shelters. Experiments and finite element analyses, based on non-linear fracture mechanics, were conducted to evaluate a new design proposal. The work presented in this thesis was carried out from November 1994 to November 1996 at the Division of Concrete Structures, Chalmers University of Technology. The project is financed by the Swedish Rescue Service Agency.

I wish to thank my supervisor, Professor Kent Gylltoft, for his guidance and support. I would also like to thank Björn Ekengren, M.Sc., and Magnus Kjellman, M.Sc., from the Swedish Rescue Service Agency for their encouraging engagement in the project. Special thanks are due to Mario Plos, Ph.D., who was an invaluable support in the first year of the project. For their joyful, never ending support and encouragement, I thank my fellow colleagues at the Structural Engineering Division. Further, I owe thanks to the staff of the Structural Engineering Laboratory for their assistance in constructing and testing the frame corner specimens. Finally, I thank Wanda Sobko, Diploma Engineer, and Lars Wahlström, Engineer, for help with figures and photos, respectively.

Göteborg, November 1996

Morgan Johansson

CONTENTS

ABSTRACT

The reinforcement detailing prescribed by the present Swedish regulations for the design of frame corners in concrete civil defence shelters is complicated which makes it difficult to carry out correctly. Therefore, a simpler method, by which all reinforcement bars are spliced within the corner region, has been worked out. The aim of the study is to evaluate a new design proposal and determine whether it is appropriate to replace the conventional reinforcement detailing with the new kind.

Eight full-scale tests of frame corners subjected to a negative moment (closing of the corner) were carried out. The parameters varied in the tests were the reinforcement detailing, the reinforcement ratio, the reinforcement type and the configuration of the reinforcement bars. Finite element analyses, with material models based on non-linear fracture mechanics and plasticity, were carried out for frame corners with the new and the conventional reinforcement detailings. Furthermore, the effects of the weakness of the construction joint, the interaction between reinforcement and concrete, and the mechanical properties of the steel reinforcement were examined using this method.

The tests and analyses showed that the conventional and the new reinforcement detailings for practical purposes are equivalent when using a low reinforcement ratio; they indicated that this is also the case when using a high reinforcement ratio. Accordingly, this work supports the idea that the new detailing is suitable to use instead of the conventional reinforcement detailing. The analyses showed that the bond-slip relation affects the stiffness of the structure and that it also affects the total deformation capacity. However, its effect on the maximum load capacity was found to be negligible. Furthermore, it was shown that the mechanical properties of the steel reinforcement can have a significant effect on the deformation capacity; after the initial cracking, the weakness of the construction joint has a negligible effect on the structural behaviour of the frame corner.

Keywords: Concrete, frame corners, splicing of reinforcement, non-linear fracture mechanics, finite element analysis, bond, shelters for civil defence.

NOTATIONS

Roman upper case letters

A_s	cross section area of reinforcement
D_{ij}	component in stiffness matrix
E_c	Young's modulus for concrete
E_s	Young's modulus for steel
F	load
F_s	force carried by reinforcement
G_f	fracture energy
L	length
P	projection matrix

Roman lower case letters

c	cohesion
dF_s	differential quantity of force carried by reinforcement
$f(w)$	softening function
f_c	compressive strength of concrete
$f_{c,cube}$	compressive cube strength of concrete (150 x 150 x 150 mm)
$f_{c,cyl}$	compressive cylinder strength of concrete (ϕ150 x 300 mm)
f_{su}	ultimate strength of reinforcement
f_{sy}	yield strength of reinforcement
f_t	tensile strength of concrete
$f_{t,split}$	cube splitting strength of concrete (150 x 150 x 150 mm)
l	longitudinal direction
l_{bar}	length of reinforcement bar
$l_{element}$	length of finite element representing reinforcement bar
n	normal direction
r	radius of reinforcement loop
s	slip
s_{rm}	mean crack spacing
s_y	slip at the point where yielding is obtained
t	traction (stress vector acting on a plane or surface), tangential direction, time
u	displacement
w	crack opening
w_u	ultimate crack opening
x	co-ordinate along reinforcement bars in corner region
y	co-ordinate along reinforcement bars in beam and column

Greek letters

α	stress block factor
α_f	scalar quantity used to describe the Drucker-Prager yield surface
α_g	scalar quantity used to determine the hardening parameter
β	stress block factor, scalar quantity used to describe the Drucker-Prager yield surface
γ	ratio of ultimate strength to yield strength of the reinforcement
γ_{mod}	modified value of γ
γ_{normal}	value of γ corresponding to "normal ratio" steel
Δ	incremental, increment of
$\Delta\varepsilon_{mod}$	modified incremental strain
δ	displacement
ε_c	concrete strain
ε_h	strain at steel hardening
ε_s	steel strain
ε_u	ultimate steel strain
$\varepsilon^p{}_{uniaxial}$	plastic strain in the direction of uniaxial stress
κ	hardening parameter
μ	factor describing the change in ductility of reinforcement
π	projection vector
ρ	reinforcement ratio
σ	stress
σ_1, σ_2, σ_3	principal stresses
σ_c	concrete stress
σ_s	steel stress
τ	bond stress
τ_f	bond strength in frictional phase
τ_{max}	maximum bond strength
τ_y	bond stress at the point where yielding is obtained
ν	Poisson's ratio
ϕ	bar diameter, internal angle of internal friction
ϕ_0	initial angle of internal friction
ψ	dilatancy angle

1 INTRODUCTION

1.1 Background

When a concrete frame structure is constructed, it is usually cast in two separate stages: first the casting of the wall, then the casting of the slab. After the casting of the wall, the reinforcement bars, which will later be bent and spliced into the slab, stick up into the air, see Figure 1a. According to the regulations of anchorage length and splicing methods used in Boverket's Handbook for Concrete Structures BBK 94, Boverket (1994), these bars may be several meters long. This type of frame corner reinforcement detailing can be difficult to realise at a building site and is complicated to carry out correctly. Therefore, it would be an advantage to use a simplified reinforcement detailing. If all the reinforcement could be spliced within the corner area a simpler procedure, with less risk of incorrect detailing, would be the result, see Figure 1b.

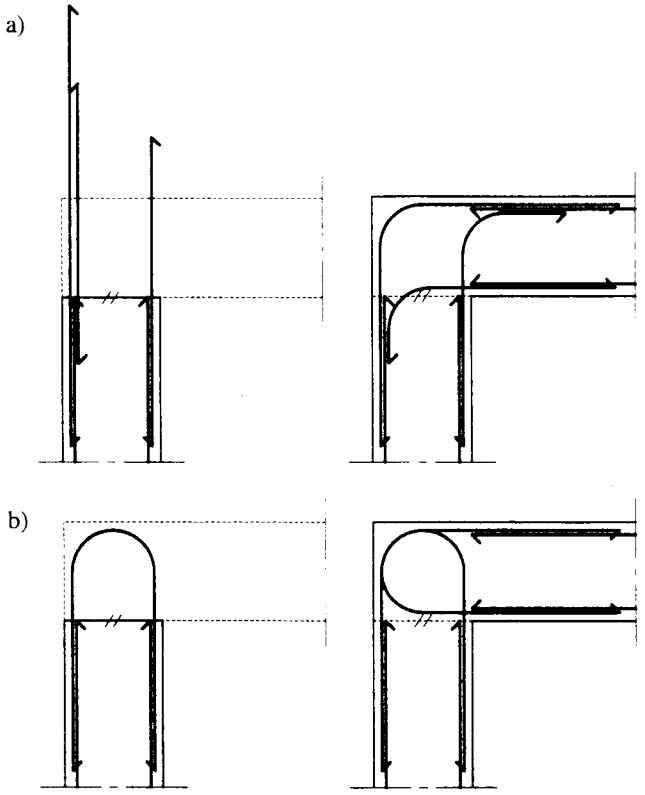

Figure 1 Schematic figure of the construction of a concrete frame corner using different reinforcement detailings: a) splicing in the slab, b) splicing within the corner area.

The present Swedish regulations for the design of civil defence shelters allow the reinforcement to be spliced in the immediate vicinity of the frame corner, with parts of the reinforcement splice extended into the corner, Swedish Rescue Service Agency (1994). This

results in a building procedure similar to that described above (Figure 1a) with a reinforcement detailing that is time consuming and quite difficult to carry out correctly. Consequently, the Swedish Rescue Service Agency wanted a simpler reinforcement detailing to be used in frame corners in civil defence shelters. Therefore, a new design proposal, in which all the reinforcement bars are spliced within the corner area, was worked out. To study the behaviour of splicing in the reinforced frame corners of shelters, a research project was initiated at the Division of Concrete Structures at Chalmers University of Technology, see Plos (1994a, b).

1.2 Aim of the Study

The aim of this research project is to evaluate a new design proposal and to determine whether it is appropriate to replace the conventional reinforcement detailing with the new kind. To do this, it is necessary to establish the service criterion that the final structure must fulfil. The load bearing capacity is of great importance and for safety reasons it is also important that a concrete structure shows a ductile behaviour that allows redistribution of forces so that a total collapse of the structure can be avoided. To obtain this, the structure must be capable of large deformations before final failure. Especially in a civil defence shelter, such ductile behaviour is of great importance in enabling the structure to withstand severe impact loading without collapse. The service criterion set up by the Swedish Rescue Service Agency is that the new reinforcement detailing must withstand loading at least as well as the conventional detailing so that a safe and ductile structure is obtained.

To determine whether the service criterion is fulfilled, a better understanding of the behaviour of frame corners under loading to failure and of the structural response in the corner area is required. Accordingly, two test-series, i.e. a total of eight full-scale test specimens subjected to negative moment (closing of the corner), were carried out, Plos (1994a, b) and Johansson (1995). The parameters varied in the tests were the reinforcement detailing, the reinforcement ratio, the reinforcement type and the configuration of the reinforcement bars.

To study the structural behaviour of the frame corner more thoroughly, the finite element method was used. Four of the test specimens were analysed using material models based on non-linear fracture mechanics and plasticity. By using this approach, the progressive cracking and the strain and stress states can be followed under increased load; which allows a better understanding of the structural behaviour of the frame corner. Once results obtained using the finite element models have been confirmed by test results, the finite element method provides a valuable tool for further studies. Accordingly, in combination with experiments, finite element analyses significantly increase the feasibility of carrying out parametric studies. In addition to the difference in the reinforcement detailing, the effects that different parameters have on the load and deformation capacity of the frame corner, were studied for frame corners with a low reinforcement ratio, using the non-linear finite element method. The parameters of interest were:

- the weakness of the construction joint between the first and second castings,
- the bond-slip relation between the reinforcement bars and the surrounding concrete, and
- the mechanical properties of the reinforcing steel bars.

Furthermore, the consequences of incorrect positioning of the reinforcement loops in the new reinforcement detailing were examined. Detailed analyses of the effect of the parameters listed above have not been carried out for frame corners with a high reinforcement ratio.

Due to numerical difficulties, it was not possible to study the effect of differences in the mechanical properties of the reinforcing steel bars using finite element models of the frame corner. Instead, a simpler model of a cantilever beam was used. This model was then also used to study more thoroughly the effect of different bond-slip relations for structures with both high and low amounts of reinforcement.

A limitation of the study carried out so far in this project is that all tests and analyses have been carried out for static loads. However, a civil defence shelter must withstand impulse loading such as explosions and falling buildings. Consequently, the behaviour of the new reinforcement detailing when subjected to impulse loading needs to be studied.

2 LITERATURE SURVEY

2.1 Frame Corners

The bearing capacity of a frame structure depends on the strength of its independent structural members. To obtain a ductile behaviour in the structure, considerable redistributions of forces and deformations must be possible. The capacity for this relies heavily on the detailing of the joint connections; i.e., the connections between different members (e.g. beams and columns) are of great importance for a sound structural behaviour. Thus, a joint connection must be at least as strong as the structural members connected to it and show a ductile behaviour in the ultimate limit state. In this section, studies of different reinforcement detailings in frame corners are briefly presented; the term "frame corner" is used to describe a corner joint connecting two structural members, such as a beam and a column or a slab and a wall, at an angle of 90°.

Concrete frame corners can be separated into two principal types: those subjected to a positive moment (opening of the corner) and those subjected to a negative moment (closing of the corner), see Figure 2. It has been found by testing that the reinforcement detailing in frame corners subjected to positive moment is more sensitive than that in frame corners subjected to negative moment, see Mayfield *et al.* (1971), Nilsson and Losberg (1976); consequently, the main effort of experimental studies has been concentrated on positive moment. Extensive experimental studies on frame corners subjected to positive moment have been conducted by several researchers, see Swann (1969), Mayfield *et al.* (1972), Nilsson (1973), Skettrup *et al.* (1985). Many different reinforcement detailings with different reinforcement ratios have been investigated; the experimental work done by Nilsson has resulted in detailing recommendations, Nilsson (1973), Nilsson and Losberg (1976).

Some studies of frame corners subjected to negative moment have also been reported, see Swann (1969), Mayfield *et al.* (1971), Yuan *et al.* (1982), Zouzou and Haldane (1993), Plos (1994b) and Luo *et al.* (1994). A literature survey of work done, before 1973, on corners and joints subjected to positive and negative moment can be found in Nilsson (1973). However, only tests on frame corners subjected to a negative moment and with reinforcement detailings similar to that examined in this study are mentioned here, see Table 1. The work of Plos is of special interest since it has functioned as a basis for the study presented in this thesis.

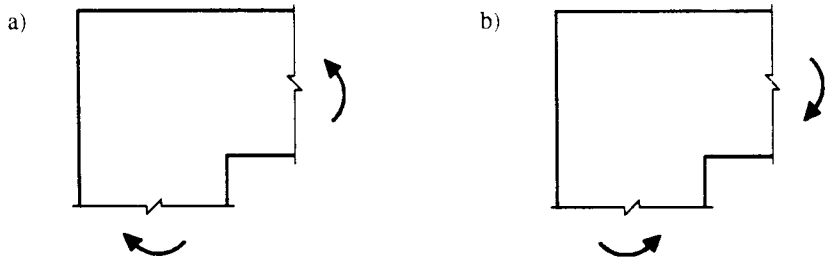

Figure 2 Frame corner subjected to: a) a positive bending moment and b) a negative bending moment.

Table 1 Test results on frame corners with reinforcement detailings similar to that presented in this study. Efficiency is defined as the ultimate load observed in the test divided by the estimated load capacity.

Researcher	Researcher's reference number	Detailing	Reinforcement ratio [%]	Efficiency
Swann (1969)	103	conventional	3.0	0.78
	104	new	- " -	0.76
	106	new	- " -	0.80
Mayfield *et al.* (1971)[1]	1-3	conventional	0.66	1.25
	1-4	conventional	- " -	1.37
	3-2	conventional	- " -	1.27
	4A-2	conventional	- " -	1.34
	2-3	new	- " -	0.94
	2-4	new	- " -	1.17
Luo *et al.* (1994)[2]	CJSa-4	new	1.39 / 1.23	1.00
	CJSa-6	new	1.04 / 0.82	1.27
	CJSb-1	new	1.39 / 1.23	1.09

[1]Lightweight concrete used

[2]Different reinforcement ratios in column (first value) and beam (second value)

The frame corner specimens tested by Swann (1969) had a very high reinforcement ratio. Due to bearing failure of the concrete within the corner, all of his specimens failed at a value below estimated strength. However, Swann concluded that a larger efficiency ratio could probably be attained by using a lower reinforcement ratio or bars of smaller dimensions (Swann used bars 19 mm in diameter).

In the tests carried out by Mayfield et al. (1971), light weight concrete was used. In all but one of the test specimens the efficiency ratio exceeded unity. They concluded that in frame corners subjected to a negative moment the "corner detailing is not important".

All specimens reached a load level equal to or higher than estimated in the tests carried out by Luo *et al.* (1994). It was concluded that the reinforcement ratio together with the yield strength of the steel and the compressive concrete strength had a significant effect on the mode of failure.

Sections with spliced reinforcement bars are possible zones of weakness; therefore, it is a common practice to splice the bars where the moments are as small as possible. In the current

practice for design of frame structures, the structural members are usually represented with their system lines. Thus, when the assumption of beam theory is used, the largest forces are obtained in the joints; this is the reason why the reinforcement must not be spliced in joint connections, according to Boverket's Handbook for Concrete Structures, BBK 94, see Boverket (1994). However, the assumption of beam theory is not applicable in a disturbed region such as a corner joint, Collins and Mitchell (1991). In a frame corner subjected to negative moment, the tensile forces in the reinforcement bars are, prior to cracking within the corner, very low compared with that in the members connecting the joint where the plastic hinges develop. Hence, it should be appropriate to splice the reinforcement bars within the corner region. To study this alternative, two test series have been conducted at Chalmers University of Technology, see Plos (1994b). It was concluded in both static and fatigue tests (reinforcement ratio = 0.56 %), that splicing of the reinforcement within the corner area had no significant effect of the behaviour of frame corners subjected to negative moment. There were no indications of anchorage failure along the lap lengths. Detailed finite element analyses using non-linear fracture mechanics have since been carried out to further study the static tests; the analyses supported the idea that it would be appropriate to splice the reinforcement within the corner area, see Plos (1995), Lundgren and Plos (1996). Another test series of reinforcement detailing in frame corners for civil defence shelters has also been carried out, see Plos (1994a, b). However, since the work is closely related to the study presented in this thesis, it is not discussed here; it is instead treated in the Sections 3 and 4, where it is referred to as the first test series.

The constant threat of earthquakes in some regions of the world have led to the dedication of significant effort, in the three past decades, to the study of structures subjected to seismic loading. The high risk of loss of lives in earthquakes makes it most important to obtain a ductile behaviour in structures subjected to this kind of loading. Consequently, the behaviour of the connections between different parts of a structure (e.g. beams and columns) is crucial, since it is here that the largest forces often occur. Therefore, several researchers have been studying beam-column joint connections subjected to seismic loading, e.g. Hanson and Connor (1967), Paulay *et al.* (1978), Tsonos *et al.* (1991), Robertson and Durrani (1992), Cheung *et al.* (1993), Restrepo *et al.* (1995). A parametric investigation of the joint mechanics for tests carried out by researchers in the USA, Japan and New Zealand, is presented in Bonacci and Pantazopoulou (1993). The behaviour of structures subjected to seismic loading is not dealt with in this thesis.

2.2 Fracture Mechanics for Concrete

The fracture mechanics models commonly used for concrete originate from studies of the initiation and propagation of a crack in a uniaxial concrete tensile test. In a concrete structure, cracking occurs mainly perpendicular to the maximum tensile stress when the tensile strength of concrete is reached. In Figure 3 the failure development of a crack in a concrete specimen subjected to increasing tensile deformation is sketched; a typical mean stress-displacement relation for such a test specimen is shown in Figure 4. When the specimen is loaded in tension, microcracks form at local weak points (Figure 3b) and under increasing load these microcracks become connected to each other and are localised to a fracture zone at the weakest section (Figure 3c). After the maximum load is reached, the tensile strength in the fracture zone decreases with increasing deformation, while the strain outside the zone decreases (Figure 3d). Eventually, a true crack that cannot transmit any tensile stresses is

formed in the zone (Figure 3e). The concrete around the formed crack, which has never reached the tensile strength, will then unload and a redistribution of stresses and deformations in the structure takes place.

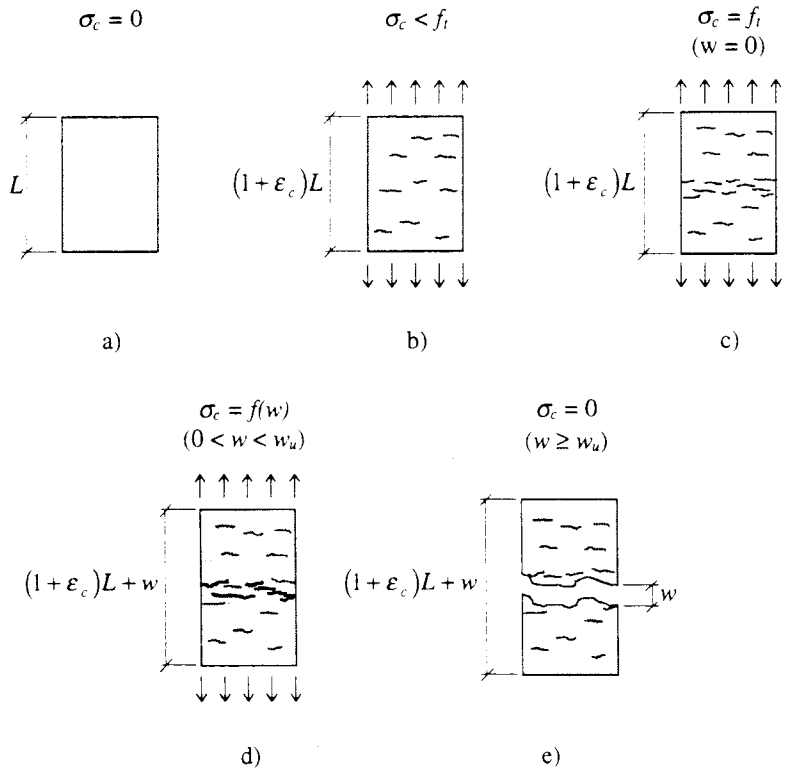

Figure 3 Stages in the formation of a crack in a concrete specimen subjected to increasing tensile deformation.

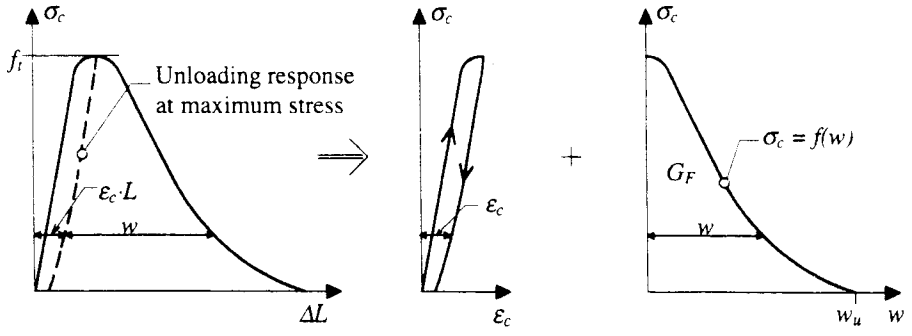

Figure 4 Mean stress-displacement relation for a uniaxial tensile test specimen. The displacement is separated into a stress-strain relation and a stress-crack opening relation. The area under the softening curve $f(w)$ represents the fracture energy G_F.

Once a fracture zone has formed, the stress transferred through the zone depends upon the crack opening w and can be defined as $\sigma_c = f(w)$, see Figure 4. Here, $f(w)$ is a function that describes the softening behaviour of the pure concrete. The area under the softening curve, $f(w)$, represents the energy release when concrete cracks and is, according to Hillerborg *et al.* (1976), the mean energy per unit area of a formed crack. This energy is called the fracture energy and is denoted G_F. Fracture mechanics for concrete and concrete structures in general is treated by Elfgren *et al.* (1989).

In finite element modelling of cracks in concrete, there are two common concepts for treating cracks: the discrete crack approach and the smeared crack approach. In this section, only the principal differences in the two approaches are mentioned. More thorough descriptions of the discrete and the smeared crack approaches have been published by for instance Rots (1988) and Plos (1995). A review of previous studies of concrete structures using the finite element method can be found in Kwak and Filippou (1990).

In the discrete crack approach, the crack is modelled as a geometrical discontinuity and separate elements are used to simulate the cracks and the material between the cracks. In the fictitious crack model presented by Hillerborg *et al.* (1976), the fracture zone is modelled as a fictitious crack of initial width equal to zero. The behaviour of the crack is then described by a stress-crack opening relation. The crack band model of Bazant and Oh (1983) is a similar approach; here the fracture zone is modelled with a band of a given width. However, in this model, the localised deformations are smeared out within the band, resulting in a response that can be described by a stress-strain relation. Thus, the continuum of strains and stresses are preserved in the model. Since separate elements are used to model a crack in the discrete crack approach, the possible crack path must be assumed in advance and the finite element mesh arranged so that the crack path follows the element boundaries. This is a serious drawback of the approach; a great amount of work is required to establish the FE mesh since the user has to decide where and how the cracks may arise. It also imposes a limitation on the spontaneous crack pattern.

According to Rots (1988), the smeared crack approach is the counterpart of the discrete crack approach. Here, the localised non-linearity of the crack is "smeared" out over the finite element, i.e. all the material deformations, including the crack, is considered in the same element. Accordingly, a cracked solid is modelled as a continuum allowing the cracked material to be described with a stress-strain relation. As this means that the crack pattern need not be taken into account in advance, the smeared crack approach is a more attractive procedure than the discrete crack approach.

2.3 Interaction between Steel and Concrete

In a composite material such as reinforced concrete, the interaction between the reinforcement bars and the surrounding concrete is of great importance. The forces transmitted between a deformed reinforcement bar and the concrete can be described by a relation between shear stresses, also known as bond stresses, and the local displacement (slip) of the bar. According to Lutz and Gergely (1967), bond is made up of three components: chemical adhesion, friction, and the mechanical interaction between concrete and steel. However, according to Gambarova *et al.* (1989), adhesion and friction are quickly lost when a bar is loaded in tension; consequently, the bond stresses for deformed bars are transferred mainly by contact

between the reinforcement ribs and the concrete. The difference in strain of steel and concrete causes a reinforcement bar to slip in relation to the surrounding concrete. According to Tepfers (1973), the slip of the reinforcement bar causes both shear stresses along the bar and stresses normal to the mean surface, see Figure 5; the normal stresses generate splitting forces radiating out from the bar.

An interface model can be used to describe the constitutive relation in terms of tractions acting on the mean contact surface and of localised deformations that occur in addition to the overall strains in the concrete closest to the reinforcement bar. The general incremental traction-displacement relation for the interface can be expressed as

$$\begin{bmatrix} \Delta t_l \\ \Delta t_n \\ \Delta t_t \end{bmatrix} = \begin{bmatrix} D_{11} & D_{12} & D_{13} \\ D_{21} & D_{22} & D_{23} \\ D_{31} & D_{32} & D_{33} \end{bmatrix} \begin{bmatrix} \Delta s_l \\ \Delta s_n \\ \Delta s_t \end{bmatrix} \tag{1}$$

where index l denotes longitudinal direction, index n normal direction, and index t tangential direction of the interface which is oriented along the mean surface of the reinforcement bar. The traction and the slip in the tangential direction are often negligible, which results in an approximate relation according to equation (2). Various bond-slip relations, D_{ll} in equations (1) and (2), based on work carried out by Eligehausen *et al.* (1983), can be found in the CEB-FIP Model Code, CEB (1993).

$$\begin{bmatrix} \Delta t_l \\ \Delta t_n \end{bmatrix} = \begin{bmatrix} D_{11} & D_{12} \\ D_{21} & D_{22} \end{bmatrix} \begin{bmatrix} \Delta s_l \\ \Delta s_n \end{bmatrix} \tag{2}$$

Research on the effect of bond in reinforced concrete using non-linear fracture mechanics has been carried out by, among others, Rots (1988), Kwak and Filippou (1990), and Noghabai (1995); a review of the use of fracture mechanics in modelling bond can be found in Noghabai. For a more thorough description of the bond concept, see CEB (1981), Engström (1992) and Magnusson (1997).

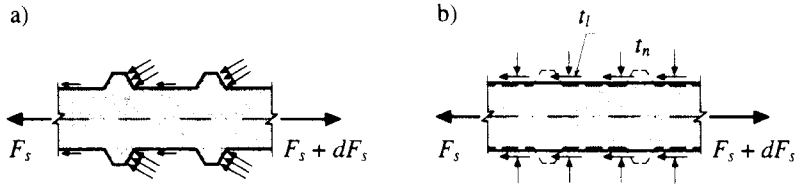

Figure 5 a) Contact stresses on a deformed bar embedded in concrete. b) Representation of these stresses by traction components on the mean contact surface.

3 EXPERIMENTS

3.1 Test Specimens

3.1.1 Dimensions and reinforcement

To gain a better understanding of the behaviour of frame corners under loading to failure, two test series, each containing of four full-scale specimens, were carried out. In this thesis the emphasis is on the second test series; more thorough information about the first test series can be found in Plos (1994a, b). The dimensions of the specimens in the second test series were the same as in the test series carried out by Plos, and are shown in Figure 6. The test specimens were reinforced with deformed bars of reinforcement type K500; this type has higher strength but lower ductility than the Ks 40 S reinforcement used by Plos, see Figure 7. All four specimens were cast with the new reinforcement detailing shown in Figure 8; that is all reinforcement bars were spliced within the frame corners. This was accomplished by using reinforcement loops. The legs of the loops were spliced to the main reinforcement in both the column and the beam. To compensate for the risk of lower structural strength at the frame corner due to the construction joint, the reinforcement ratio of the loops was increased by 25 %, in accordance with the Swedish Shelter Regulations, Swedish Rescue Service Agency (1994). However, for the specimens with new detailing tested by Plos, the amount of reinforcement was unequal in the sections adjacent to the frame corner, see Figure 8 and Table 2.

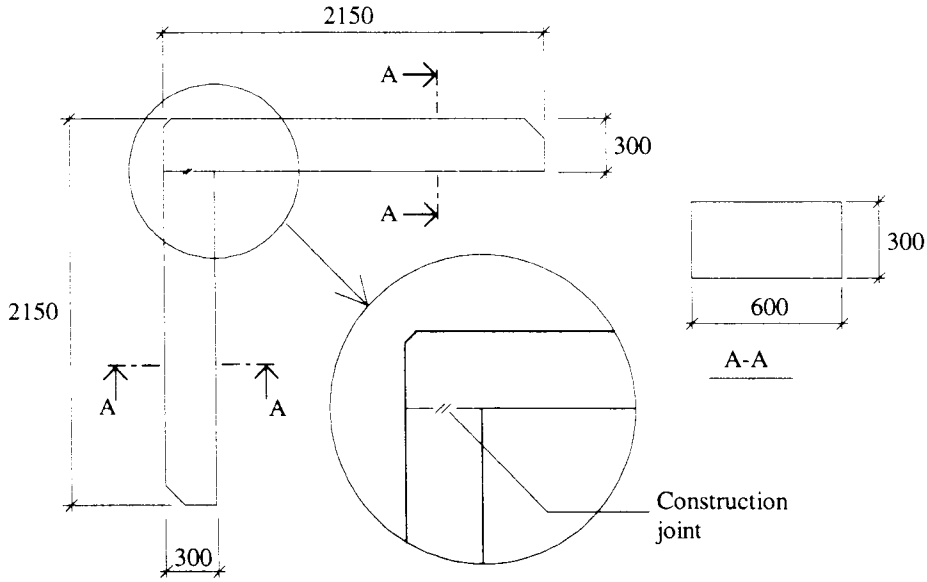

Figure 6 Dimensions of the full scale specimens used in the two test series.

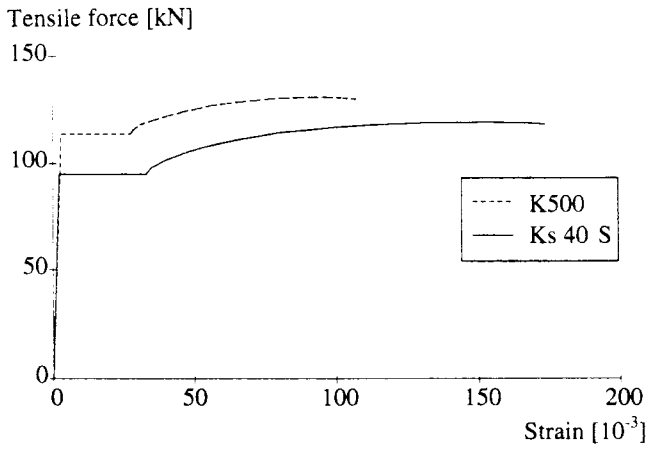

Figure 7 Mechanical properties of 16 mm diameter reinforcement bars of two types: Ks 40 S used in the first test series, Plos (1994a, b), and K500 used in the second test series.

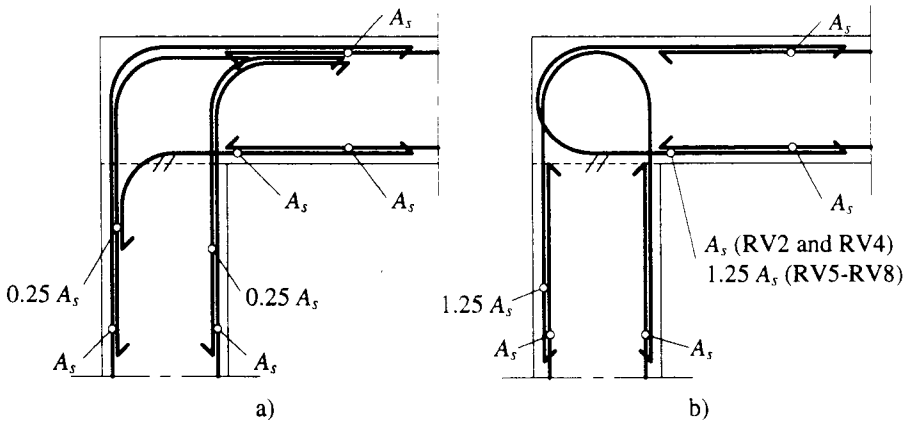

Figure 8 Detailing of the reinforcement according to: a) the conventional method, and b) the new alternative.

Two of the specimens (denoted RV5 and RV6) had a large amount of longitudinal reinforcement, 5 ϕ16, approximately equal to the maximum allowed reinforcement ratio in agreement with the Swedish Shelter Regulations. The other two specimens (denoted RV7 and RV8) had a longitudinal reinforcement amount of 3 ϕ10, approximately equal to the corresponding minimum allowed reinforcement ratio. The same amount of longitudinal reinforcement was used on both the compressive and tensile sides of the beam and the column, see Figure 8 and Table 2. For each reinforcement ratio, one specimen was reinforced with the spliced reinforcement loops placed in contact with each other (RV5 and RV7); in the other specimens, the loops were placed with space between each other (RV6 and RV8), see Figure 9. Drawings of the specimens in the second test series is shown in Appendix A; for further information, see Johansson (1995).

Table 2 Reinforcement amount and configurations for the test specimens. The same number of reinforcement bars was placed on both the compressive and the tensile sides of the beam and the column. The specimens tested by Plos (1994a, b) are included.

Test specimen	Bar diameter [mm]	Number of reinforcement bars		Configuration of reinforcement bars in the splices	Reinforcement detailing
		in beam and column	in frame corner (loops)		
RV1[1]	16	2 x 6	2 x 8	in contact	conventional
RV2[1]	16	2 x 6	2 x 6 / 2 x 8 [3]	in contact	new
RV3[1]	10	2 x 4	2 x 5	in contact	conventional
RV4[1]	10	2 x 4	2 x 4 / 2 x 5 [3]	in contact	new
RV5[2]	16	2 x 5	2 x 7	in contact	new
RV6[2]	16	2 x 5	2 x 7	space between	new
RV7[2]	10	2 x 3	2 x 4	in contact	new
RV8[2]	10	2 x 3	2 x 4	space between	new

[1]Reinforcement type Ks 40 S used. Plos (1994a, b)
[2]Reinforcement type K500 used
[3]The number of bars were not equal in the beam and the column, see Figure 8

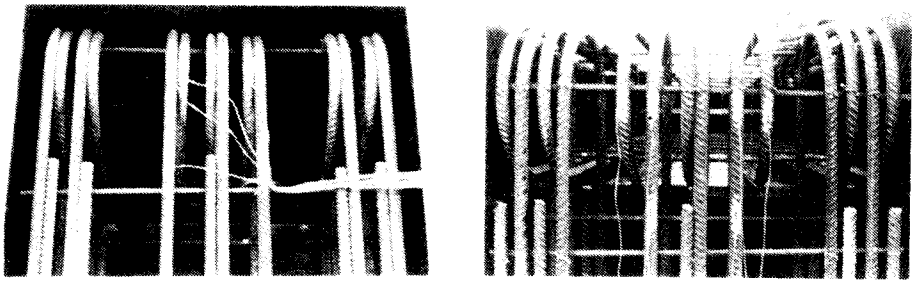

Figure 9 Specimens with a large amount of reinforcement (RV5 and RV6). The reinforcement loops were spliced in contact with each other (left) or with space between the loops (right).

3.1.2 Material properties

The specimens were cast with the column in a vertical position, see Figure 6. To obtain a construction joint, the frame columns were cast first and four days later the beams and corner joints, were cast. The specimens were made in pairs; the two specimens that would be directly compared with each other were cast at the same time and with concrete from the same batch. Concrete quality K30, according to Boverket's Handbook for concrete Structures, BBK 94, see Boverket (1994), with a target cylinder compressive strength of 30 MPa was chosen. For the

specimens in the second test series with low reinforcement ratio, a different concrete quality was delivered for the casting of the beams. This quality exhibited a somewhat higher splitting and compressive strength but a lower value of Young's modulus of elasticity. However, the fracture energy was only about half that of the ordinary concrete of quality K30. The strength of the concrete used was determined by tests on cubes (150 mm) and cylinders (ϕ150 x 300 mm), according to Swedish standard, BST Byggstandardiseringen (1987), and is presented in Table 3. The strength of the concrete was determined at the age of 28 days and on the day that the specimens were tested. The fracture energy was determined according to the recommendations of RILEM (1985) at a concrete age of between 29 and 32 days. The mechanical properties of the reinforcement are presented in Figure 10.

Table 3 The strength of the concrete used in the test specimens (mean value of three specimens).

Test specimen	Object	28 days				Testing day					Fracture Energy[1]
		$f_{t,split}$ [MPa]	$f_{c,cube}$ [MPa]	$f_{c,cyl}$ [MPa]	E_c[1] [GPa]	Age [days]	$f_{t,split}$ [MPa]	$f_{c,cube}$ [MPa]	$f_{c,cyl}$ [MPa]	E_c[1] [GPa]	[N/m]
RV1, RV2	column	3.0	34.8	23.2	—	32	3.1	34.9	23.1	—	—
- " -	beam	3.6	39.4	29.7	—	28	3.6	39.4	29.7	—	—
RV3, RV4	column	—	—	—	—	58	3.0	29.1	19.1	—	—
- " -	beam	—	—	—	—	56	3.6	39.8	28.7	—	—
RV5, RV6	column	3.2	37.3	30.0	26.6	43	3.5	39.9	31.3	26.9	131
- " -	beam	3.1	35.6	29.8	24.6	39	3.1	36.6	30.6	25.0	110
RV7, RV8	column	3.2	36.6	27.3	24.3	34	3.2	37.3	27.8	24.6	108
- " -	beam	3.4	40.7	34.0	23.5	30	3.5	41.6	33.8	23.5	66

[1]Not determined for the concrete used in the specimens in the first test series

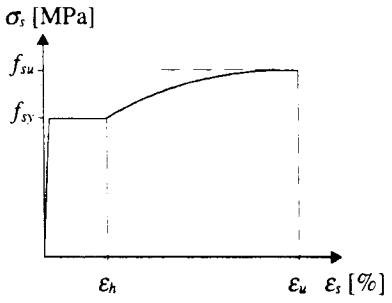

Reinforce-ment type	f_{sy} [MPa]	f_{su} [MPa]	ε_h [%]	ε_u [%]	E_s [GPa]
ϕ16 Ks 40 S	473	652	3.3	17.3	210
ϕ10 Ks 40 S	504	675	3.5	14.5	214
ϕ16 K500	567	652	2.7	10.0	189
ϕ10 K500	573	675	2.8	12.0	191

Figure 10 Mechanical properties of the reinforcement bars (mean value of five specimens). The values of Young's modulus and the strength of the steel have been calculated to correspond to a cross section area of 201 mm^2 and 78.5 mm^2 for the ϕ16 and ϕ10 bars, respectively.

3.2 Test Set-up and Test Procedure

The frame corner specimens were tested in a vertical test rig, see Figure 11. The specimens were braced in the horizontal direction at the loading and support points, allowing displacements only along the loading line. The load was applied by a hydraulic jack and the magnitude of the load was measured by a load cell. The total deflection along the loading line was measured by electronic displacement transducers. Strain gauges were used to measure the strain in the reinforcement loops (length 6 mm) as well as on the concrete (length 60 mm) at the inside of the frame corner, see Figure 12.

The load was initially applied in load increments of 5 kN for the specimens with the low reinforcement ratio and in load increments of 10 kN for the specimens with the high reinforcement ratio. To make it easier to follow the behaviour of the frame corner near the maximum load, the load increment was halved when a non-linear structural response was observed (at 25 kN and 120 kN for the specimens with low and high reinforcement ratios, respectively). When large time dependent deformations started to occur, the load level was kept constant until the displacement was less than 0.01 mm/s.

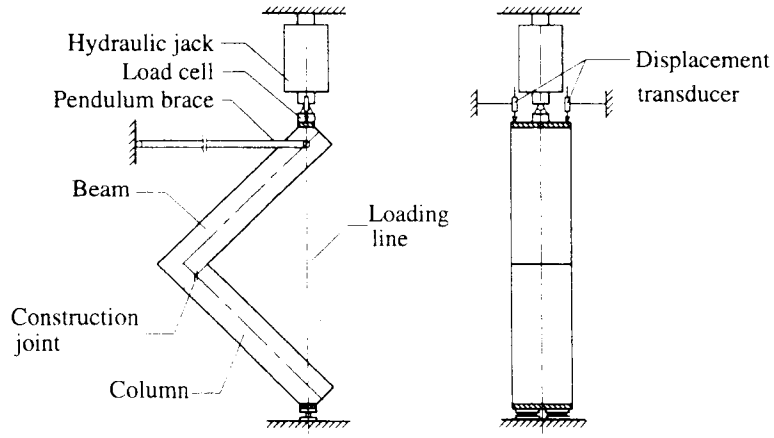

Figure 11 Test set-up of frame corner specimens.

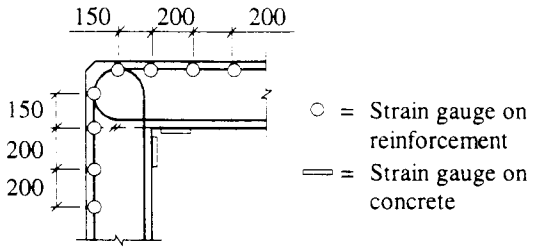

Figure 12 Position of strain gauges on reinforcement and on concrete.

3.3 Failure Development

3.3.1 General observations

During the initial loading, two primary cracks were observed close to the frame corner in all the specimens, one in each section adjacent to the corner, see Figure 13. In all specimens except RV5, the first crack was observed at the construction joint. When yielding was reached in the reinforcement bars, the deformations were concentrated to the frame corner region and plastic hinges developed on both sides of the corner for all specimens. All specimens showed ductile behaviour.

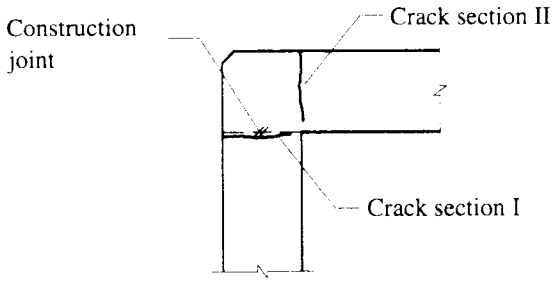

Figure 13 Sections where the two primary cracks were first observed during the initial loading.

3.3.2 Specimens with high reinforcement ratio

For specimens RV5 and RV6, very few cracks were observed outside the immediate vicinity of the frame corner. The behaviour of the two specimens was similar and the maximum load was determined for both specimens by spalling of the concrete side cover in the frame corner, see Figure 14. According to Boverket's Handbook for concrete Structures, BBK 94, Boverket (1994), this failure should not have occured for the combination of bar diameter, bending radius of the reinforcement loops and concrete cover used in the specimens. That the concrete side cover spalled off anyway indicates that the recommendations in BBK 94 are not applicable for this kind of reinforcement detailing. Before the spalling occurred, the largest cracks for both specimens were observed in crack section II (according to Figure 13).

Both specimens obtained considerable plastic rotation and the maximum load was approximately the same. Specimen RV5 still showed ductile behaviour when the test had to be stopped because of the obliquity of the hydraulic jack. Specimen RV6 was deformed until two of the reinforcement loops were torn off.

3.3.3 Specimens with low reinforcement ratio

In tests of the specimens with low reinforcement ratio, cracks were formed with a spacing of approximately 0.2 meters between them in both the beam and the column. The two specimens behaved similarly and the maximum load was the same. The cracks that led to failure

appeared in crack section II for specimen RV7. For specimen RV8, the decisive crack appeared in section I, along the construction joint, see Figure 15. For both specimens, the first crack was observed in the construction joint at a load level lower than expected (at about 10 kN compared to an expected load of about 20 kN). This indicates that the tensile strength across the construction joint was lower than in the concrete close to it, which resulted in a localised weakness in the column adjacent to the corner area.

For the specimens with low reinforcement ratio the maximum load was reached after considerable plastic rotation in the sections adjacent to the frame corner. The maximum deformation for both these specimens was limited by rupture of the reinforcement (three reinforcement loops in each specimen were torn off).

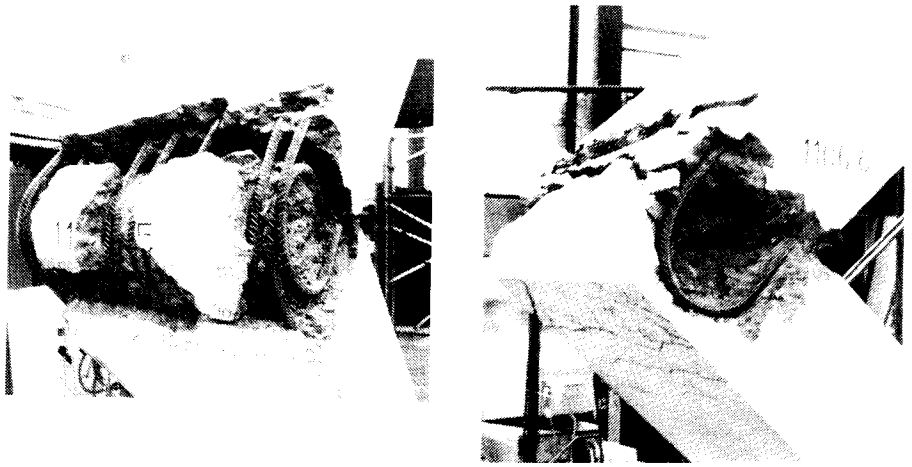

Figure 14 Specimens RV5 (left) and RV6 (right) at the end of the test.

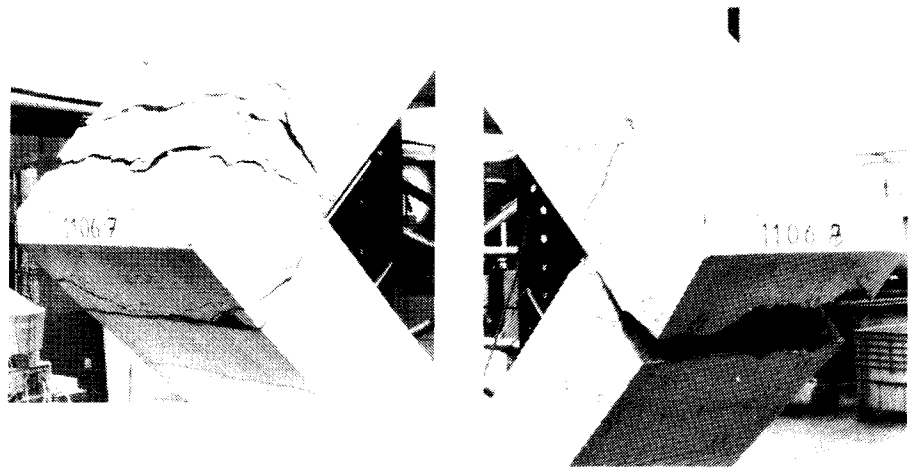

Figure 15 Specimens RV7 (left) and RV8 (right) at the end of the test.

3.4 Test Results

The structural behaviour of the frame corner specimens is described by the load-displacement relation and the distribution of tensile forces along the reinforcement bars in the corner. The relations between load and vertical displacement for test specimens RV5 to RV8 are shown in Figures 16 and 17. Except for RV5, all specimens had some of their reinforcement bars torn off. A plateau can be seen clearly in the load-displacement curves for the specimens with the low reinforcement ratio. Due to spalling of the concrete side cover, this was not the case for the specimens with high reinforcement ratio. The load-displacement relations for test specimens RV1 to RV4, presented by Plos (1994a, b), are shown in Figure 18. That the load capacities obtained for the specimens with conventional detailing were higher than those for the specimens with the new detailing is explained by the unequal capacities of the sections adjacent to the corner with the new detailing, Figure 8 and Table 2. The maximum load and the maximum displacement at the end of the test are shown for all specimens in Table 4.

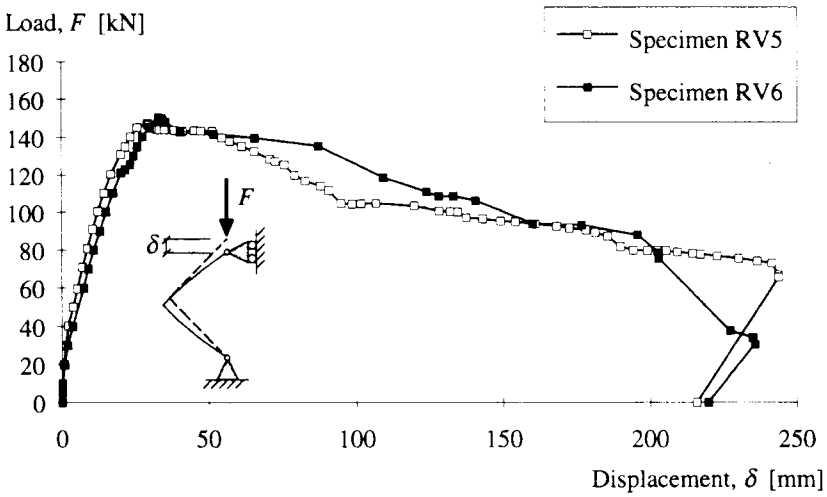

Figure 16 Load-displacement relations for the test specimens with high reinforcement ratio. In both specimens, the maximum load capacity was limited due to spalling of the side concrete cover in the frame corner.

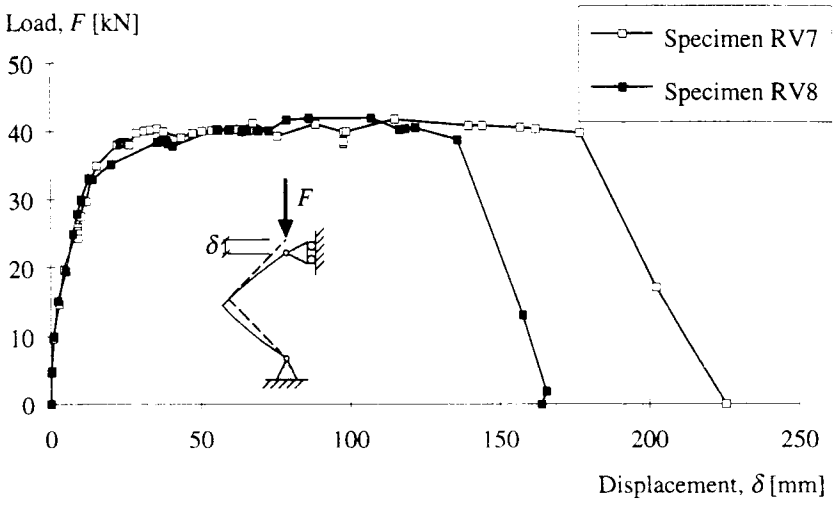

Figure 17 Load-displacement relations for the test specimens with low reinforcement ratio. Both specimens had their maximum displacement limited by rupture of the reinforcement bars.

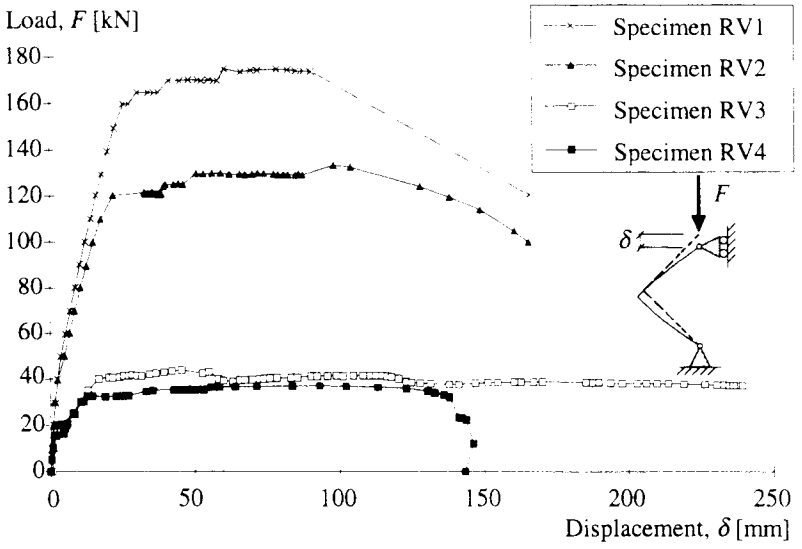

Figure 18 Load-displacement relations for the frame corner specimens of the test series carried out by Plos (1994a, b).

Table 4 Test results for the eight specimens. Results for specimens RV1 to RV4 have been taken from Plos (1994a, b).

Test series	Test specimen	Reinforcement ratio[1] [%]	Reinforcement ratio[2] [%]	Maximum load [kN]	Displacement at maximum load	Maximum displacement [mm]
1	RV1	0.75	1.00	175	61	165
	RV2	- " -	0.75 / 1.00 [3]	134	98	165
	RV3	0.19	0.23	44	45	239
	RV4	- " -	0.19 / 0.23 [3]	37	93	144
2	RV5	0.63	0.88	147	29	244
	RV6	- " -	- " -	150	33	236
	RV7	0.14	0.19	42	115	225
	RV8	- " -	- " -	42	107	167

[1]Reinforcement ratio in beam/column
[2]Reinforcement ratio in corner (loops)
[3]Unequal amount of reinforcement in beam and column, see Figure 8 and Table 2

The distribution of tensile forces along the reinforcement bars in the frame corner for different load levels is shown in Figures 19 and 20; the force-curves overlap in the middle of the frame corner where the reinforcement bars were overlapped. The tensile force varied in a similar way for all four test specimens. The highest values of the tensile forces were reached in the cross sections adjacent to the corners (sections I and II according to Figure 13). For all test specimens, yielding was initiated in the reinforcement bars before the maximum load was reached. Measured strain (mean value over a length of 60 mm) in the concrete at the inside of the frame corner never exceeded $2.5 \cdot 10^{-3}$ and $2.0 \cdot 10^{-3}$ for the specimens with high and low reinforcement ratios, respectively.

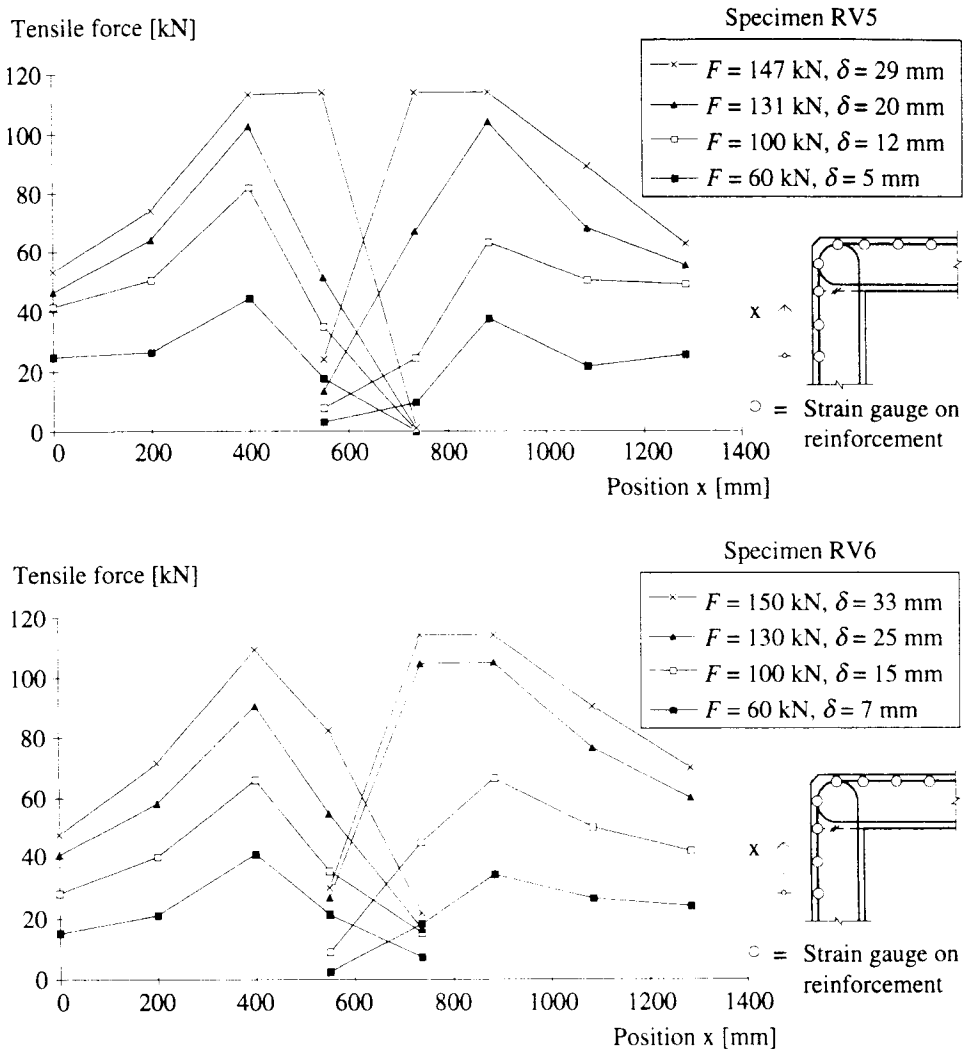

Figure 19 Distribution of tensile forces along the reinforcement bars in the frame corner at different load levels for the specimens with high reinforcement ratio.

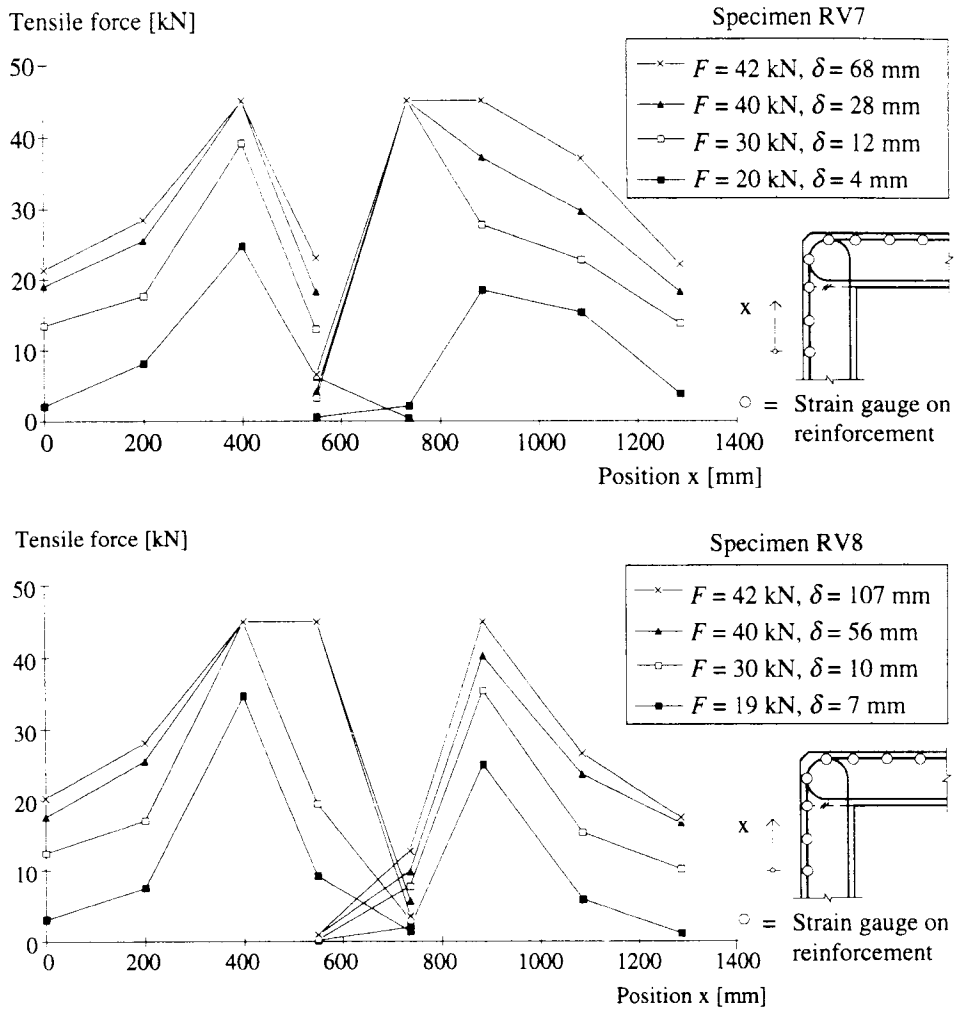

Figure 20 Distribution of tensile forces along the reinforcement bars in the frame corner at different load levels for the specimens with low reinforcement ratio.

3.5 Discussion

In the first test series, carried out by Plos, the specimens with conventional reinforcement detailing were found to have a somewhat higher load capacity than those with new detailing. This was because of the greater amount of reinforcement, prescribed for the cross-section with the construction joint (section I in Figure 13), that continued through the other critical cross-section (section II in Figure 13) for the conventional reinforcement detailing. For the new detailing, the amount of reinforcement crossing section II was less than that crossing section I, see Figure 8, which resulted in unequal strength in the sections adjoining the corner. Consequently, a plastic hinge developed only in the weaker cross section of the specimens

with new detailing, and at a lower load than for the specimens with conventional detailing. Therefore, in the second test series, the adjoining sections of the frame corner were designed to be of equal strength, see Figure 8. With this modification, plastic hinges developed at both sides of the frame corner, i.e. a similar behaviour was exhibited for specimens reinforced with either type of detailing.

In the second test series, the specimens with high reinforcement ratio behaved similarly. The maximum load was nearly the same and the load-displacement curves were similar. Because of the spalling of the concrete side cover in the frame corners, a somewhat lower maximum load capacity than expected was obtained. Also, the plateau in the load-displacement relation, observed for the specimens with high reinforcement ratio in the first test series, did not appear. One can assume that when the concrete spalling occurred, the outermost reinforcement bars ceased to carry any load and the remaining reinforcement bars were left to balance the compression force in the concrete. This means that the load capacity of the structure decreased and that the load-displacement plateau would appear at a lower load level. The response of the test specimens, in particular of specimen RV5, corresponded fairly well to this assumption. When the maximum load was reached, it fell because of the spalling after which a plateau can be discerned in the load-displacement curve for a load of about 90 kN. Thus, theoretically, if the spalling had not occurred, the specimens with high reinforcement ratio probably would have obtained a plateau at the maximum load level.

Both of the specimens with low reinforcement ratio, in the second test series, showed similar ductility. The plateau in the load-displacement relations at maximum load did appear clearly for these specimens. The maximum loads were the same and the displacements were of the same magnitude. There were no indications that the difference in the configuration of the reinforcement bars had any influence on the response of the specimens.

Three of the specimens in the second test series had some reinforcement bars torn off. The use of a less ductile reinforcement type, K500, contributed to this behaviour. Thus, if the more ductile reinforcement type Ks 40 S had been used, a greater deformation before collapse of the specimens would have been obtained. No tests with the conventional reinforcement detailing and the new, less ductile, reinforcement type were carried out.

An approximate comparison was made between the load capacity of the specimens used in the second test series and that of the specimens with conventional reinforcement detailing tested by Plos (specimens RV1 and RV3). Classic calculation methods for reinforced beam analyses, with the compressive zone described by stress block factors α and β according to the Concrete Handbook design, AB Svensk Byggtjänst and Cementa AB (1990), were used to estimate the load capacities of the specimens. Estimated load capacities for the specimens compared are listed in Table 5.

Table 5 Comparison of load capacity between the specimens in the second test series and the specimens with the conventional reinforcement detailing tested by Plos. Efficiency is defined as ultimate load observed in test divided by the estimated maximum load capacity.

Test series	Test specimen	Estimated maximum load [kN]	Maximum load in the tests [kN]	Efficiency
1	RV1	157	175	1.11
	RV3	40	44	1.10
2	RV5	165	147	0.89
	RV6	- " -	150	0.91
	RV7	37	42	1.14
	RV8	- " -	42	1.14

The estimated maximum load capacities were lower than those observed in the tests, except for the specimens where the concrete side cover spalled off (RV5 and RV6). Because of the spalling of the concrete side cover for the specimens with high reinforcement ratio, a direct comparison cannot be made between the specimens with conventional and new detailing. However, the calculated estimations indicate that the load capacity of specimens RV5 and RV6 would have been somewhat higher than that of specimen RV1, if the spalling of the concrete side cover had not occurred, and provided the two different reinforcement detailings of the specimens were equivalent.

For the specimens with low reinforcement ratio, a direct comparison is possible. The differences between the estimated and the observed maximum load capacities for specimens RV1, RV7 and RV8 are similarly small. Furthermore, a similar plateau in the load-displacement relation was observed in all three specimens. Accordingly, for the specimens with low reinforcement ratio, approximately the same load and deformation capacity were obtained when using the conventional and the new reinforcement detailing.

4 NON-LINEAR FINITE ELEMENT ANALYSES

4.1 General

One of the aims of this study was to gain a better understanding of the structural behaviour of frame corners under loading to failure and of the response in the corner area. One way to achieve this is by carrying out many experiments in which different parameters are varied. However, not only is this quite expensive but it cannot be counted on to give all the information needed. Another approach is to make use of the advanced computational techniques available today. By using the non-linear finite element method, in which the concrete material models are based on non-linear fracture mechanics to account for cracking, together with plasticity models for the reinforcement steel and the concrete in compression, the need for experiments can be greatly reduced. In such a finite element analysis, it is possible to evaluate the stresses and deformations of a structure more thoroughly than can be done in an experiment. However, the experiments cannot be completely replaced, since they are still needed to check that the finite element simulations correspond to the tests. This means that even if both methods have their advantages when used alone, they can become an even more powerful tool when used together. Accordingly, in combination with the experiments, the use of non-linear finite element analyses will result in a better understanding of the mechanical behaviour in a structure during loading to failure.

The test specimens were analysed using the finite element programme DIANA, TNO (1993). Two-dimensional plane stress models were used to simulate the concrete. The cracking of the concrete was modelled using the smeared crack concept with fixed cracks. The non-linearity of concrete in compression and the steel reinforcement were accounted for by plasticity models. The specimens were modelled at two different levels of detail. A relatively coarse mesh, assuming perfect bond between the reinforcement bars and the concrete, was used to simulate the general response of the specimens. To compare the new and the conventional reinforcement detailings a refined element model, taking into account the interaction between reinforcement and concrete, with a more dense mesh was used. This model was also used to examine the influence of such parameters as the interaction between the reinforcement and the concrete, the weakness of the construction joint, and the mechanical properties of the reinforcing steel. Thorough information about the material data used in the FE analyses can be found in Johansson (1995, 1996).

4.2 Material Models

4.2.1 Modelling of the concrete

4.2.1.1 The crack model for tension

In the analyses used here, cracking is taken into consideration by using a constant stress cut-off criterion. This means that once the maximum principal tensile stress reaches the tensile strength, independent of the other principal stresses, a crack is initiated perpendicular to the principal stress, see Figure 21. The orientation of the crack is then stored and the material response perpendicular to the crack is determined by a stress-strain relation, reflecting the effect of the softening relation $f(w)$, for the cracked material volume. Additional cracks may

appear at the same location but their formation is restricted to a minimum angle (here set to 60°) to previous cracks. When the cracked concrete is unloaded, the secant unloading modulus is used as tangent stiffness so that the strain across the crack is reduced linearly to zero as the stress approaches zero, see Figure 22. Thus, in the model used, a crack closes completely when the stress reaches zero.

To simulate the softening curve of the concrete, a bilinear stress-crack opening relation, according to recommendations given in Gylltoft (1983), was used, see Figure 23. The fracture energy, G_F, was together with the tensile strength, f_t, used to calculate the value of the ultimate crack opening, w_u. To get the stress-strain relation for the concrete where the reinforcement bars were modelled assuming perfect bond, the mean crack distance, s_{rm} (= 0.2 m), observed from the test specimens was used. Approximate strain values were determined by dividing the ultimate crack opening by the mean crack distance. However, as an approximation to consider the higher stiffness in the structure, due to the effects of tension stiffening, the gradient of the descending part of the stress-strain curve was halved for the concrete where perfect bond was assumed. In the models where the interaction between the reinforcement and the concrete is simulated by using separate elements for the reinforcement bars and the concrete, the crack distribution is given by the analysis, which means that the tension stiffening effect is considered automatically. Since the smeared cracking of each element represents the development of one real crack, the stress-strain relation of the cracked concrete depends on the length of the finite element. Therefore, in the area where the interaction was taken into account, the crack width was divided by the element lengths to determine the softening stress-strain relation.

The tensile strength in MPa used in the analyses was determined, according to the CEB-FIP Model Code, CEB (1993), as

$$f_t = 0.30\left(f_{c,cyl}\right)^{2/3} \tag{3}$$

where $f_{c,cyl}$ was the cylinder compressive strength of the specimens on the testing day, see Table 3.

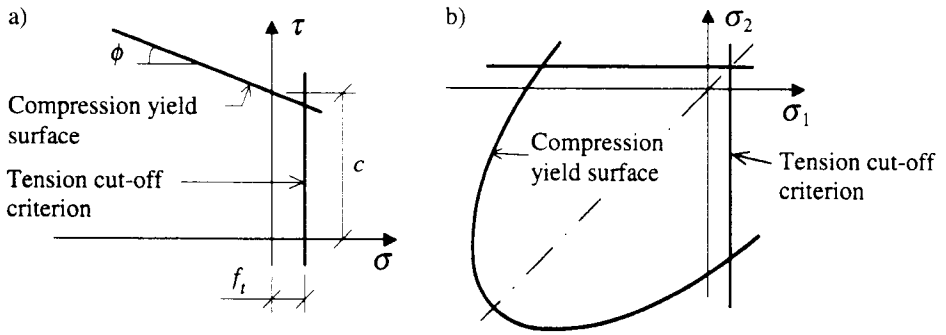

Figure 21 Tension cut-off criterion and compression yield surface in: a) the σ-τ plane when $\sigma_1 = \sigma_2 > \sigma_3$, and b) in the σ_1-σ_2 plane (plane stress: $\sigma_3 = 0$).

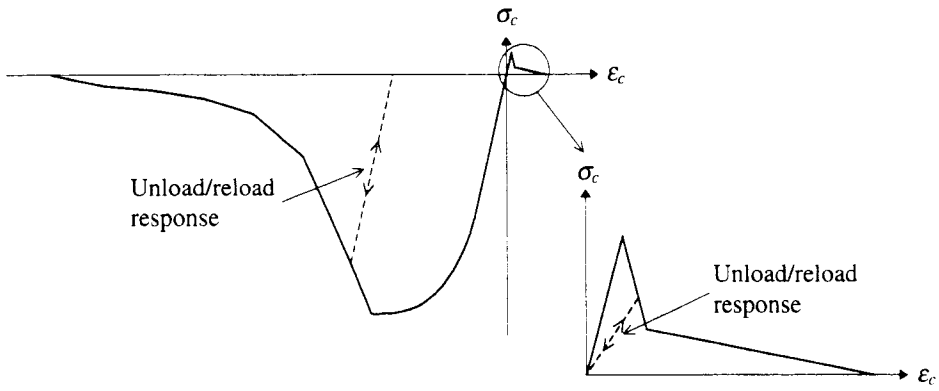

Figure 22 Stiffness used in the analyses for unloaded concrete in compression and tension.

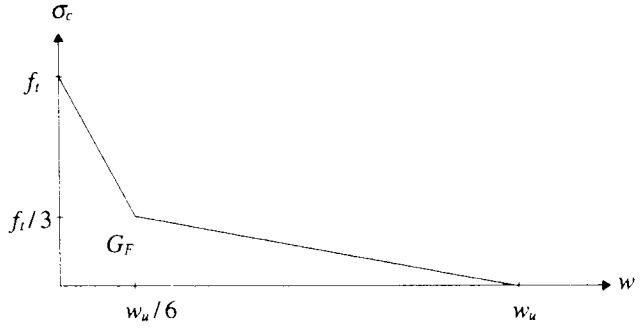

Figure 23 Bilinear stress-crack opening relation simulating the concrete softening curve. The shape of the curve was based on recommendations given in Gylltoft (1983).

4.2.1.2 The plasticity model for compression

In compression, the response of the concrete was accounted for by an elastic-plastic model. The elastic stress-state was limited by a Drucker-Prager yield surface, see Figure 21. Once yielding had occurred, an associated flow rule with isotropic hardening was used. In DIANA, the Drucker-Prager yield surface is evaluated from the current stress state, the angle of internal friction, ϕ, and the cohesion, c, see Appendix B. When concrete in compression is unloaded, the initial elastic stiffness is used, see Figure 22.

The angle of internal friction in concrete was, in accordance with recommendations given in the DIANA manual, approximated to be $\phi = 30°$ and the cohesion, c ,used in the analyses was calculated as

$$c = f_{c,cyl}(\varepsilon^p_{uniaxial})\frac{1-\sin\phi}{2\cos\phi} \tag{4}$$

where $f_{c,cyl}(\varepsilon^{p}_{uniaxial})$ was the compressive strength as a function of the plastic strain in the direction of the uniaxial stress, evaluated from standard uniaxial tests on cylinders, see Table 3. Poisson's ratio was, according to recommendations in BBK 94, Boverket (1994), approximated to $\nu = 0.20$.

The strain hardening of the concrete, specified in the analyses, were determined on uniaxial cylinder tests in which concrete from the same batch as the test specimens was used. In these tests the stress-strain curve could be registered only to the maximum stress, which is why the remaining part of the stress-strain curve was determined using the cylinder compression strength in accordance with the Concrete Design Handbook, AB Svensk Byggtjänst and Cementa AB (1990) and CEB-FIP Model Code, CEB (1993). In the analyses, the strain hardening of the compressed concrete was described by a cohesion-hardening parameter relation, see Appendix B.

4.2.2 Modelling of the reinforcement

The reinforcement bars in the specimens were modelled with either the DIANA option "embedded reinforcements" or separate steel elements using truss elements. In the embedded reinforcement option, the reinforcement does not have separate degrees of freedom; instead the strength and stiffness of the concrete elements are increased in the direction of the embedded reinforcement. With this model, perfect bond is assumed between the reinforcement and the surrounding material. When the interaction between the reinforcement and the concrete was taken into consideration, the reinforcement bars were modelled by separate elements, using truss elements in combination with interface elements, see Section 4.2.3. The von Mises yield criterion with associated flow and isotropic strain hardening was used to describe the constitutive behaviour of the reinforcement. The modulus of elasticity and the mechanical properties of the reinforcement used in the FE analyses are shown in Appendix B. The Poisson's ratio was set to 0.3.

When testing a reinforcement bar to obtain its material properties, the plastic deformations will localise to a short length of the bar once the ultimate strength of the steel material has been reached. However, the strain in the stress-strain relation obtained from such a test is calculated from the extension of the bar divided by the length of the bar. Thus, the localised deformations are smeared out over the whole length of the bar tested. Therefore, to take this into consideration when determining the stress-strain relation of the steel used in the analyses, the localised deformations were smeared out over one reinforcement element, which resulted in a less steep stress-strain relation for the softening branch. The strain exceeding the strain at maximum stress was modified according to equation (5), see Figure 24.

$$\Delta\varepsilon_{mod} = \Delta\varepsilon \frac{l_{bar}}{l_{element}} \tag{5}$$

Here, l_{bar} denotes the length of the reinforcement bar used when determining the stress-strain relation of the steel (= 400 mm) and $l_{element}$ denotes the length of the finite element representing the bar in the FE analyses (= 50 mm).

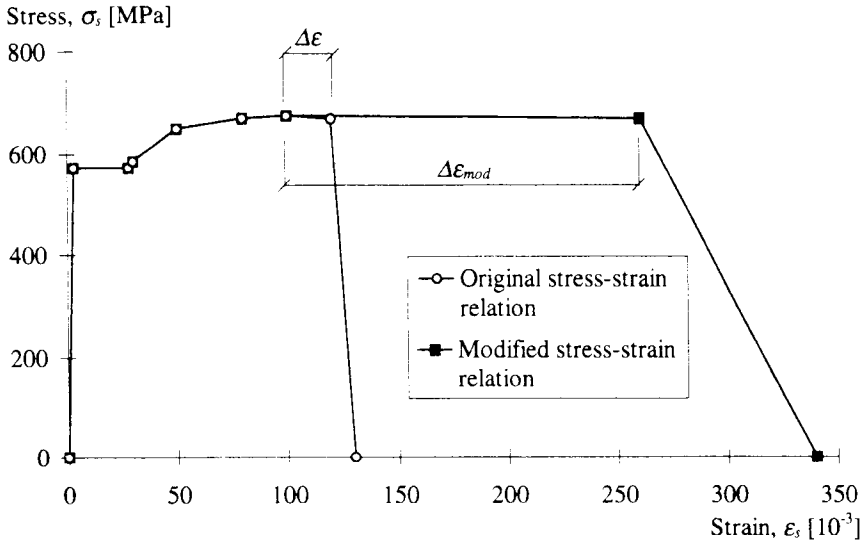

Figure 24 Determination of the modified stress-strain relation used in the FE analyses to take into consideration the localised deformations of the reinforcement bar after maximum stress. The modified strain $\Delta\varepsilon_{mod}$ is determined according to equation (5).

In this work, the importance of the mechanical properties of the reinforcing steel in the deformation capacity of the frame corner was studied. The ratio γ of the ultimate strength f_{su} to the yield strength f_{sy} can, according to Öberg (1976), have a considerable effect on the rotational capacity of a structure. A high value of γ, see equation (6), means that the yielding of the reinforcement bars is more likely to occur over a larger area, resulting in an enhanced deformation capacity of a structure.

$$\gamma = \frac{f_{su}}{f_{sy}} \tag{6}$$

Here f_{sy} and f_{su} denote the yield strength and ultimate strength, respectively, of the "normal ratio" stress-strain relation, see Figure 25. In the detailed FE analyses, three different stress-strain relations of the steel reinforcement, denoted "high ratio", "normal ratio" and "low ratio", were studied; the "normal ratio" corresponded to the stress-strain relation of the steel used in test specimens RV7 and RV8 and the "high ratio" and "low ratio" stress-strain relations were evaluated from the "normal ratio" relation using a factor μ according to equation (7). For detailed information about the determination of the "high ratio" and the "low ratio" stress-strain relations, see Johansson (1996).

$$\mu = \frac{\gamma^{mod}}{\gamma^{normal}} \tag{7}$$

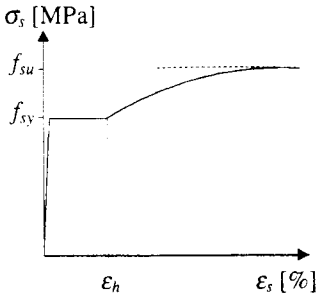

Stress-strain relation	f_{sy} [MPa]	f_{su} [MPa]	γ	μ
High ratio	573	743	1.30	1.1
Normal ratio	573	675	1.18	1.0
Low ratio	573	608	1.06	0.9

Figure 25 Determination of the three different stress-strain relations of the steel reinforcement used in the detailed FE analyses. The "normal ratio" stress-strain relation is based on the reinforcement used in test specimens RV7 and RV8, Johansson (1995).

4.2.3 Interaction between reinforcement and concrete

The interaction between the reinforcement bars and the surrounding concrete was taken into consideration only in the detailed analyses. In the analyses of the general response, perfect bond was assumed, see Section 4.2.2. In DIANA, the bond-slip relation between the reinforcement and the concrete is modelled using interface elements. The off-diagonal terms are set to zero and a non-linear bond-slip relation in the longitudinal direction is used together with a linear relation in the normal direction, see equation (8). In the model no normal expansion is caused by the slip of a bar; thus, radial stresses do not arise in the concrete around a bar. Consequently, splitting failures cannot be modelled. Instead, the effect of splitting has to be included in the non-linear bond-slip relation.

$$\begin{bmatrix} \Delta t_l \\ \Delta t_n \end{bmatrix} = \begin{bmatrix} D_{11}(s_l) & 0 \\ 0 & D_{22} \end{bmatrix} \begin{bmatrix} \Delta s_l \\ \Delta s_n \end{bmatrix} \tag{8}$$

An example of the FE modelling of the reinforced concrete used in the detailed analyses is shown in Figure 26. The steel reinforcement bars, modelled by truss elements, are positioned at the edge between the two concrete elements. Separate nodes are used to define the truss elements and the concrete elements although the co-ordinates of the nodes are identical. Interface elements are then used to model the bond-slip relation between the reinforcement and the concrete. The width i of the interface elements (see Figure 26) is initially equal to zero, while the thickness of the interface elements is equal to the circumference of the reinforcement bars.

Since the truss elements, modelling the reinforcement bars, have to be positioned at the edge of the concrete elements, the finite element mesh is dependent on the positioning of the reinforcement bars. Consequently, when modelling the interaction between the reinforcement and the concrete, a more complex finite element mesh is usually necessary than when a perfect bond is assumed and the embedded reinforcement option is used.

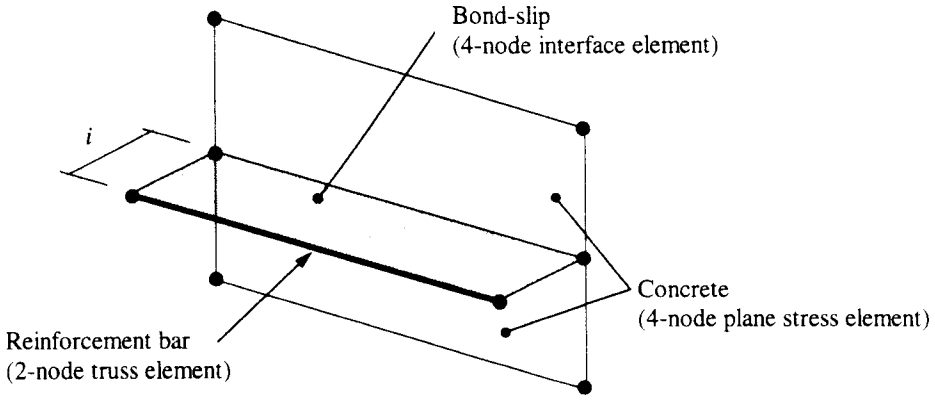

Figure 26 Finite element idealisation in DIANA of reinforced concrete elements using truss and interface elements.

The bond-slip relation between the reinforcement and the concrete used in the detailed analyses was approximated according to the CEB-FIP Model Code, CEB (1993) where the bond stress, τ, is given as a function of the relative displacement, s.

The CEB-FIP Model Code accounts for the effect of splitting cracks by giving different bond-slip relations for confined and unconfined concrete. Since no splitting cracks were observed in the test specimens, "confined concrete" was assumed in the FE analyses. According to Engström (1992), the bond stress decreases considerably when the reinforcement steel yields, see Figure 27. In the bond-slip relation proposed by Engström, the bond stress is not given explicitly, but depends on when the steel reinforcement yields. However, the principal bond-slip relation for this yield case is similar to the relation given when "unconfined concrete" is assumed; therefore, as an approximation, "unconfined concrete" was assumed for the reinforcement bars where yielding of the reinforcing steel was likely to occur.

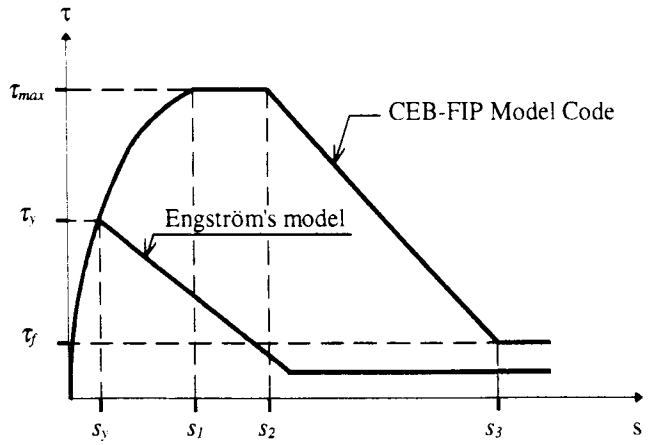

Figure 27 Bond-stress-slip relationship according to the CEB-FIP Model Code, CEB (1993) and the modified model according to Engström (1992).

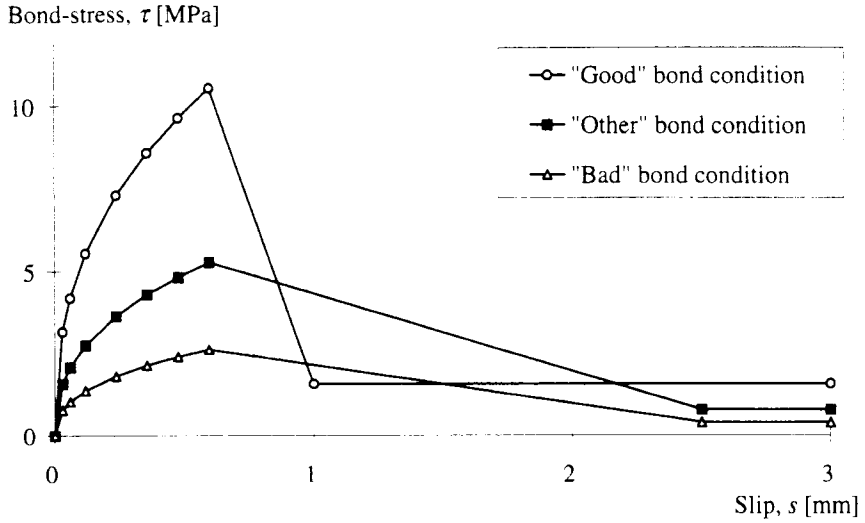

Figure 28 The principal difference between "good", "other" and "bad" bond conditions for "unconfined concrete", CEB (1993).

Different bond-slip relations were used in the analyses to study the effect of the structural behaviour of various bond conditions. "Good" and "other" bond conditions according to the CEB-FIP Model Code, CEB (1993), and a third bond-slip relation, denoted "bad" bond condition, were used. The "bad" bond condition was defined as having half the bond stress at the same amount of slip as the "other" bond condition, see Figure 28. The different bond-slip relations used in the FE analyses can be found in Johansson (1996).

4.3 The Numerical Approach

In a finite element analysis, where the non-linear behaviour of the material, the structure, or both is taken into consideration, a system of simultaneous non-linear equations results. The relation between load and displacement then becomes non-linear, and the displacement at a given stage usually depends on previous displacements. To solve this system, the load is subdivided into increments, see Figure 29. At each load increment a linear approximation of the stiffness, representing a kind of linearised form of the relation between the load and the displacement, is established and the corresponding equilibrium equations are solved. Since the stiffness varies with the displacement, the internal forces of the structure are not in equilibrium with the external forces; this produces an error in the solution. Therefore, to minimise this error, an iterative solution procedure is used within each load increment and the solution is refined until a specified convergence criteria is satisfied.

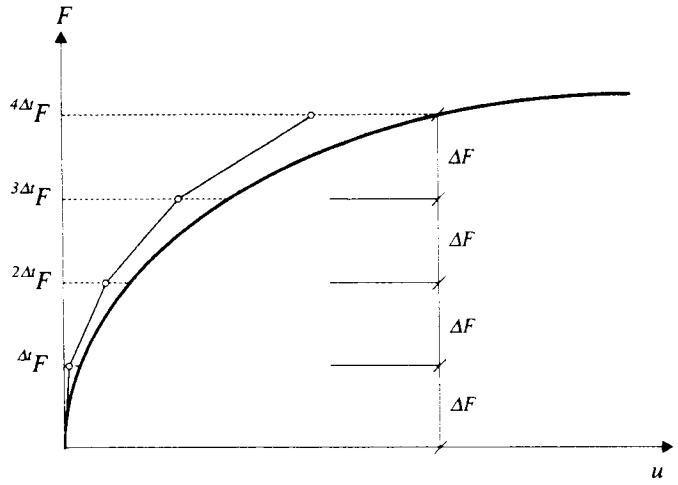

Figure 29 Increasing error of the solution when using the incremental load method without correction for a one degree of freedom system.

There are several different iteration methods available that can be used in the solution process. According to TNO (1996), the general procedure is the same for all iteration methods; the difference is in how the stiffness matrix is determined. The iterative methods can be divided roughly into three categories: the tangent stiffness method, the initial stiffness method and the secant stiffness method, see Figure 30. In the tangent stiffness method, the stiffness matrix is determined at each iteration, resulting in a method that requires few iterations, but there every iteration is relatively time consuming. In the initial stiffness method, the stiffness is determined at the beginning of each load step and it is then used throughout the whole iteration process within an increment. This method requires more iterations to reach convergence than the tangent stiffness method. However, since the same stiffness matrix is used in each iteration within the increment, every iteration is faster. The secant stiffness method uses the information from previous solutions to update the inverse stiffness matrix in each iteration, which results in a convergence rate somewhere between that of the tangent and the initial stiffness methods.

In this study, the Modified Newton-Raphson method (initial stiffness method) and the BFGS method (secant stiffness method) have been used in combination with a displacement controlled incremental loading. Experience indicates that these methods provide a solution process with fewer numerical difficulties, see Plos (1995). A tolerance given as a percentage (usually 0.01 %) of the energy norm was used as the convergence criterion. Further information of these iteration methods can for instance be found in Bathe (1996) and TNO (1996).

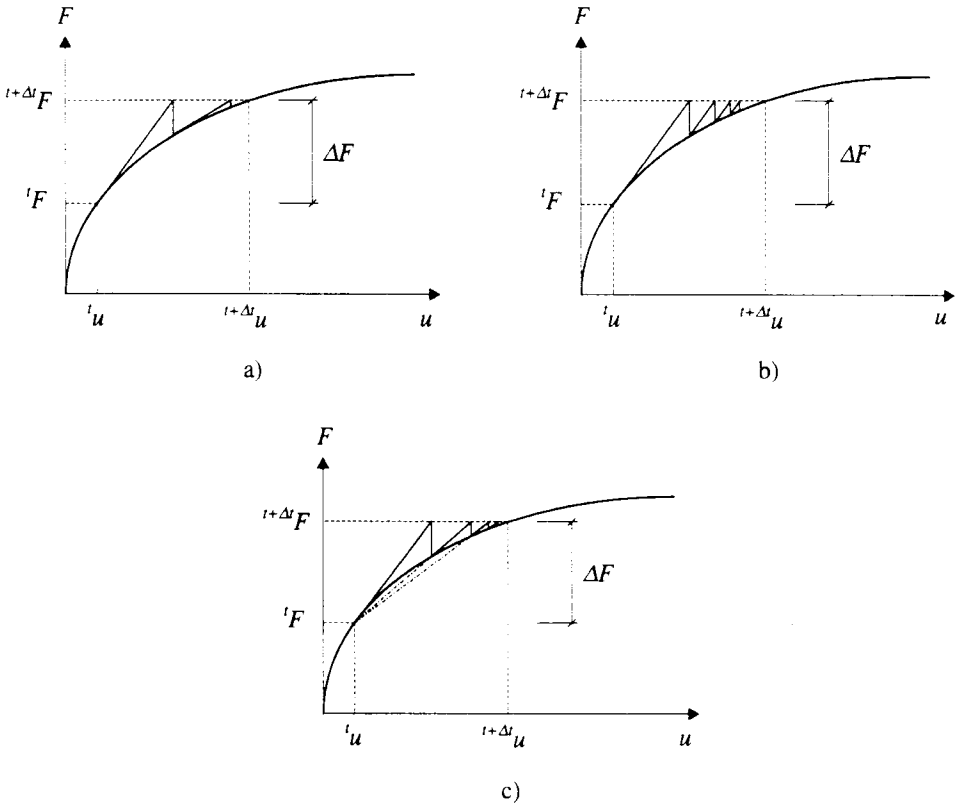

Figure 30 Schematic figure of different iteration methods for a one degree of freedom system: a) tangent stiffness method, b) initial stiffness method, c) secant stiffness method.

4.4 Analyses of Frame Corners

4.4.1 General

The frame corner specimens tested in the second test series were analysed using the finite element method. The analyses were carried out at two different detail levels. In the analyses of the general response, perfect bond between the reinforcement bars and the concrete was assumed, using the embedded reinforcement option. In the more detailed analyses, truss elements in combination with interface elements were used to simulate the reinforcement bars in the region close to the frame corner area; thus, the interaction between the reinforcement and the surrounding concrete was included. Embedded reinforcement was used in the remaining part of the model, to model the reinforcement bars. In the tests of specimens with high reinforcement ratio, the side concrete cover in the corner area spalled off. As this behaviour could not be simulated in the FE models used, these specimens were analysed using only the less detailed model. The specimens with low reinforcement detailing were analysed

using both models. The FE models used do not take into account the placement of the reinforcement bars, i.e. whether they are in contact with each other or not. Therefore, the same models were used in the analyses of the specimens whether or not the reinforcement bars were in contact with each other; i.e. one model was used to simulate specimens RV5 and RV6, and another model was used to simulate specimens RV7 and RV8.

Due to numerical difficulties, the effect of different mechanical properties of the reinforcing steel bars was not studied using finite element models of the frame corner. Instead, a simpler model of a cantilever beam was used, see Section 4.7. This model was also used to study more thoroughly the effect of different bond-slip relations for structures with high and low amounts of reinforcement.

In the FE analyses, two-dimensional plane-stress elements, consisting of four-node quadrilateral elements and three-node triangular elements, were used to model the concrete. The reinforcement bars were modelled using either the embedded reinforcement option available in DIANA or two-node truss elements, see Section 4.2.2. Where the reinforcement was modelled by truss elements, four-node interface elements were used to simulate the interaction between the reinforcement and the concrete, see Section 4.2.3. A Gauss integration scheme was used: 2 x 2 integration points for the four-node quadrilateral elements, one integration point for the three-node triangular elements, one integration point for the two-node truss elements, and two integration points for the four-node interface elements.

For the detailed analyses of the frame specimens, the accuracy of the model was investigated; an analysis using a comparative model consisting of elements of higher polynomial order were carried out. The four-node plane stress elements, two-node truss elements and four-node interface elements were replaced by nine-node plane stress elements, three-node truss elements and six-node interface elements, respectively. As the difference in the results was negligible, the model using the lower order elements was chosen.

4.4.2 The FE model for analyses of general response

The model used to analyse the general response of the frame corners consisted of 158 two-dimensional plane stress elements, see Figure 31. Since embedded reinforcement was used to model the reinforcement, the same element mesh could be used to model the test specimens with both the high and low amounts of reinforcement. The position and amount of reinforcement bars used in the model were determined by taking into account the anchorage capacity of the reinforcement according to the simplified splitting stress model, AB Svensk Byggtjänst and Cementa AB (1990), see Figure 32.

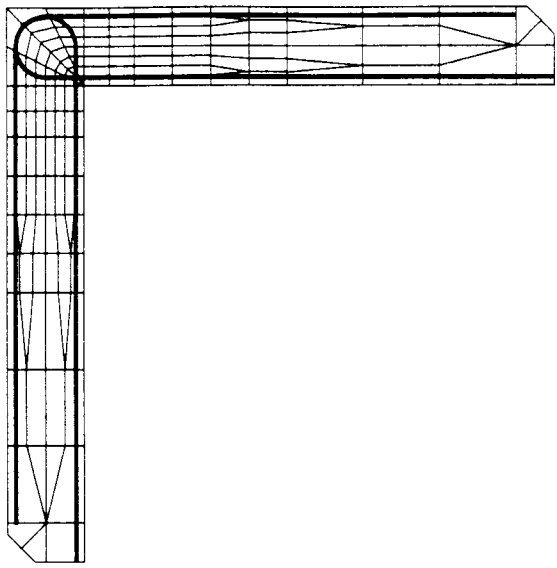

Figure 31 The finite element mesh and the position of steel reinforcement in the model for analysing the general response of the frame corner.

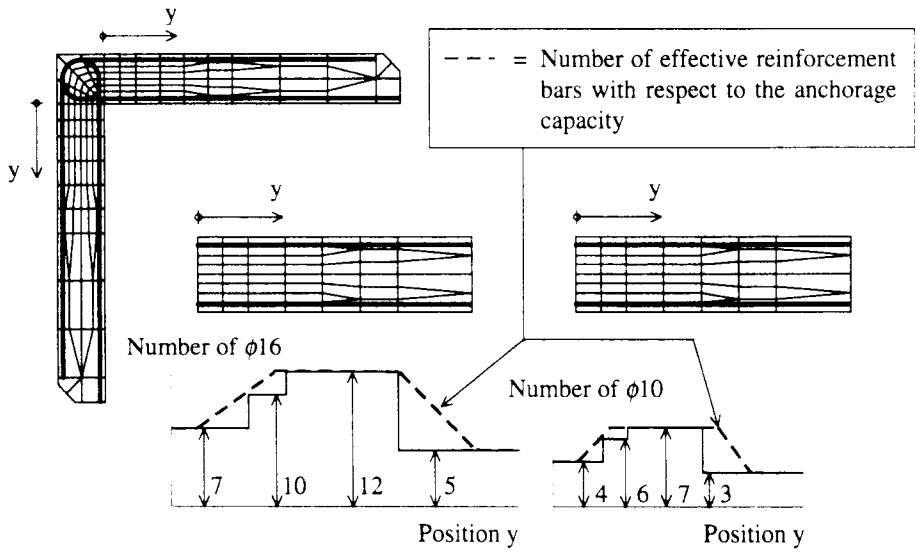

Figure 32 Position and amount of the steel reinforcement when the anchorage capacity has been taken into account. The steel area used in the different sections of the model correspond to the area of the number of reinforcement bars listed in the diagrams.

4.4.3 The FE model for detailed analyses

4.4.3.1 New reinforcement detailing

To model the geometry of the test specimens, a total of 322 two-dimensional plane stress elements were used, see Figure 33. Truss elements in combination with interface elements (a total of 137 each) were used to model more accurately the reinforcement bars within 1.0 m of the corner, where cracking of the concrete was expected. Outside this area, the reinforcement bars were modelled with embedded reinforcement, see Figure 34.

The test specimens were cast with a construction joint, see Figure 6. The test results indicated that this joint exhibited a zone of weakness in the material in which cracking first occurred, see Section 3.3.3. To model the weakness of the construction joint, a thin row of elements was used in which weaker material parameters were given, see Figure 35. In this way, the construction joint was smeared out in the FE model, meaning that any reinforcement bars placed in the element row simulating the construction joint would be affected. The straight reinforcement bars in the column did not reach into the corner area and were not, therefore, affected by the construction joint. Thus, the straight tensile reinforcement bars in the columns of the frame corners tested were modelled to end just below the row of elements modelling the construction joint, see Figure 35.

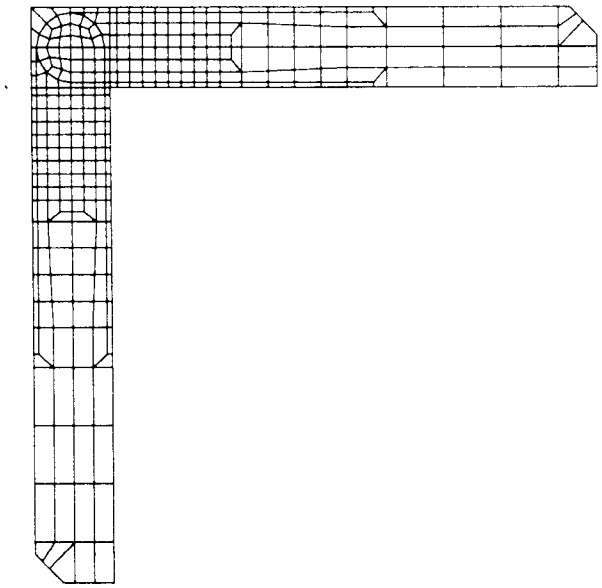

Figure 33 The finite element mesh of the frame corner with new reinforcement detailing.

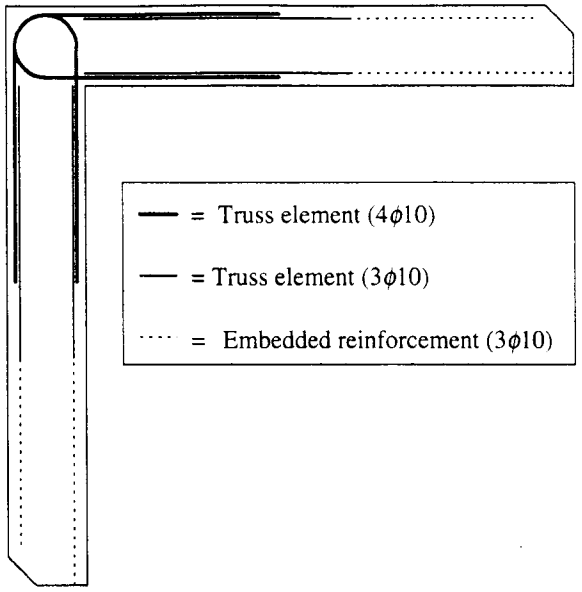

Figure 34 Modelling of the reinforcement bars in the frame corner with new reinforcement detailing.

The concrete in the construction joint was assumed to have reduced tensile strength and fracture energy although the compressive strength was unmodified. Since the first cracks in the test specimens with low reinforcement ratio were observed at a load level approximately half of that expected, the tensile strength of the concrete modelling the construction joint was reduced to 50 %. The effect of the weakness in the construction joint on the structural behaviour of the frame corner was examined. By modelling the construction joint with a slight weakness, the first crack was made to form at the same place as in the tests. Therefore, an FE analysis with a tensile strength and fracture energy of 90 %, of that used in the rest of the model was carried out.

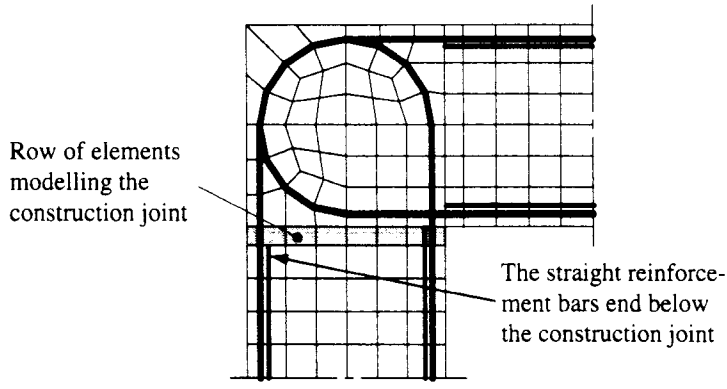

Figure 35 Modelling of the construction joint and the reinforcement bars in it.

On the construction site, it sometimes happens that the reinforcement bars are not positioned according to the designers' drawings. In this work, it is of interest to study the consequences of incorrectly positioned reinforcement loops. Therefore, an analysis of reinforcement loops incorrectly positioned in the column was carried out, see Figure 36. When using truss elements in combination with interface elements, the element mesh modelling the concrete depends on the reinforcement detailing, see Section 4.2.3. To use truss elements in combination with interface elements for modelling the reinforcement detailing shown in Figure 36, quite a complicated finite element mesh for the concrete elements is necessary. In the analyses where all reinforcement bars in the corner area were modelled with a combination of truss elements and interface elements, the crack propagation in the corner was limited; thus, the slip of the reinforcement in the bend of the reinforcement bars was tolerably small. This means that the assumption of perfect bond for the bend part of the reinforcement loops is appropriate. Therefore, as an approximation, embedded reinforcement was used to model the loop of the reinforcement bars in the corner area. Parallel to this, a new, less complicated element mesh in the corner area was used to study its effect on the crack pattern in the corner and the structural behaviour of the specimen, see Figure 37.

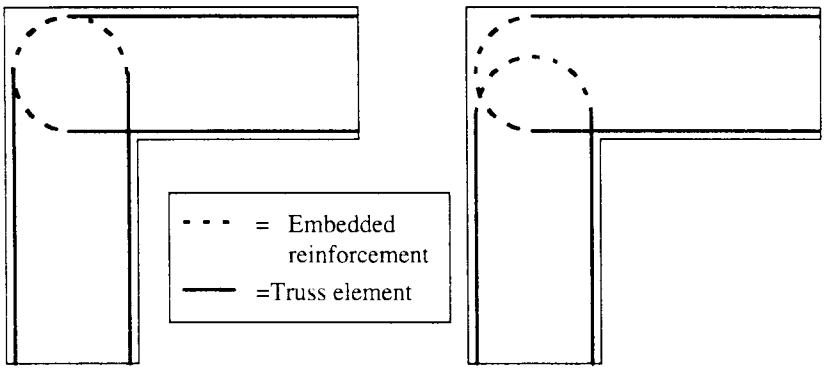

Figure 36 Position and modelling of the reinforcement in the corner area for analyses of correct (left) and incorrect (right) positioned reinforcement loops. The bends of the reinforcement bars were modelled using embedded reinforcement.

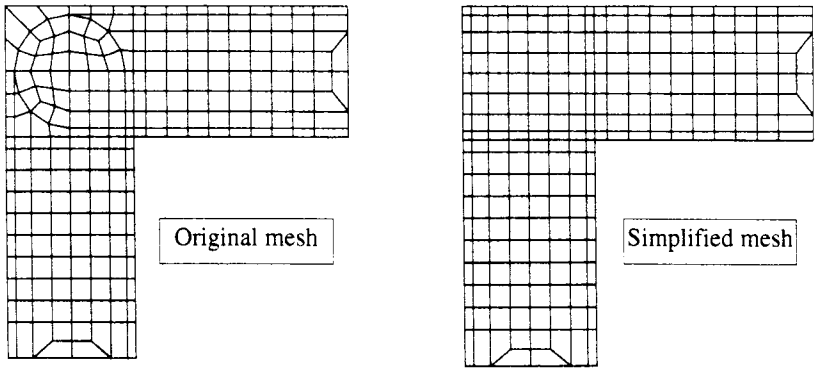

Figure 37 Different element meshes in the corner area when the loops of the reinforcement were modelled with embedded reinforcement.

4.4.3.2 Conventional reinforcement detailing

A comparison of the new and the conventional reinforcement detailings was carried out. The reinforcement detailing in the FE model was in accordance with that used by Plos for test specimen RV3. The material parameters for concrete and reinforcing steel, including the weakness of the construction joint, were identical to those used in the corresponding analyses of the frame corner with the new reinforcement detailing. To study the different detailings of the reinforcement in and near the corner area, a new model with a total of 336 two-dimensional plane stress elements was used to model the geometry, see Figure 38. As in the model with the new reinforcement detailing, a combination of truss elements and interface elements (203 of each) were used to model the reinforcement bars within 1.0 m of the corner. The remaining reinforcement bars were modelled using embedded reinforcement, see Figure 39.

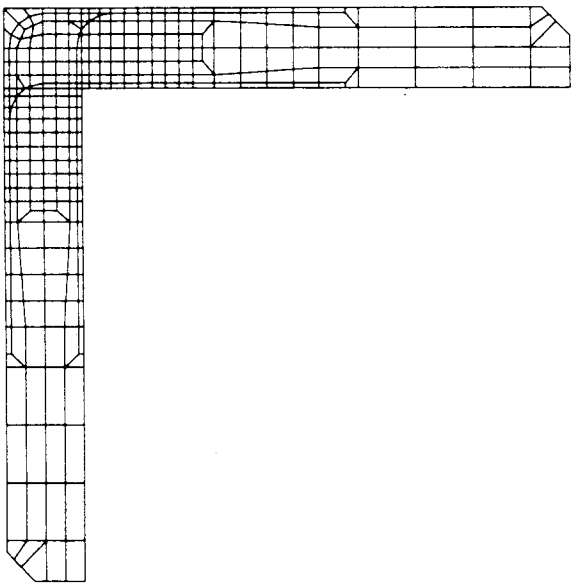

Figure 38 The finite element mesh of the frame corner with conventional reinforcement detailing.

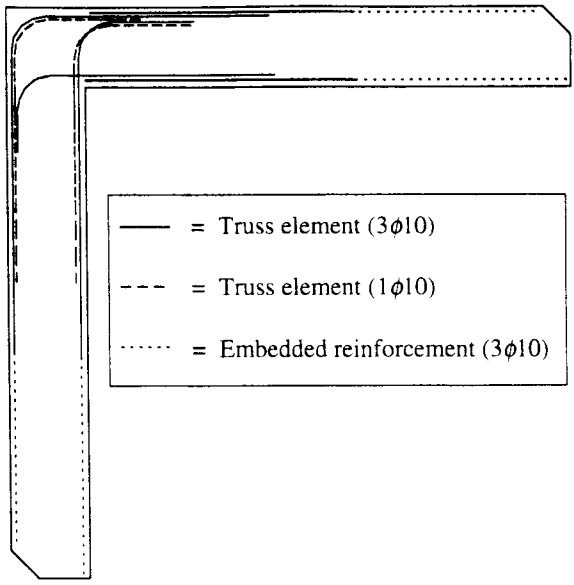

Figure 39 Modelling of the reinforcement bars in the frame corner with conventional reinforcement detailing.

4.5 Results of the Analyses

4.5.1 General

Two different iteration methods, the Modified Newton-Raphson method and the BFGS secant stiffness method, were used in the FE analyses, see Section 4.3. In the analyses of the general response, only the Modified Newton-Raphson method was used. However, in the analyses of the refined FE model it was found that fewer numerical problems were encountered with the BFGS secant method; accordingly, this was the main iteration method used. Although the Modified Newton-Raphson method gave a somewhat smoother load-displacement relation than that achieved with the BFGS secant method, the difference in the effect of these iteration methods on the results was negligible, see Figure 40.

Unless otherwise stated, the following assumptions were made in the detailed FE analyses:

- bond condition = "good" (see Section 4.2.3),
- reinforcement type = "normal ratio" (see Section 4.2.2),
- strength of construction joint = 50 % (see Section 4.4.3.1), and
- iteration method = BFGS secant stiffness method.

It was found that incorrect parameters for the modelling of the concrete in compression had been used in the FE analyses; this resulted in a stronger and less ductile concrete, see Appendix B. To examine what effect this error had on the structural behaviour of the frame corner, a comparative detailed analysis with a more accurate stress-strain relation was carried out. The difference in the load-displacement relation is shown in Figure 41.

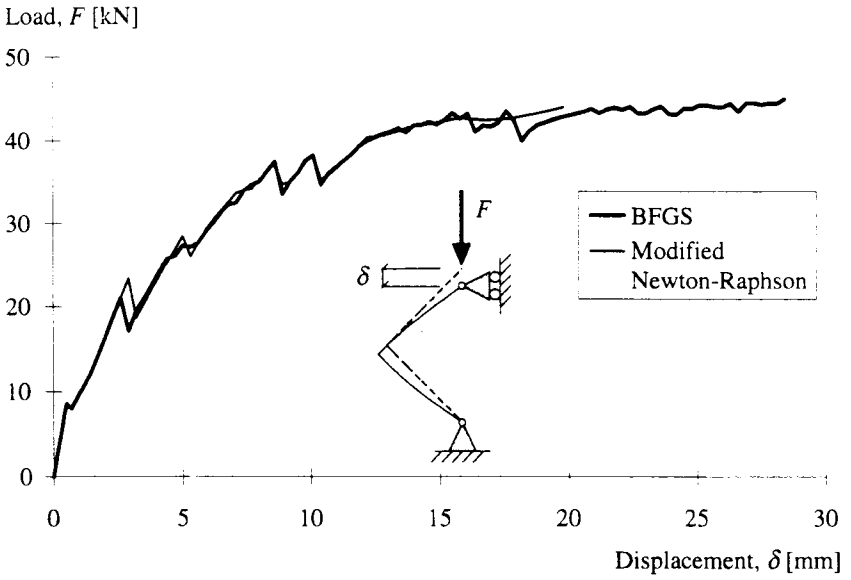

Figure 40 Comparison of the FE analyses of the frame corner with new reinforcement detailing when using different iteration methods.

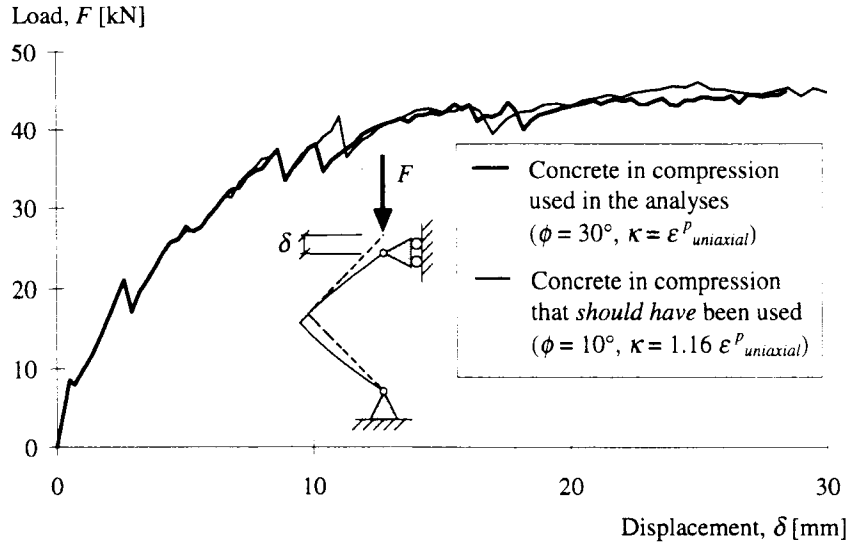

Figure 41 Comparison of the FE analyses when using different stress-strain relations for the concrete in compression, see Appendix B.

As can be seen, the incorrect usage of stronger and less ductile concrete had a negligible effect on the structural behaviour of the frame corner. The load capacity and the stiffness of the structure were, more or less, the same in the FE analyses carried out. This was due to the small compressive zone obtained in the structure (about 20 mm), which meant that the inner

lever arm remained approximately the same, independent of the strength of the concrete. Unless otherwise stated, the results presented in this study are from analyses in which the incorrect modelling of the concrete in compression was used. However, the negligible difference in the behaviour of the structure shown in Figure 41, when using different values of the concrete in compression, shows that the results are still valid.

4.5.2 FE analyses of the general response

An objective of the FE analyses of the general response, besides predicting the maximum load, was to describe the plateau in the load-displacement relations observed in the tests. In the analysis of the specimens with low reinforcement ratio, such a plateau was obtained and the analysis was disrupted when the deformation capacity of the steel reinforcement was almost reached. In the analysis of the specimens with high reinforcement ratio, yielding of the steel reinforcement was reached but, due to numerical problems caused by the concrete in compression, the plateau could not be simulated.

With the models used, it was not possible to simulate the spalling of the side concrete cover in the frame corners that was observed in the tests for the specimens with high reinforcement ratio. Consequently, the maximum load obtained in the analysis of the general response for these specimens do not coincide with the test results. Instead, the maximum load level reached in these analyses reflects the capacity of the test specimens, providing the spalling of the concrete had not occurred. The load-displacement relation for the FE analyses and the test results are compared in Figures 42 and 43. The distribution of tensile forces along the reinforcement bars in the frame corner for the analyses and the tests are displayed in Figures 44 and 45. The relatively high tensile force obtained in the middle of the corner for the analysis of the specimens with high reinforcement ratio was due to large cracks in this region. In the analysis of the specimens with low reinforcement ratio, no cracks were formed in the corner; this explains the low tensile forces in the reinforcement bars in this region.

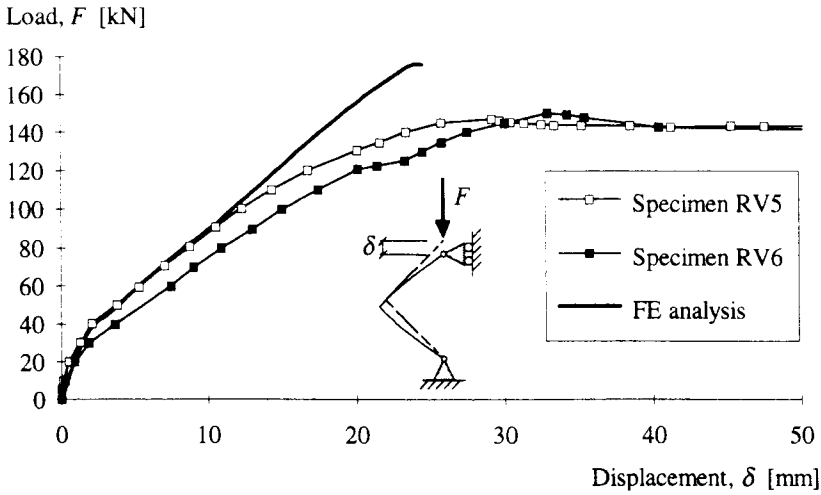

Figure 42 Comparison of the FE analyses of the general response and the test results for the specimens with high reinforcement ratio.

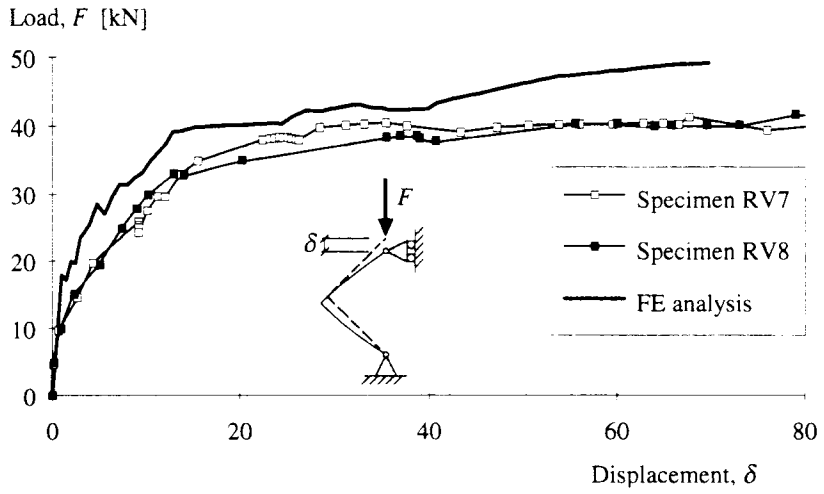

Figure 43 Comparison of the FE analyses of the general response and the test results for the specimens with low reinforcement ratio.

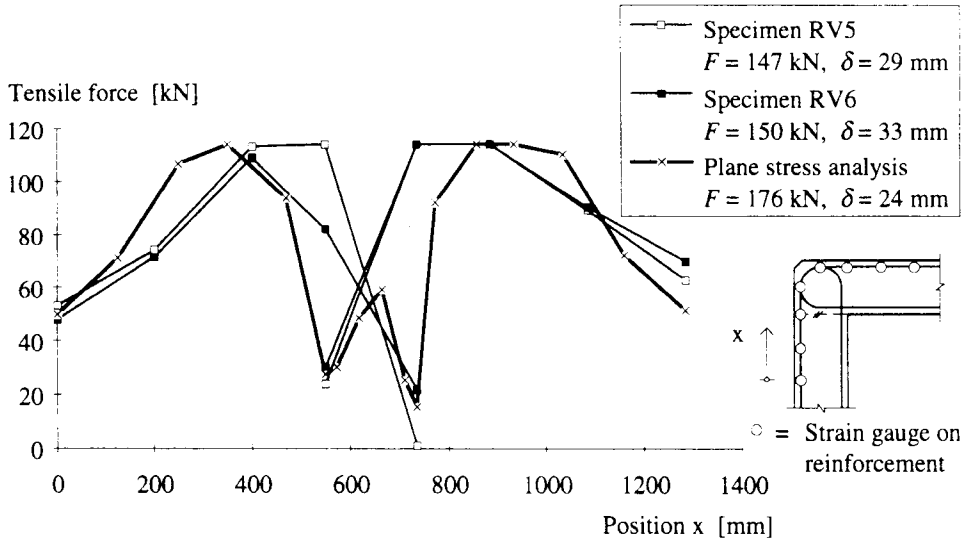

Figure 44 Distribution of tensile forces along the reinforcement bars in the frame corner. Results from the analysis of the general response are compared with results from the test specimens with high reinforcement ratio.

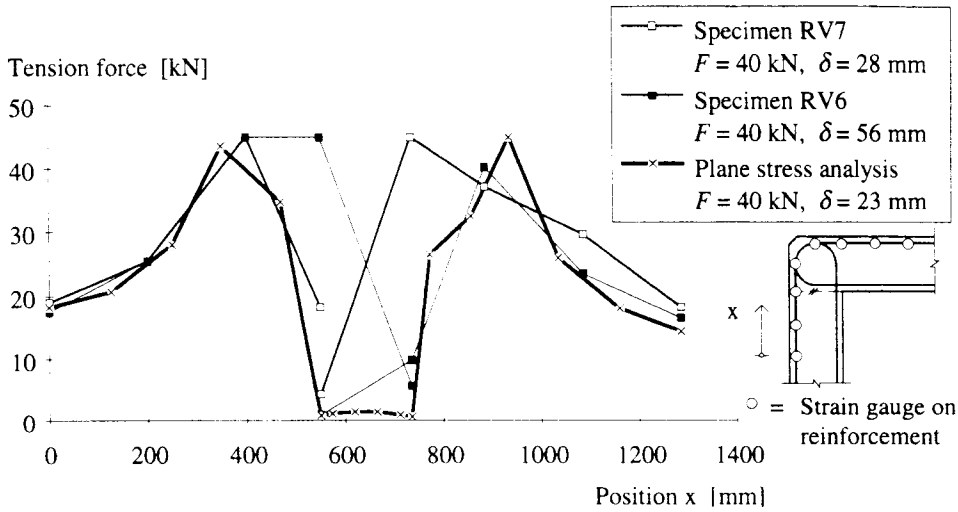

Figure 45 Distribution of tensile forces along the reinforcement bars in the frame corner. Results from the analysis of the general response are compared with results from the test specimens with low reinforcement ratio.

4.5.3 Detailed FE analyses

4.5.3.1 Objectives and preconditions

In the detailed FE analyses, the main objective was to examine the effect of different parameters, such as bond condition, mechanical properties of the steel reinforcement, and the weakness of the construction joint, on the maximum load and the deformation capacity of a frame corner structure. Also, the structural behaviour of frame corners with the new and the conventional reinforcement detailing was to be compared. In addition the effect of incorrect positioning of the reinforcement loops in the new reinforcement detailing was examined.

As in the analyses of the general response, it was not possible to predict the behaviour of the frame corner throughout total failure. All the detailed analyses of the frame corner were disrupted due to numerical problems when the ultimate compression strength of the concrete was reached at one integration point in the corner area. At this stage, yielding of the reinforcement bars had occurred and, in some cases, also started to harden. To study the effect that different mechanical properties of the steel reinforcement have on the frame corner, substantial hardening of the steel is presumed. However, in the analyses of the frame corner, sufficient strain of the reinforcing steel was not reached and, therefore, the mechanical property study was not made with the frame corner model. Instead a simpler model of a cantilever beam was used for this study, see Section 4.7.

4.5.3.2 New reinforcement detailing

The specimens with low reinforcement ratio of the second test series was analysed using the detailed model. In the first stage of the analyses, the bond condition corresponding to that of the test specimens was to be determined. Two criteria can be used for this determination: the mean spacing of the major cracks observed in the test specimens and the load-displacement relation obtained in the tests. The former criterion was assumed the better one to use since some factors of uncertainty, such as the fracture energy and the generally stiffer behaviour of the FE analysis, have less effect on it. The crack pattern of the analyses was compared with the crack pattern obtained in the tests, see Figure 46 The crack pattern (at the end of the analysis) and the load-displacement relations for three different bond-slip relations, "good", "other" and "bad", see Section 4.2.3, were examined, see Figures 47 to 50. The FE analysis assuming "good" bond condition showed the best agreement with the mean crack spacing of 0.2 m observed in the tests. When comparing the load-displacement relations, the analysis using "bad" bond condition correlated best with the tests. However, as explained above, the crack pattern was assumed to be more important when deciding what bond condition was present in the test specimens. Therefore, a bond-slip relation corresponding to "good" bond condition was assumed to be the closest to that of the test specimens even though it was somewhat too stiff in comparison with the tests. Accordingly, the "good" bond condition has been used as a basis when comparing the FE analyses.

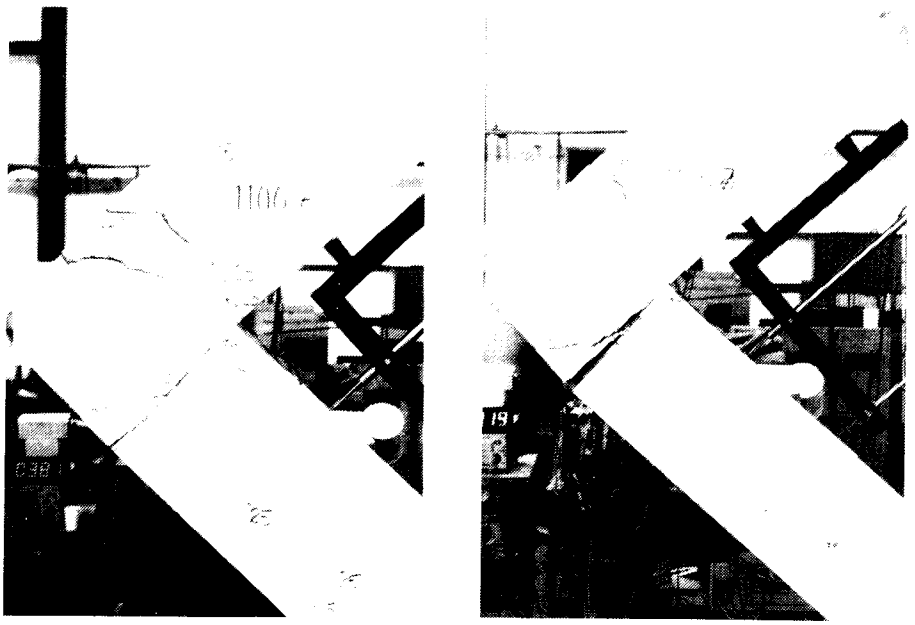

Figure 46 Crack patterns obtained for test specimens RV7 (left) and RV8 (right).

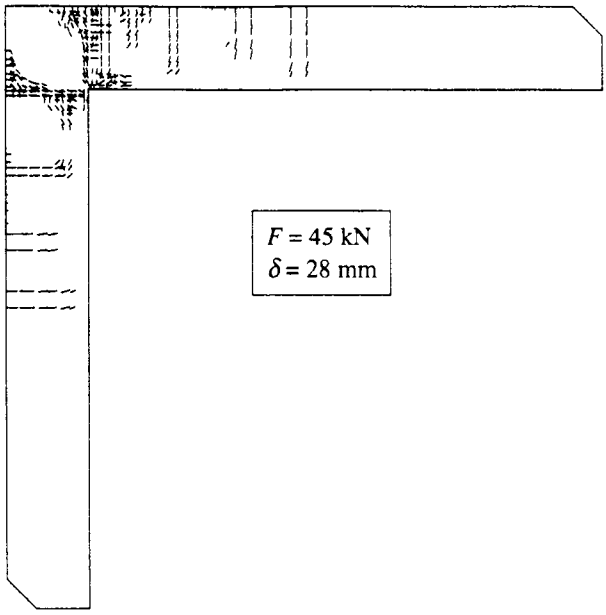

Figure 47 Crack pattern at the end of the analysis for a frame corner with the new reinforcement detailing when assuming "good" bond condition.

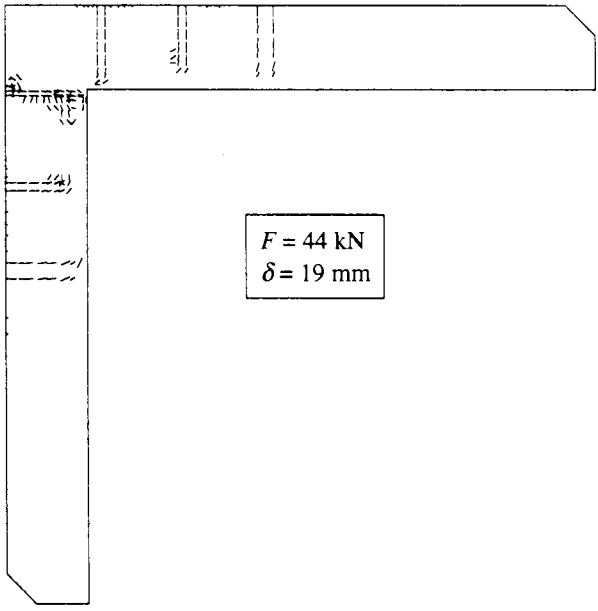

Figure 48 Crack pattern at the end of the analysis for a frame corner with the new reinforcement detailing when assuming "other" bond condition.

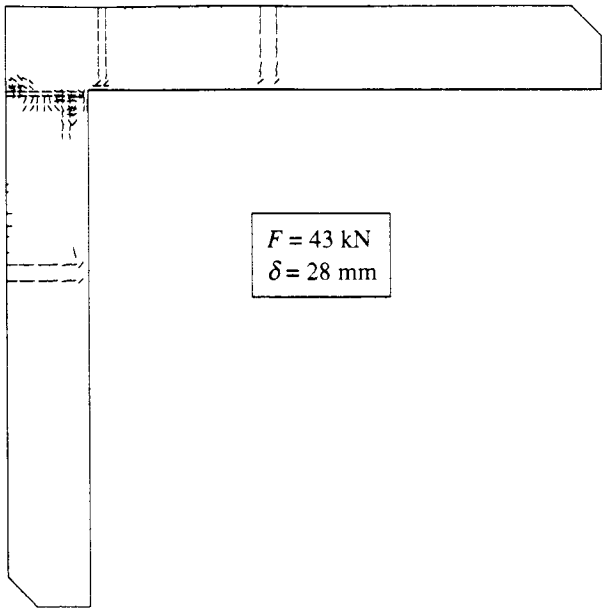

Figure 49 Crack pattern at the end of the analysis for a frame corner with the new reinforcement detailing when assuming "bad" bond condition.

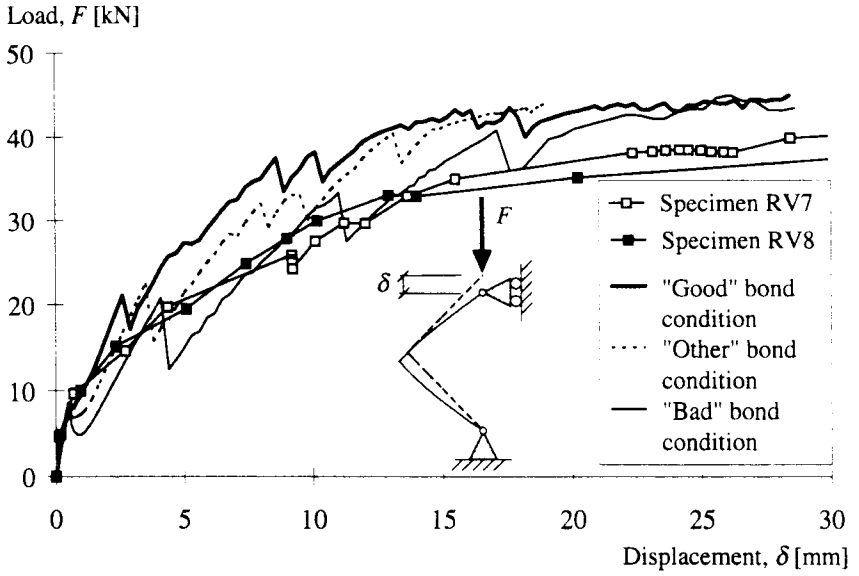

Figure 50 Comparison of the load-displacement relations for three different bond conditions.

The distribution of the tensile forces along the reinforcement loops, in the tests and analyses, when yielding of the steel reinforcement has occurred, are presented in Figures 51 and 52. The difference in the distributed tensile forces, observed for the different bond-slip relations, was

due to the appearance of major cracks in the column and the beam near the corner area. In the analysis where "bad" bond condition was assumed, the variation of the tensile force was approximately linear. This was because of the large space between the cracks in the column and the beam. For the "good" and "other" bond-conditions, a shift in the tensile force resulted due to the appearance of a crack near the corner, see Figures 47 to 49.

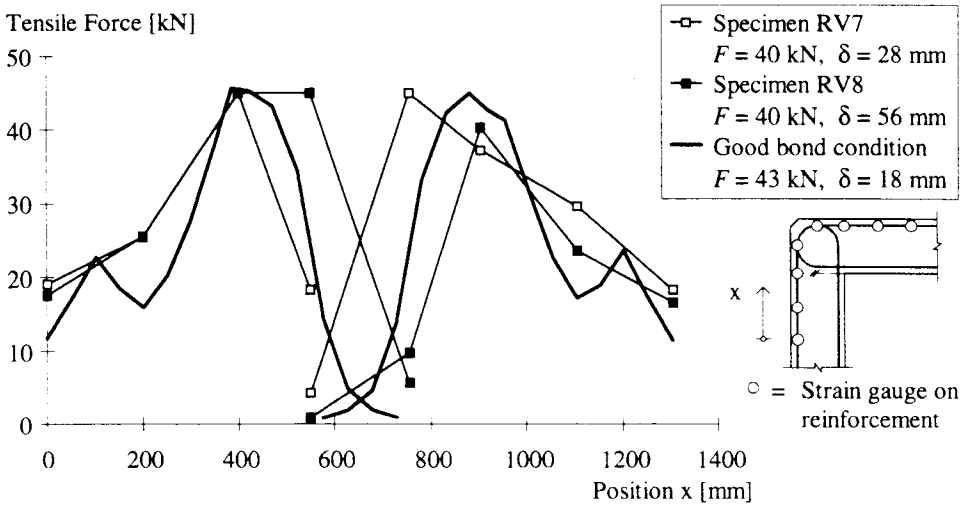

Figure 51 Distribution of the tensile forces along the reinforcement bars in the frame corner for the tests and the FE analysis where "good" bond condition was assumed.

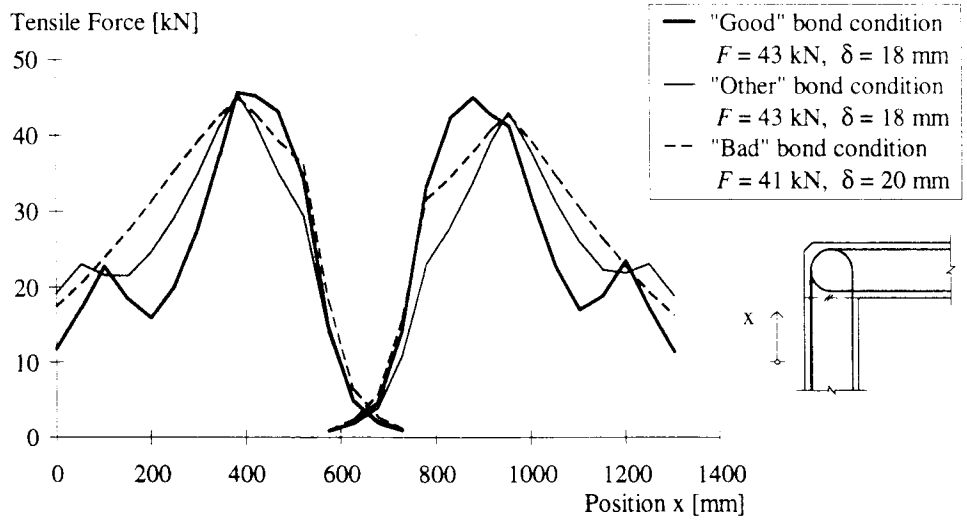

Figure 52 Distribution of the tensile forces along the reinforcement bars in the frame corner for the FE analyses of different assumptions of the bond condition.

The effect of the weakness in the construction joint on the structural behaviour of the frame corner was examined. By modelling the construction joint with a slight weakness, the first crack was made to form at the same place as in the tests. Therefore, an FE analysis with a tensile strength and fracture energy of 90 %, of that used in the rest of the model, was carried out. The load-displacement relations of the FE analyses using different strength of the construction joint are compared in Figure 53. The changes in the crack pattern and the distribution of tensile forces in the frame corner area, caused by the weakness of the construction joint, are shown in Figures 54 and 55, respectively.

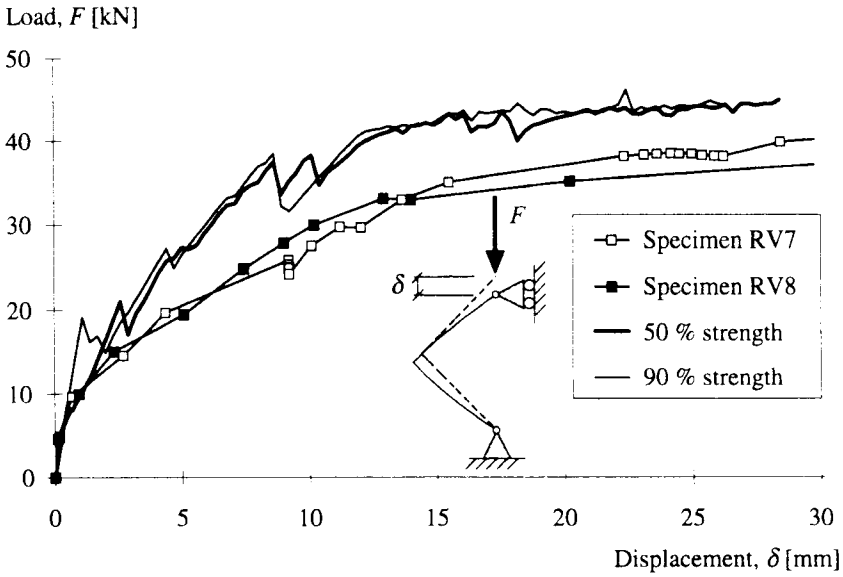

Figure 53 Comparison of the load-displacement relations using different strengths of the construction joint for the frame corner with new reinforcement detailing.

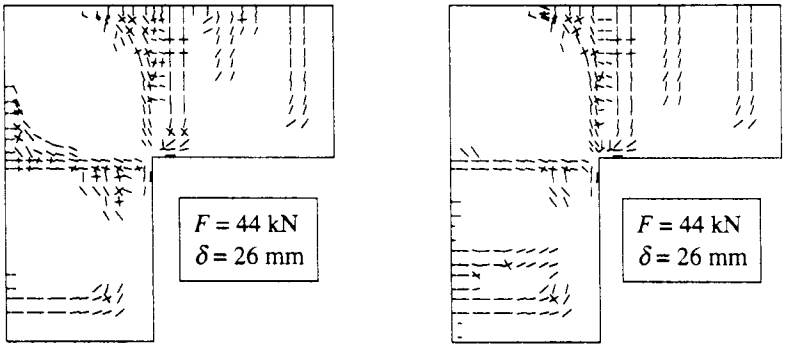

Figure 54 Difference in crack pattern in the corner area when using 50 % strength (left) and 90 % strength (right) for the concrete in the construction joint.

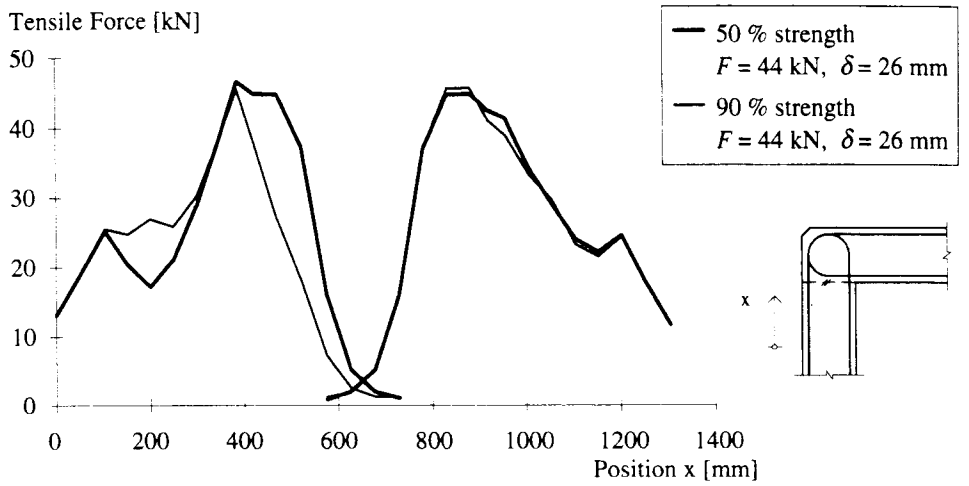

Figure 55 Comparison of the tensile forces in the frame corner when using different strengths for the concrete in the construction joint.

When examining the consequence of incorrect positioning of the reinforcement loops, an approximate approach was used to model the reinforcement bars in combination with a simplified FE mesh, see Section 4.4.3.1. The load-displacement relations compared in Figure 56 confirm that the approximations made were appropriate. The slightly higher load capacity obtained, in the analyses where the reinforcement loops were modelled using embedded reinforcement, was due to the assumption of perfect bond in the bend. When the bend of the

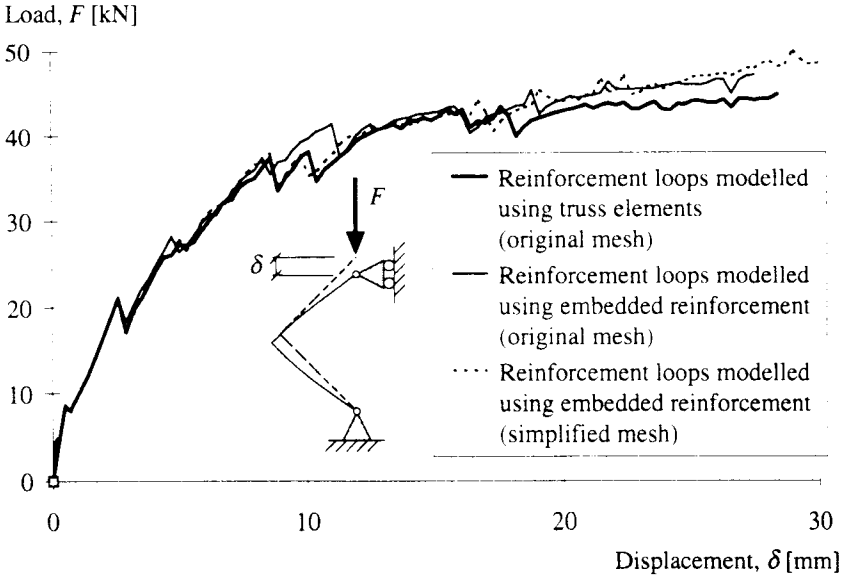

Figure 56 Comparison of the load-displacement relations for different modelling schemes of the corner area, see Section 4.4.3.1.

reinforcement loops was prevented from slipping, a somewhat higher tensile strain with consequent higher tensile stress in the reinforcement bars was the result. Parallel to this, the effect of different element meshes for the crack pattern in the corner area, was examined. In Figure 57, the resulting crack patterns in the corner, when using the original and the simplified mesh shown in Figure 37, are compared. It can be seen that the crack pattern is affected by the element mesh and that the direction of the cracks tends to be parallel to the edges of the elements. The effect of the load-displacement relation when the reinforcement loops in the column are positioned incorrect is shown in Figure 58.

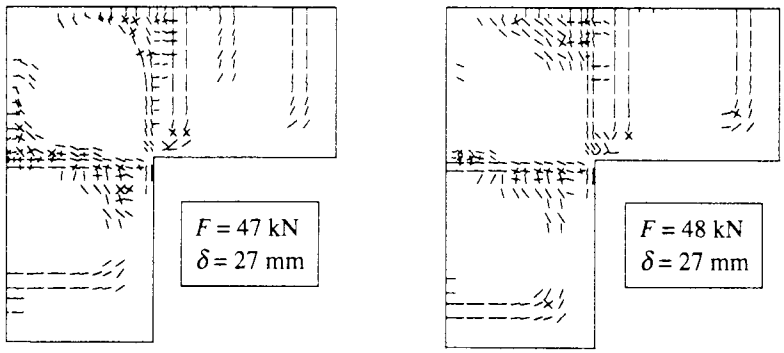

Figure 57 Crack pattern in the frame corner when using the original FE mesh (left) and the simplified mesh (right), see Figure 37. Embedded reinforcement was used to model the bend of the reinforcement loops.

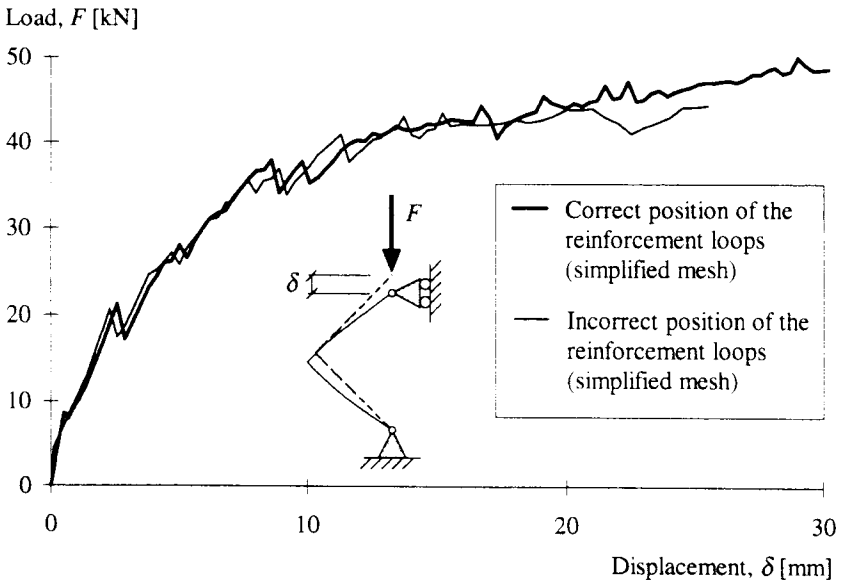

Figure 58 Comparison of the load-displacement relations for the frame corner when the reinforcement loops were modelled in the positions according to Figure 36.

4.5.3.3 Conventional reinforcement detailing

The crack pattern of a test specimen with low reinforcement ratio (specimen RV3), Plos (1994a, b), carried out with the conventional detailing is shown in Figure 59. Although the strength of the concrete and the steel reinforcement used in this specimen were not the same as in the FE analyses, a comparison of the crack pattern can still be made. The crack pattern (at the end of the analyses) and the load-displacement relation for the "good" and the "other" bond conditions are shown in Figures 60 to 62. The denser crack pattern obtained in the analyses of the frame corner with conventional reinforcement detailing, compared with the frame corner with the new detailing, was due to the greater amount of reinforcement in the vicinity of the corner area, see Figures 34 and 39. The distribution of the tensile forces along the reinforcement bars in the frame corner for the FE analyses where "good" and "other" bond conditions were assumed, are shown in Figure 63.

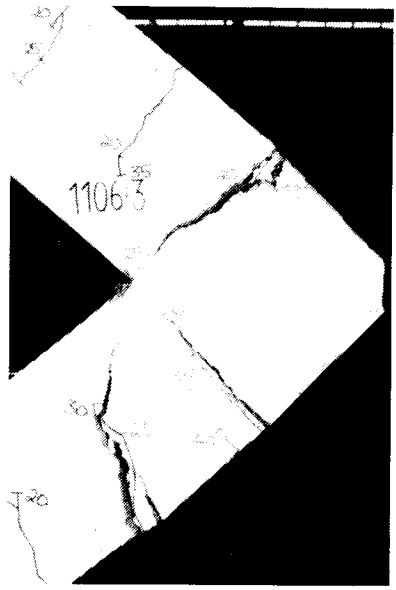

Figure 59 Crack pattern of a test specimen (specimen RV3) carried out with the conventional reinforcement detailing, Plos (1994a, b).

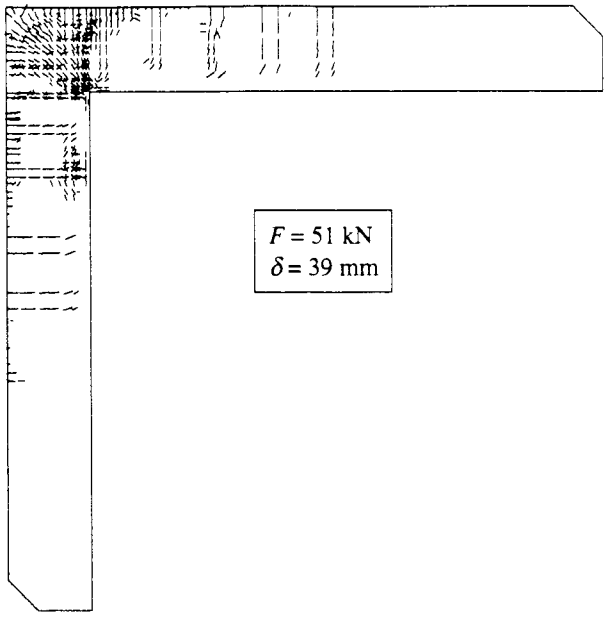

Figure 60 Crack pattern at the end of the analysis for a frame corner with the conventional reinforcement detailing when assuming "good" bond condition.

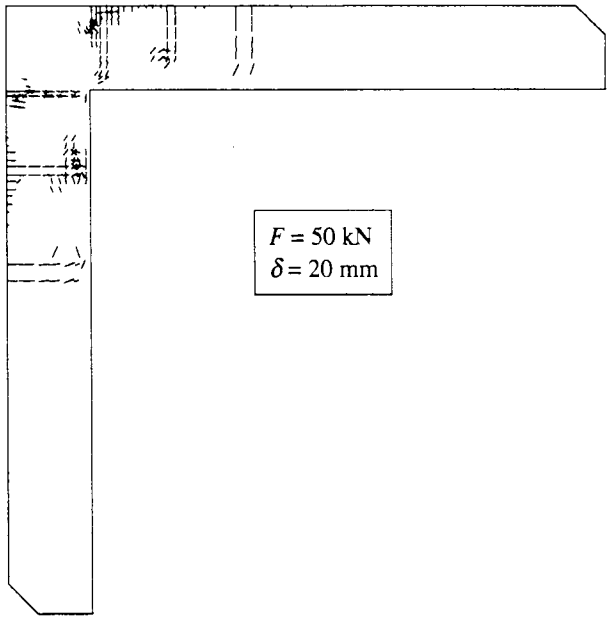

Figure 61 Crack pattern at the end of the analysis for a frame corner with the conventional reinforcement detailing when assuming "other" bond condition.

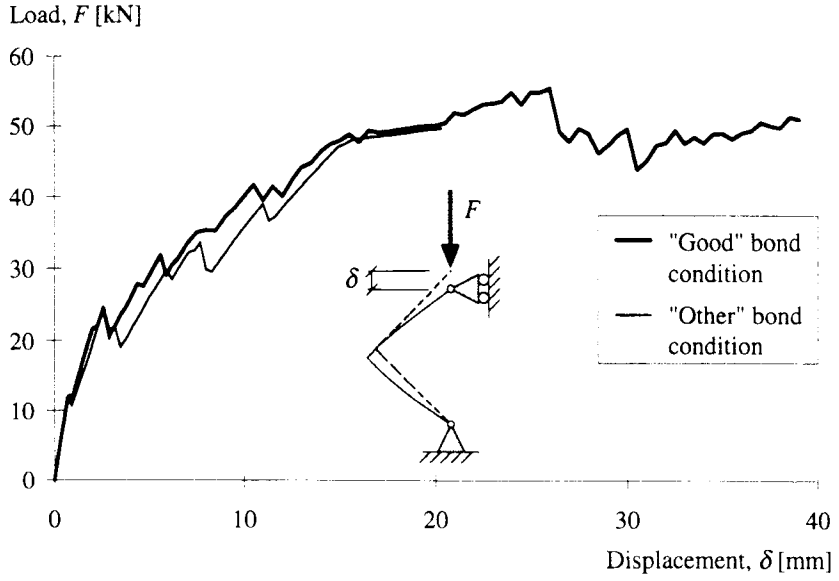

Figure 62 Comparison of the load-displacement relations for two different bond conditions.

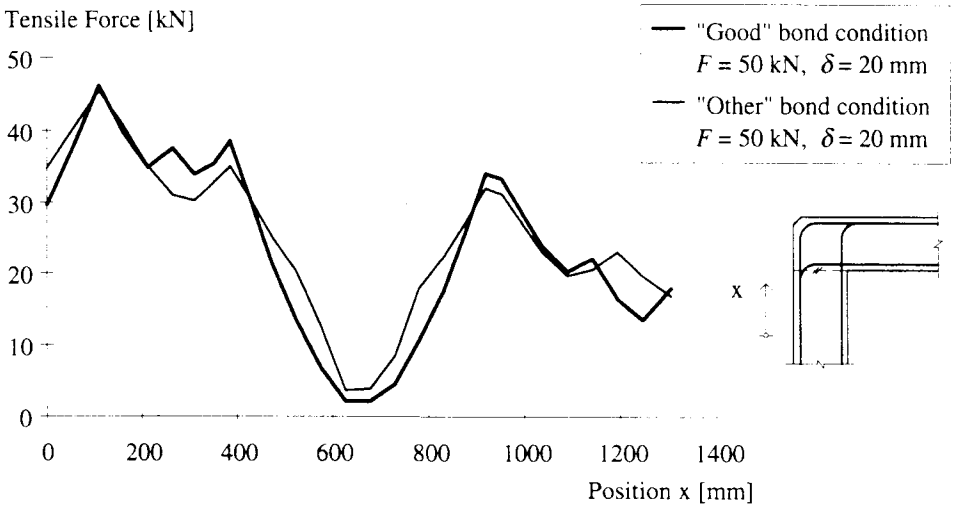

Figure 63 Distribution of the tensile forces along the reinforcement bars in the frame corner for the FE analyses with two different assumptions of the bond condition.

As for the frame corner with new reinforcement detailing, a comparison of the effect of different weaknesses of the construction joint on the structural behaviour, was carried out. The load-displacement relations for different strengths of the construction joint are shown in Figure 64.

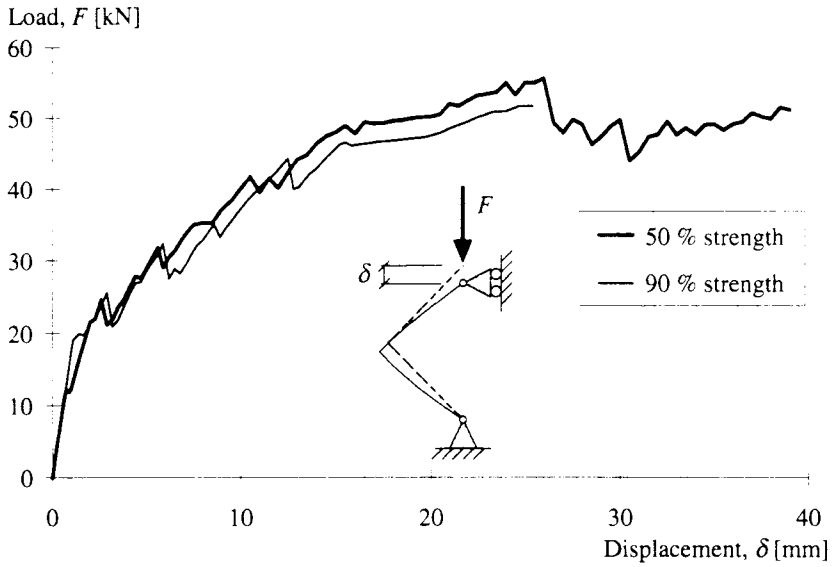

Figure 64 Comparison of the load-displacement relations for different strengths of the construction joint in the frame corner with conventional reinforcement detailing.

4.5.4 Comparisons of the FE analyses

4.5.4.1 Comparison of conventional and new reinforcement detailings

In Figure 65, the load-displacement relation of the FE analyses for the frame corner with the new reinforcement detailing is compared with that of the frame corner with the conventional reinforcement detailing. The distribution of tensile forces along the reinforcement bars in the frame corners for the analyses with new and with conventional reinforcement detailing are shown in Figure 66.

The structural behaviour of the frame corners was similar up to a load of about 40 kN at which the reinforcement bars in the frame corner with new reinforcement detailing started to yield. Due to the greater amount of reinforcement in the sections adjacent to the corner (see Figures 34 and 39), the load capacity of the frame corner with conventional reinforcement detailing continued to increase until yielding at a load level just below 50 kN was reached. Then a load plateau similar to that observed in the tests was formed for both reinforcement detailings. The increase in load capacity obtained for the frame corner with conventional detailing, once yielding was reached, was due to substantial hardening of the steel reinforcement. The sudden loss of load capacity (approximately 7 kN) at a displacement of about 26 mm was caused by a redistribution of forces. This occurred because of the propagation of large cracks in the corner area, the result of the critical section moving from a section in the column approximately 300 mm below the construction joint to the section where the beam meets the corner, see Figure 67. This behaviour corresponded well with that

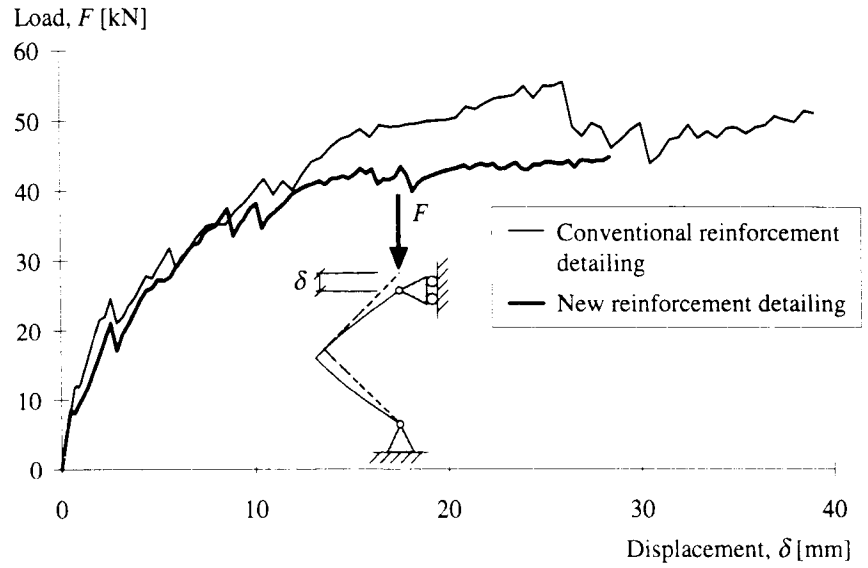

Figure 65 Comparison of the load-displacement relation for frame corners carried out with new and with conventional reinforcement detailing.

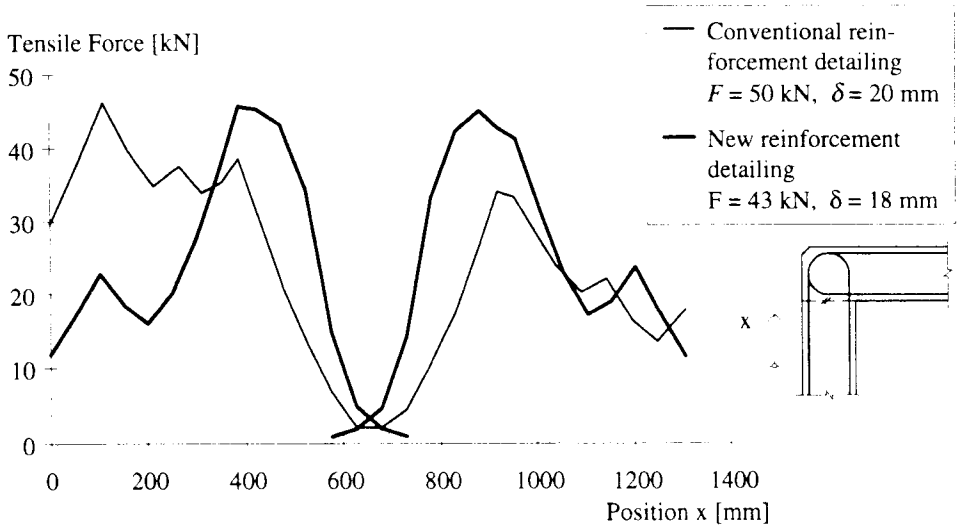

Figure 66 Comparison of the tensile forces of the reinforcement bars in the frame corner for the frame corners carried out with new and with conventional reinforcement detailing.

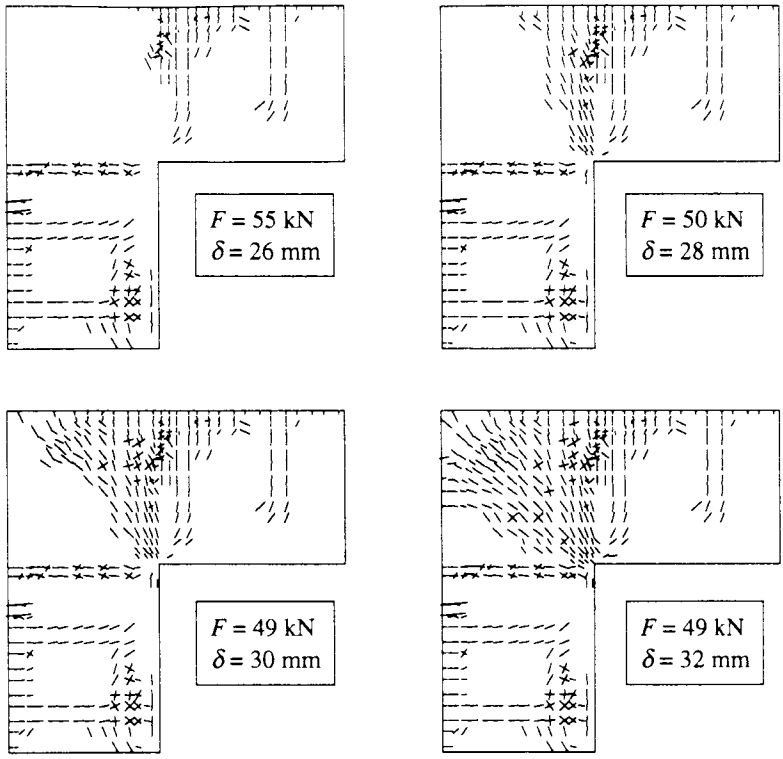

Figure 67 Crack propagation in the corner area for the conventional reinforcement detailing at different load levels.

observed for test specimen RV3, where plastic hinges developed in a region approximately 300 mm below the construction joint, as well as in the section where the beam meets the corner, see Figure 59. The propagation of cracks in the corner area also caused the tensile forces in the reinforcement bars in that area to increase considerably, see Figure 68. The frame corner with new reinforcement detailing showed a quite symmetric distribution of the tensile forces, with yielding of the reinforcement bars in the sections adjacent to the corner. The distribution of the tensile forces in the frame corner with conventional detailing was shifted to the left (into the column). This was because of the unsymmetric amount of reinforcement used in the sections adjacent to the corner, see Figure 39. Yielding of the reinforcement bars was reached about 300 mm below the construction joint, coinciding with the section where the bent reinforcement bars, extending from the beam, ended. This behaviour corresponded well with that observed for test specimen RV3, where a plastic hinge developed in a section below the construction joint, see Figure 59.

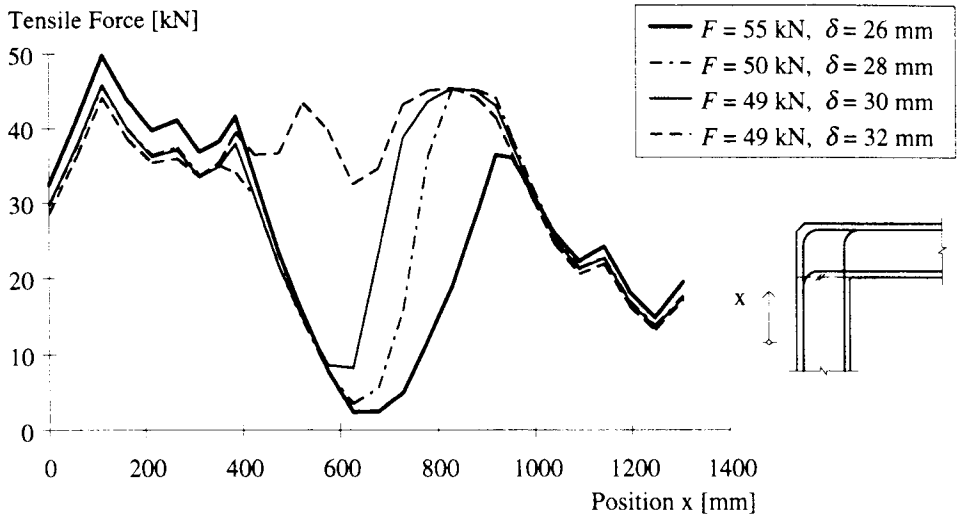

Figure 68 Distribution of the tensile forces along the reinforcement bars in the frame corner carried out with conventional reinforcement detailing. The tensile forces are shown at the same load levels as the crack patterns, see Figure 67.

4.5.4.2 The effect of fracture energy

The importance of the fracture energy used in the analyses was examined. The fracture energy was halved and an analysis of the specimens with high reinforcement detailing (general response model) and low reinforcement detailing (refined model) was carried out. In the analysis of the specimens with high reinforcement ratio, the change of stiffness due to cracking occurred somewhat earlier than when the halved value of the fracture energy was used. However, the stiffness was then independent of the fracture energy, which resulted in a slightly lower maximum load capacity at the same displacement, see Figure 69. In the detailed analysis of the specimen with low reinforcement ratio, the effect of the fracture energy was somewhat more distinct; an earlier change in stiffness was observed and it was then slightly affected until yielding of the steel reinforcement was reached. Furthermore, the maximum load capacity became lower due to the decrease in fracture energy; this resulted in a load-displacement relation better corresponding to that obtained in the tests, see Figure 70. In Table 6, the maximum load capacities (and corresponding displacements) obtained in the FE analyses, for full and halved fracture energy, are compared with the maximum load observed in the tests. It is important to note that the maximum load levels obtained in the analyses, listed here, depend on the tensile stress of the reinforcement bars; thus, an analysis in which the reinforcement bars have obtained a substantial hardening would show a higher load capacity. This is the case in the analysis of the general response for the specimens with low reinforcement ratio, in which the deformation capacity of the steel reinforcement was almost reached, see Section 4.5.2. Therefore, the load levels when the plateau in the load-displacement relation (i.e. yielding of the steel reinforcement) is reached are compared in Table 7. For the specimens with high reinforcement ratio (both tests and analyses), this load was considered to have been reached at the maximum load.

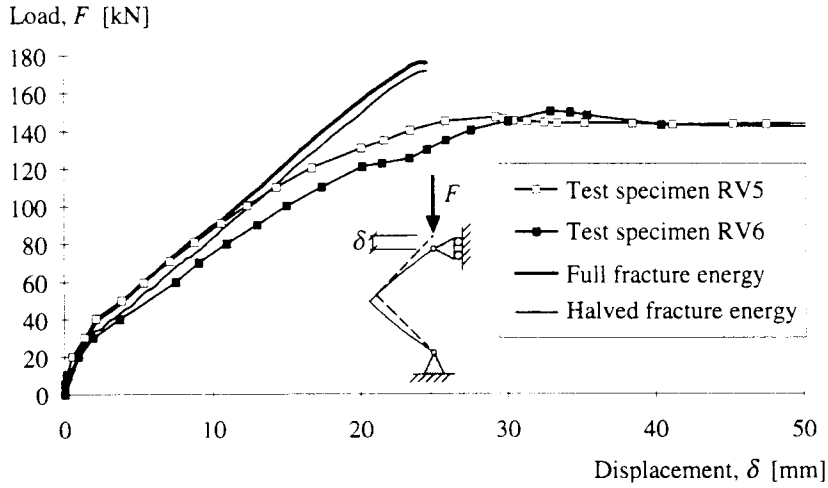

Figure 69 The effect of fracture energy in the FE analysis of the general response for the specimens with high reinforcement ratio.

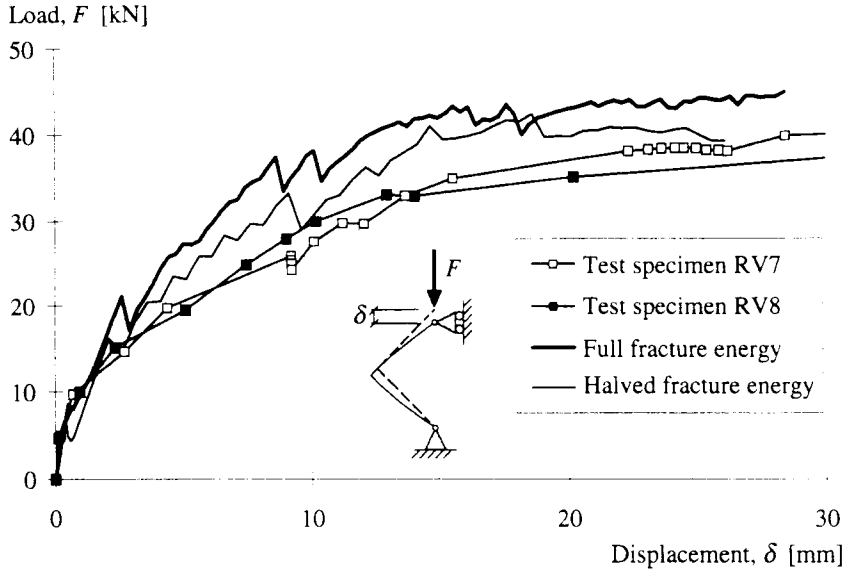

Figure 70 The effect of fracture energy in the detailed FE analysis for the specimens with low reinforcement ratio when assuming "good" bond condition.

Table 6 Comparison of the maximum load capacities and corresponding displacements obtained in the FE analyses and observed in the tests.

Test specimen	Maximum load / Displacement				
	General response		Detailed analysis		Observed in test
	Full fracture energy [kN] / [mm]	Halved fracture energy [kN] / [mm]	Full fracture energy [kN] / [mm]	Halved fracture energy [kN] / [mm]	[kN] / [mm]
RV5	176 / 24	171 / 24	—	—	147 / 29
RV6	- " -	- " -	—	—	150 / 33
RV7	49 / 70	—	45 / 28	41 / 19	42 / 115
RV8	- " -	—	- " -	- " -	42 / 107

Table 7 Comparison of the load levels and corresponding displacements in the FE analyses and the tests when the plateau in the load-displacement relation was reached.

Test specimen	Load / Displacement				
	General response		Detailed analysis		Observed in test
	Full fracture energy [kN] / [mm]	Halved fracture energy [kN] / [mm]	Full fracture energy [kN] / [mm]	Halved fracture energy [kN] / [mm]	[kN] / [mm]
RV5	176 / 24	171 / 24	—	—	147 / 29
RV6	- " -	- " -	—	—	150 / 33
RV7	40 / 13	—	41 / 14	40 / 14	39 / 22
RV8	- " -	—	- " -	- " -	39 / 35

4.5.4.3 Comparison of plane stress and plane strain analyses

In the analyses of the test specimens a state of plane stress was assumed. However, in a real civil defence shelter structure, a state of plane strain is probably a more accurate assumption. Therefore, to examine the behaviour of a frame corner when plane strain is assumed an analysis of a frame corner with the new detailing and a low reinforcement ratio was carried out. As can be seen in Figure 71, the structural behaviour is similar for the frame corner whether a state of plane stress or plane strain is assumed. Consequently, since the state in a real structure is somewhere between plane stress and plane strain, the analyses assuming plane stress presented here should be valid for the frame corner in a real structure.

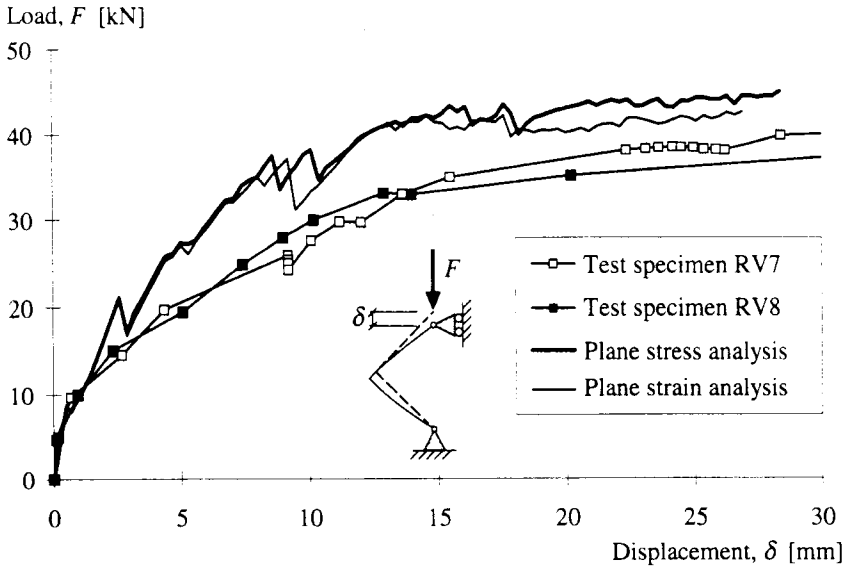

Figure 71 Comparison of the load-displacement relations for analyses where plane stress and plane strain was assumed for the specimens with new detailing and low reinforcement ratio.

4.6 Discussion

The results of the FE analyses corresponded quite well with the results from the experiments, as can be seen in Section 4.5; the behaviour was similar for both the maximum load capacity obtained and the stiffness of the structure. Furthermore, the agreement between test observations and FE analyses was quite good for the crack pattern and the distribution of tensile forces along the reinforcement bars in the frame corner.

Due to the spalling of the concrete side cover, the maximum load obtained in the analysis of the specimens with high reinforcement ratio does not coincide with the load capacities observed in the tests. Instead, the maximum load level reached in this analysis reflects the capacity that the test specimens would have had if the spalling of the concrete had not occurred. Consequently, a direct comparison of the maximum load capacities observed in the tests and obtained in the FE analysis cannot be made for these specimens. However, by using the estimated load capacities in Table 5, an indirect comparison is possible; the estimations listed there correspond well to the load capacities obtained in the FE analyses. By comparing the estimated and observed load capacities for the specimens with conventional detailing (RV1 and RV3) and for the specimens used in the second test series (RV5 to RV8), a statement on the efficiency of the reinforcement detailing can be made. The estimated load capacities listed in Table 5 suggest that the load capacity of specimens RV5 and RV6 should have been somewhat higher than that of specimen RV1, and that the load capacity of specimens RV7 and RV8 should have been somewhat lower than that of specimen RV3. Accordingly, a comparison of the maximum load observed for specimen RV1 with the load obtained in the FE analysis for the specimens with high reinforcement ratio indicates that the

conventional and the new reinforcement detailings behaved approximately the same for these specimens. This statement is still more evident for the specimens with low reinforcement ratio because of the similarities in the load-displacement relations observed in the tests with conventional and new reinforcement detailings.

The detailed FE analyses have shown that the bond-slip relation affects the crack pattern in the frame corner and that the stiffness of the structure is affected by the bond-slip relation up to the point at which the steel reinforcement yields: the higher the stiffness of the bond-slip relation, the higher the stiffness of the structure. This behaviour occurs when the reinforcement bars slip instead of stretching, which for a weaker bond-slip relation results in a lower stress level in the reinforcement at the same displacement. Consequently, when assuming a weak bond-slip relation, a larger displacement of the frame corner is obtained when the steel reinforcement starts to yield. However, once yielding of the reinforcing steel was reached in the analyses, the effect of the bond-slip relation on the load capacity was negligible. Since the bond-slip relation assumed in the analyses determined the mean crack spacing in the structure, the distribution of the tensile forces along the reinforcement bars adjacent to the frame corner was also affected. When the cracking in the corner area was limited, the reinforcement bars positioned inside the corner all showed approximately the same distribution of low tensile forces; however, once large cracks were formed in the corner, the tensile forces in the reinforcement bars increased notably.

Due to the disruption of the FE analyses, it is difficult to draw conclusions about what effect the bond condition has on the total deformation capacity of the frame corner. However, when a stiffer bond-slip relation was assumed, higher tensile strains in the steel reinforcement bars were observed. This indicates that, if rupture of the reinforcement bars is the cause of failure, then the deformation capacity of the frame corner would be lower for a stiffer bond-slip relation. The maximum concrete strain in compression was more or less unaffected by the different bond-slip relations.

The influence of the weakness of the construction joint in the frame corner was limited to the initial cracking stage and had negligible effect on the general behaviour of the structure. After the appearance of the first major crack, the behaviour of the structure was approximately the same, independent of the strength modelled in the joint. The incorrect positioning of the reinforcement loops in the column had a limited effect on the behaviour of the frame corner. The load capacity obtained from the analyses was found to be approximately the same, regardless of whether the reinforcement loops were positioned correctly or not.

The FE analyses have shown that a frame corner made with the conventional reinforcement detailing may have a somewhat higher load capacity than a frame corner with the new reinforcement detailing. This is due to the greater amount of reinforcement positioned in the sections adjacent to the corner area. However, this higher load capacity is only temporary since a redistribution of forces, reducing the load capacity to a level similar to that obtained when using the new reinforcement detailing, soon occurs. If the critical crack forms as shown in Figure 72, the contribution to the load carrying capacity of the short bent bars, extending from the beam into the column, would decrease considerably. In the analyses carried out, the weakness of the construction joint was modelled by reduction of the tensile strength and fracture energy in the element row next to the corner. Thus, cracks adjacent to the corner were made to propagate within this weakness in such a way that the marked bend had considerable effect on the load capacity. To simulate what would happen if the bars extending from the

beam into the column did not have any effect on the critical section adjacent to the corner, the bent part of them was removed, see Figure 72. Thereby, the propagation of a large crack above the bent bars was simulated in an approximate way. As can be seen in Figure 73, this modification had a notable effect on the structural behaviour after yielding of the reinforcement, resulting in a load-displacement relation similar to that obtained in the frame corner with new detailing. Furthermore, the distribution of tensile forces along the reinforcement bars in the corner was similar to that obtained when using the new reinforcement detailing. Consequently, plastic hinges may develop differently in frame corners made with the new and the conventional reinforcement detailings. With the new reinforcement detailing, plastic hinges always develop adjacent to the corner in both the column and the beam. However, in a frame corner with the conventional reinforcement detailing, the main plastic hinge may develop, depending on the crack propagation, in the section below the construction joint where the bent bars, reaching out from the beam, end. The statements made above, treating the effect of the construction joint and the bond-slip relations on the structural behaviour, hold true also for a frame corner made with the conventional reinforcement detailing.

The analyses carried out with different element meshes in the corner region have shown that the cracks tend to propagate parallel to the mesh lines. This phenomenon has also been observed by Rots (1988), who explains that it is caused by interlocking between the elements and coupling between the integration points. Improvements can be made by rotating the element mesh and thereby adapting it to the expected crack directions. However, this procedure is undesirable since it may severely decrease the simplicity of the mesh generation when using the smeared crack approach. Therefore, Rots suggests using triangular elements placed in a cross-diagonal mesh, thus increasing the number of lines which the cracks can follow, see Figure 74a. However, for the analyses carried out in this study, the use of a triangular bisectional mesh in the corner probably would have been sufficient, see Figure 74b. These possible improvements of the element mesh was not examined in the analyses.

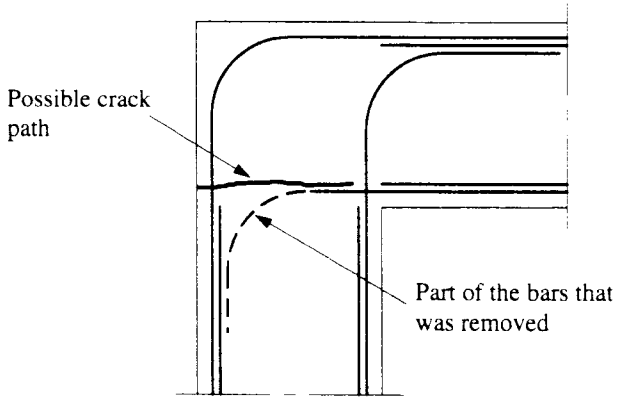

Figure 72 Possible crack path in the column-corner region. To simulate the effect of such a critical crack in an approximative manner the bent part of the bars extending from the beam into the column was removed.

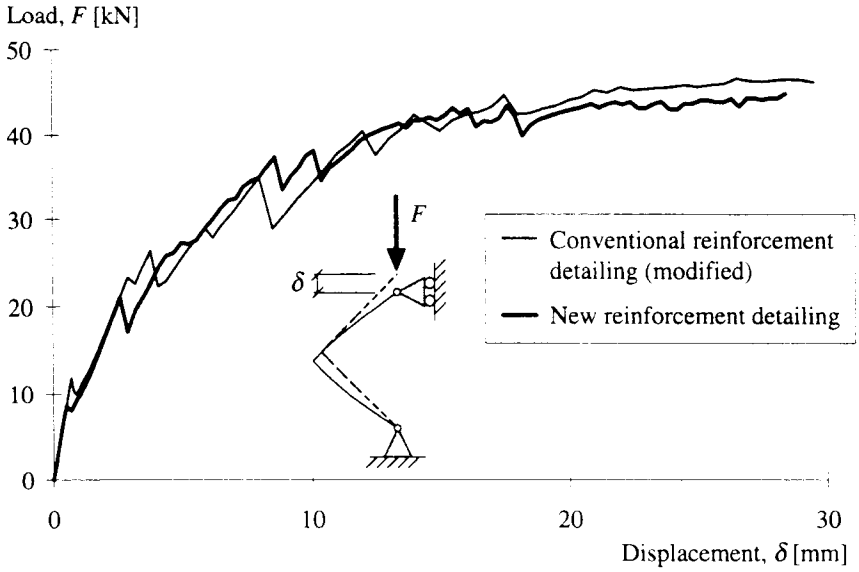

Figure 73 Load-displacement relation for frame corners carried out with new and with conventional (modified as shown in Figure 72) reinforcement detailing.

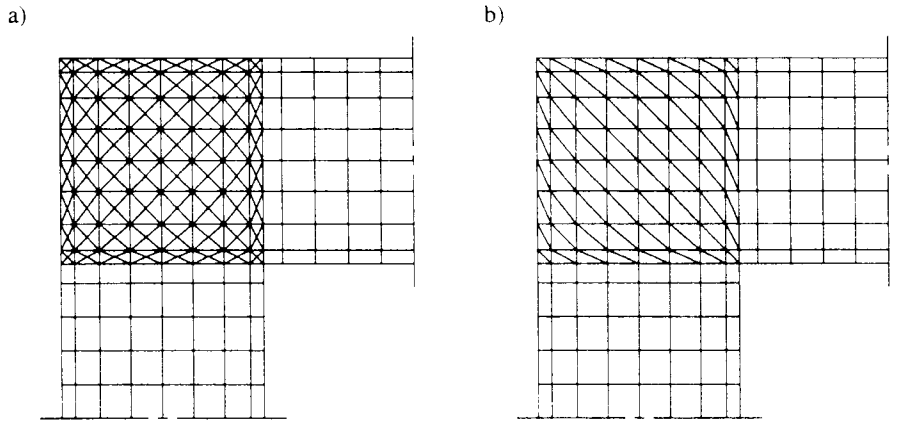

Figure 74 Possible improvement of the simplified element mesh (see Figure 37) in the corner region to obtain a more accurate crack pattern: a) cross-diagonal mesh, b) bisectional mesh.

The two-dimensional plane stress models used in the analyses have worked well up to a load level corresponding to yielding of the reinforcement; the numerical problems encountered have mostly been caused by the concrete in compression. In accordance with observations made by Claeson *et al.* (1996), it has been found that once the ultimate compressive strength of the concrete has been reached, the gradient of the descending softening branch is of great importance in further simulating the behaviour of the structure. This observation holds true also for the concrete in tension; a more gradual stress-strain relation describing the cracked

concrete introduces fewer numerical problems in the analyses, see Plos (1995). Since the fracture energy and the tensile strength determine the ultimate crack opening, and thereby also the gradient of the stress-strain relation, the value of the fracture energy can have considerable effect on the feasibility of simulating a problem. Accordingly, fewer numerical problems were encountered when the reinforcement bars were modelled using truss elements in combination with interface elements than when modelling the reinforcement bars using embedded reinforcement. This was because of the more gradual stress-strain relation obtained for the concrete softening when dividing the ultimate crack opening by the finite element length instead of the mean crack spacing, see Section 4.2.1.1. The bond-slip relation assumed in the analyses had no notable effect on reaching convergence in the analyses.

The effect of the fracture energy used in the analyses was examined. It was found that a reduction to 50 % in the fracture energy had relatively little effect of the structural behaviour in the analyses of the specimens with either the high or low reinforcement ratio; its importance was proportionally higher for the specimens with the low reinforcement ratio. In conjunction with the slightly higher load capacities obtained in the detailed analyses compared to that observed in the tests, this indicates that the fracture energy used in the analyses might have been somewhat too high. However, it does not affect the results presented and conclusions drawn in this study.

4.7 Analyses of a Cantilever Beam

4.7.1 General

Due to the numerical problems encountered in the FE analyses of the frame corner, it was not possible to state with certainty what effect the bond condition or the mechanical properties of the steel reinforcement have on the deformation capacity. Therefore, a simpler model of a cantilever beam, with reinforcement bars positioned only at the tensile side of the structure, was established, see Figure 75. Part of the connecting column was included in the model so that the anchorage of the reinforcement bars in the column could be modelled. The reinforcement bars in the wall were spliced to the reinforcement bars in the beam; the bars had approximately the same anchorage length as in the frame corner test specimens and were provided with a bend to prevent pull-out failure from the wall.

To examine the effect of the bond condition on the load and the deformation capacity of structures that have failed from different causes, the analyses of the cantilever beam were carried out with two different reinforcement ratios. A low amount of reinforcement, corresponding to 4 ϕ10 (ρ = 0.20), was used to obtain rupture of the reinforcement bars and a higher amount, corresponding to 4 ϕ16 (ρ = 0.52), was used to reach ultimate compressive stress in the concrete shortly after yielding of the reinforcement had occurred.

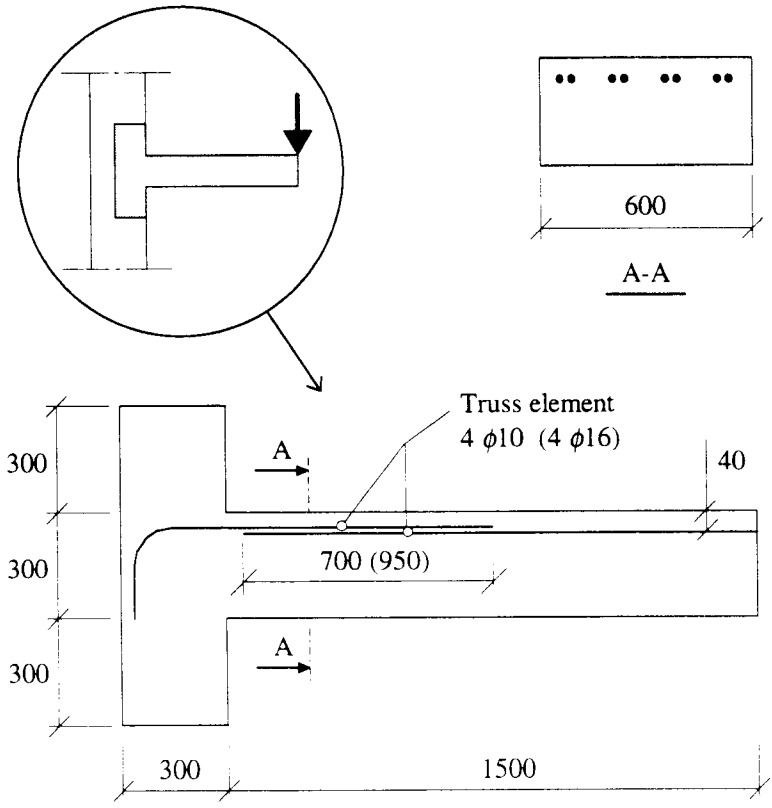

Figure 75 Dimensions of the cantilever beam model and position of the reinforcement bars. Amount of steel reinforcement and anchorage length of the beam with the high reinforcement ratio are given between brackets.

The material parameters for the steel reinforcement and the bond-slip relations used in the analyses of the cantilever beam were the same as those used in the column in the detailed analyses of the frame corner. The same incorrect parameters for concrete in compression as used in the frame corner, see Section 4.5.1 and Appendix B, were used also for the cantilever beam with low reinforcement ratio. However, in the analyses of the cantilever beam with higher reinforcement ratio, a more accurate stress-strain relation for compressed concrete was used (ϕ was set to 10°, see Appendix B).

In the analyses of the beam with low reinforcement ratio, the concrete in compression never reached its ultimate strength; consequently the use of the incorrect stress-strain relation had negligible effect on the results. However, for the cantilever beam with higher reinforcement ratio, crushing of the concrete was the cause of failure, which shows that it is more important to simulate the compressed concrete accurately. This is why the more accurate stress-strain relation for concrete in compression was used. Further, to examine the importance of the descending branch for concrete in compression, analyses using a more gradual stress-strain relation (denoted modified stress-strain relation) were also carried out, see Figure 76.

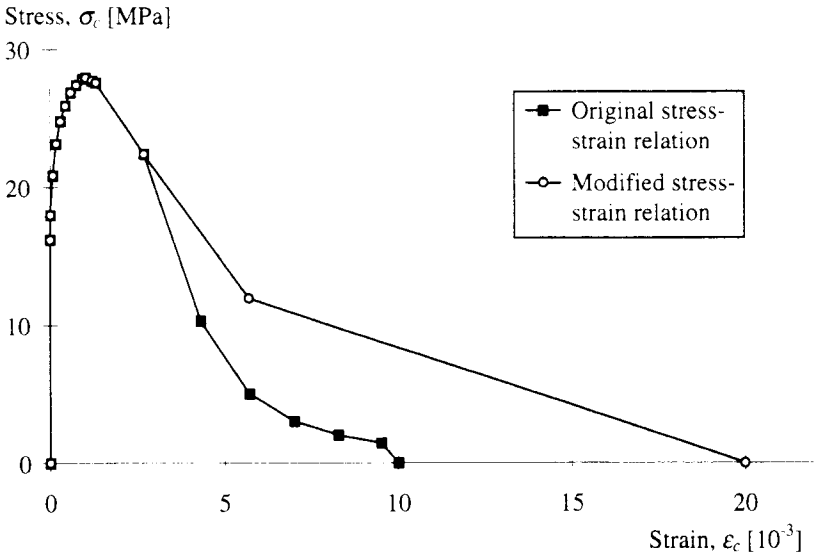

Figure 76 Uniaxial stress-strain relations for concrete in compression used in the analyses of the cantilever beam with high reinforcement ratio. The angle of internal friction, ϕ, was set to 10°, see Appendix B.

4.7.2 The finite element model

To define the geometry of the beam, 215 plane stress elements were used, see Figure 77. The reinforcement bars and the interaction between the reinforcement and the concrete were modelled using 48 truss elements in combination with 48 interface elements.

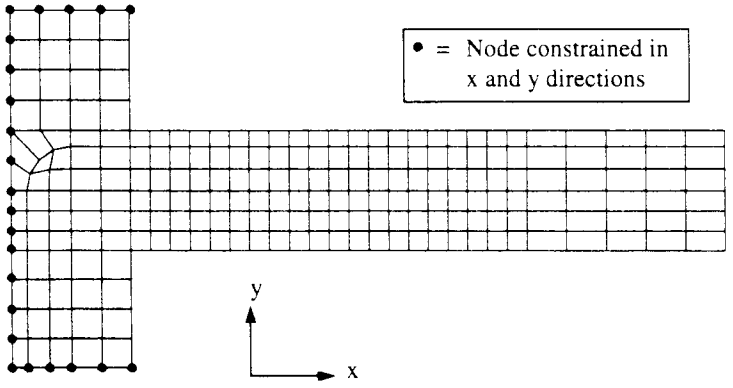

Figure 77 Finite element mesh and boundary conditions of the cantilever beam.

4.7.3 Results of the analyses

4.7.3.1 General

The general behaviour of the load-displacement relation of the cantilever beam was found to be independent of the iteration method. However, as in the detailed FE analyses of the frame corner, the results obtained when using the Modified Newton Raphson method were quite "smooth" while the results achieved when using BFGS secant method fluctuated a lot. When using the more robust BFGS secant method, it was possible to analyse the cantilever beam with low reinforcement ratio until final failure (rupture of the reinforcement bars). The load-displacement relation from the FE analyses of the cantilever beam with low reinforcement ratio are compared for the two iteration methods in Figure 78.

Unless otherwise stated, the following assumptions were made in the FE analyses:

- bond condition = "good" (see Section 4.2.3),
- reinforcement type = "normal ratio" (see Section 4.2.2), and
- iteration method = BFGS secant method (see Section 4.3).

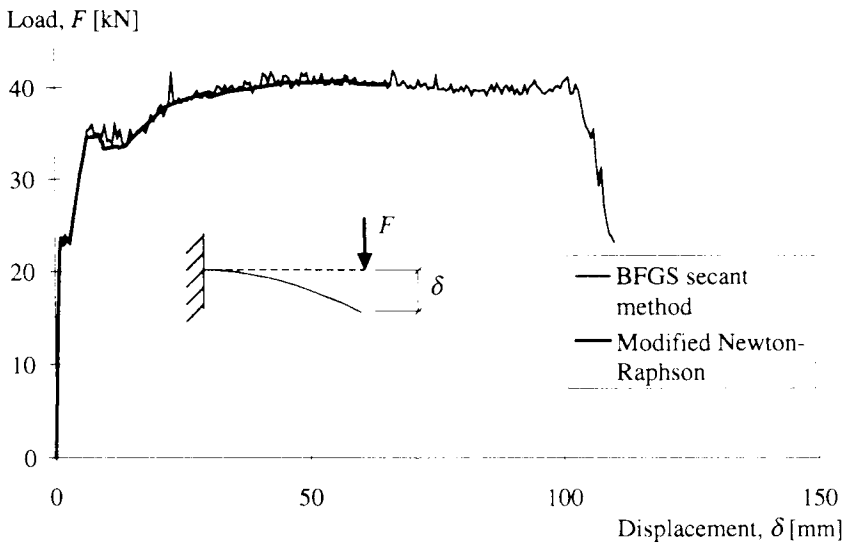

Figure 78 Comparison of the effect of the iteration methods used in the FE analyses of the cantilever beam.

4.7.3.2 Effect of the bond-slip relation

Two different bond-slip relations, denoted "good" and "other", were compared in the analyses of the cantilever beam. A comparison of the load-displacement relations for the different bond conditions is shown in Figures 79 and 80.

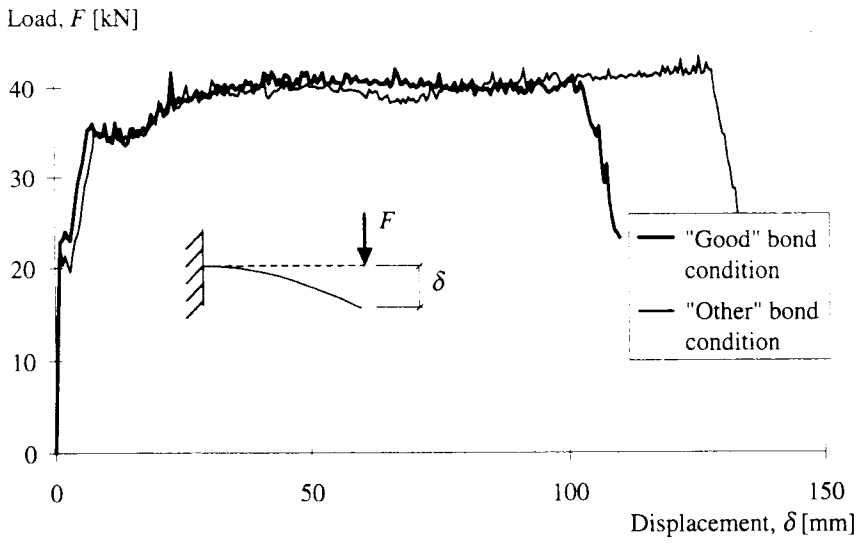

Figure 79 Load-displacement relation for the FE analyses of the cantilever beam with low reinforcement ratio for different bond conditions..

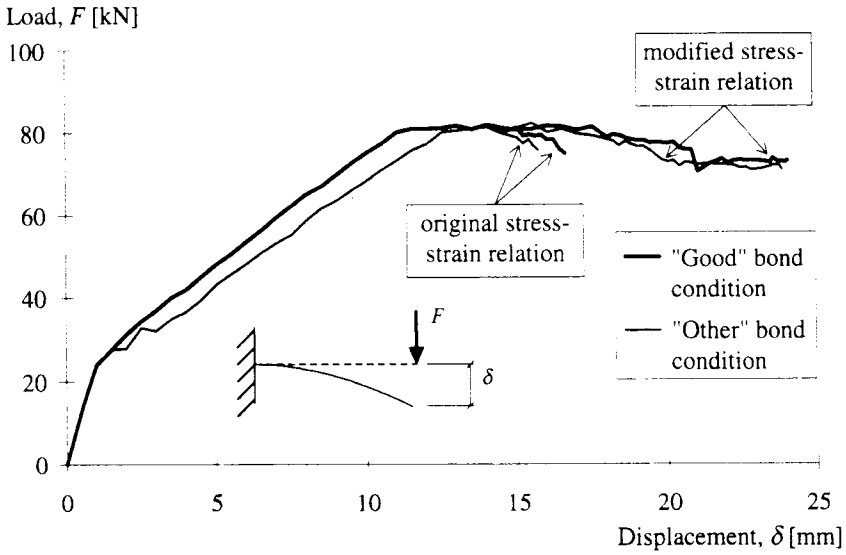

Figure 80 Load-displacement relation for the FE analyses of the cantilever beam with high reinforcement ratio for different bond conditions and different stress-strain relations of concrete in compression.

4.7.3.3 Effect of the reinforcement type

The FE analyses of the cantilever beam with low reinforcement ratio could simulate the behaviour of the structure to the extent that the maximum stress value of the steel reinforcement was reached. Thus, the effect that different mechanical properties of the reinforcing steel have on the deformation capacity of the structure could be studied. Three different stress-strain relations of the steel reinforcement were studied in the FE analyses, see Section 4.2.2. The resulting load-displacement relations for the different reinforcement types are compared in Figure 81.

The abrupt shifts obtained in the analysis assuming "high ratio" were due to a snap-through behaviour (see Bathe (1996)) obtained when the maximum bond stress was reached in one of the interface elements in the region of the beam closest to the column. This resulted in an decrease of the tensile force (unloading) in the truss element, modelling the reinforcement bars, connected to the interface element. When the bond stress reached its minimum value (at a corresponding slip, s_3, according to Figure 27) one of the two truss elements adjacent to the unloaded truss element started to harden which resulted in a corresponding increase of the external load, F. In the analyses, the amount of truss elements that had reached yielding, and thus contributing to a higher deformation capacity, depended on whether a snap-through behaviour occurred or not. In the beams with "low ratio" and "normal ratio" steel, three truss elements reached yielding (of which only one element hardened); in the beam with "high ratio" steel, five truss elements reached yielding and of these, four elements also started to harden.

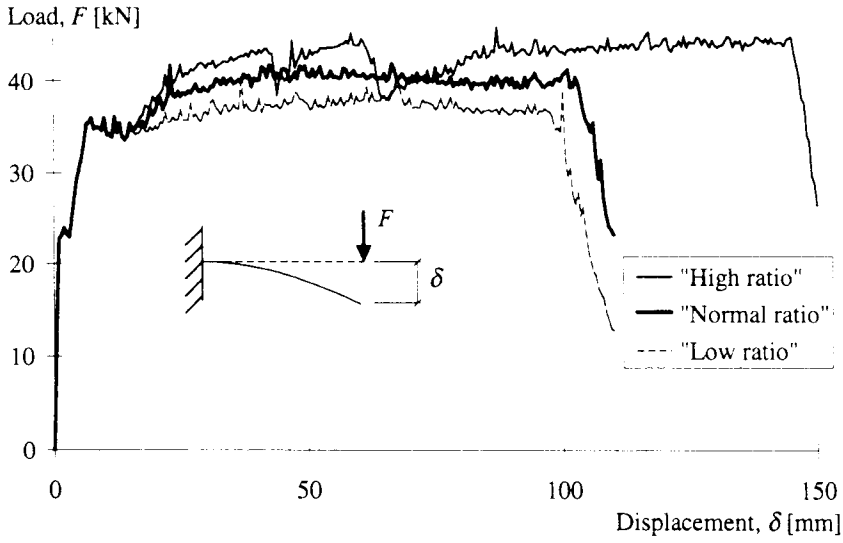

Figure 81 Load-displacement relation for the FE analyses of the cantilever beam for different mechanical properties of the steel reinforcement.

4.7.4 Discussion

The analyses of a cantilever beam were carried out to more thoroughly examine the effects of different bond-slip relations and the mechanical properties of the steel reinforcement. The displacement at final failure in the beam with low reinforcement ratio, when "other" bond condition was assumed, was approximately 30 % higher than that obtained in the beam assuming "good" bond condition. This supports the indications of the analyses of the frame corner: a weak bond-slip relation has a positive effect on the deformation capacity of a structure when rupture of the reinforcement bars is the cause of failure. The load capacity of the beam was, as for the frame corner, relatively unaffected by the bond-slip relation. In the beam with high reinforcement ratio, the bond-slip relation had negligible effect on both the maximum load capacity and the deformation capacity. However, it should be noted that the analyses indicate that a weaker bond condition has a very minor negative effect on the deformation capacity when crushing of the concrete is the cause of failure.

When a weak bond condition was assumed, the difference in tensile stress between the truss elements (modelling the reinforcement bars) connected to each other, was less than that observed when assuming a stiff bond condition. This caused a more rapid development of a large plastic hinge in the reinforcement bars once yielding had occurred, which resulted in a higher deformation capacity of the cantilever beam. In the analyses where crushing of the concrete was the cause of failure, the steel reinforcement did not start to harden. In a structure where hardening of the steel reinforcement is followed by crushing of the concrete, the bond-slip relation may still affect the deformation capacity. However, it is important to note that a stiff bond-slip relation has a positive effect on the crack width in a serviceability limit state, resulting in more but smaller cracks in a structure; thus, a stiff bond-slip relation gives the structure a greater resistance to corrosion.

The effect of three different mechanical properties of the steel reinforcement was investigated in this study. Apart from differences in the load capacity, which were due to different ultimate strengths of the reinforcement bars, the deformation capacity was noticeably affected by the mechanical properties of the steel reinforcement; the cantilever beam modelled with the "high ratio" steel produced a displacement at failure approximately 50 % larger than that obtained when using the "normal ratio" steel. In the analyses, the increase in the displacement at failure was not proportional to the ratio of the different mechanical properties; where the "low ratio" steel was assumed, the displacement at failure was approximately 95 % of that obtained in the beam which had a "normal ratio" steel. This behaviour is probably partly due to the discretisation in the finite element method. If a more dense element mesh had been used to model the region next to the column, a larger plastic region in the steel reinforcement next to the column had probably been obtained for the beam with the "normal ratio" steel and, consequently, the total displacement at failure would have been larger. Therefore, it is difficult to make a certain statement of how much the different mechanical properties of the steel reinforcement affect the deformation capacity of a concrete structure. However, the difference in total displacement at final failure of approximately 50 %, between the beams with "high ratio" and "low ratio" steel, seems quite reasonable.

When rupture of the reinforcement bars is the cause of final failure, the value of the ultimate strain of the steel reinforcement probably affects the total displacement in the analyses of the cantilever beam. For a structure where crushing of the concrete is the cause of failure, the importance of the steel ductility depends on what strain values have been reached. If the

reinforcement bars have just started to yield when this happens (as in the cantilever beam with the high reinforcement ratio analysed above) the ductility of the steel has no effect at all. However, when the reinforcement bars have started to harden, the mechanical properties of the steel may be important, since it is these that determine the capacity for redistribution of forces in a concrete structure, see Öberg (1976).

In summary, to obtain a ductile structure, the most important factor is the yielding of the steel reinforcement; the longer the reinforcement bars have yielded before final failure, the more ductile is the behaviour obtained. Furthermore, once a strain large enough to obtain hardening is reached, the mechanical properties of the steel can be of great importance; the plastic hinges in a structure then spread over a larger area which offers an enhanced deformation capacity. The stiffness of the bond-slip relation may affect the deformation capacity, provided strain hardening of the reinforcing steel is reached. When rupture of the reinforcement bars is the cause of failure, a weaker bond-slip relation, as mentioned above, has a positive effect on the deformation capacity. However, since a stiffer bond-slip relation results in higher tensile strains in the steel reinforcement, the steel hardens sooner. Consequently, provided that hardening of the steel reinforcement is reached, a stiff bond-slip relation may have a positive effect on the deformation capacity when crushing of the concrete is the cause of failure.

5 CONCLUSIONS

5.1 General

The reinforcement detailing allowed in the present Swedish regulations for the design of frame corners in concrete civil defence shelters is complicated, which makes it difficult to carry out correctly. Therefore, a new design proposal has been studied. Eight full-scale frame corners subjected to a negative moment were tested. The parameters varied in the tests were the reinforcement detailing, the reinforcement ratio, the reinforcement type and the configuration of the reinforcement bars. Finite element analyses, using non-linear fracture mechanics and plasticity, were carried out for frame corners with the new and the conventional reinforcement detailings. Furthermore, the effects of the weakness of the construction joint, the interaction between reinforcement and concrete, the mechanical properties of the steel reinforcement, and incorrect positioning of reinforcement loops were examined.

The tests and the FE analyses conducted have shown that the conventional and the new reinforcement detailings for practical purposes are equivalent for a frame corner structure with a low amount of reinforcement. Comparisons of tests and FE analyses indicate that this is also the case for a frame corner with a high amount of reinforcement. Thus, the tests and analyses support the idea that the new alternative is suitable to use instead of the conventional reinforcement detailing.

The tests have shown that, whether or not the reinforcement bars are spliced in contact with each other, there is no significant difference in the behaviour of the frame corner made with the new detailing. The concrete side cover spalled off the frame corner of the specimens with the high reinforcement ratio. This indicates that the expression to determine the minimum bending radius of the reinforcement in Boverket's Handbook for Concrete Structures, BBK 94, Boverket (1994), should not be used for reinforcement detailings of the type used in the new proposal.

To obtain a ductile structure, the most important factor is the yielding of the steel reinforcement; the longer the reinforcement bars have yielded before final failure, the more ductile is the behaviour obtained. However, the bond-slip relation and the mechanical properties of the steel reinforcement can also have significant effect on the deformation capacity. The FE analyses have shown that the stiffness of the structure is affected by the bond-slip relation up to the point at which the steel reinforcement starts to yield: the higher the stiffness of the bond-slip relation, the higher the stiffness of the structure. Depending on the cause of final failure the bond-slip relation can have a noticeable effect on the deformation capacity of a structure. When rupture of the reinforcement bars is the cause of final failure, a weak bond-slip relation has a positive effect; when crushing of the concrete is the cause of failure and hardening of the steel reinforcement is reached, a stiff bond-slip relation may have a positive effect. However, when hardening of the steel reinforcement is not reached and crushing of the concrete is the cause of failure, the bond-slip relation has negligible effect on the deformation capacity of the structure. The maximum load capacity is relatively unaffected by the bond-slip relation, independent of the amount of reinforcement. However, a stiffer bond-slip relation does have a positive effect on the crack width, resulting in more, but smaller, cracks in a structure which can be positive concerning the risk of corrosion of the

steel reinforcement. It was also shown that the mechanical properties of the steel reinforcement can have a considerable effect on how large the region of yielded reinforcement will be; consequently, it can have a significant effect on the deformation capacity of a structure.

The weakness of the construction joint affects the structural behaviour of the frame corner only in the initial cracking stage; its effect on the maximum load capacity is negligible. The FE analyses have shown that an incorrect positioning of the reinforcement loops in the column of the frame corner has a limited effect on the maximum load capacity.

It has been noted that the cracks have a tendency to propagate parallel to the element meshes and, consequently, the crack pattern in a structure is slightly dependent on the element mesh. The BFGS secant method was found to be a comparatively robust iteration method, well suited for the kind of FE analyses carried out in this study. Fewer numerical problems were encountered in the analyses when separate elements were used to model the reinforcement bars; this is due to the lower gradient in the stress-strain curve used for the cracked concrete.

5.2 Suggestions for Future Research

In this study, tests and FE analyses have been carried out only for a static loading. However, a civil defence shelter must withstand impact loading such as explosions and falling buildings; consequently, the behaviour of the new reinforcement detailing when subjected to impact loading needs to be studied.

The use of reinforcement loops has been examined only in frame corners connecting two structural members, i.e. a beam and a column. Therefore, an examination of the use of reinforcement loops in other types of connections, e.g. T-joints or corners with an angle wider than 90°, would be valuable.

6 REFERENCES

AB Svensk Byggtjänst and Cementa AB (1990): Betonghandbok Konstruktion, utgåva 2 (Concrete Handbook Design, second edition. In Swedish). AB Svensk Byggtjänst, 791 pp.

Bathe K-J. (1996): Finite Element Procedures. Prentice-Hall, Englewood Cliffs, New Jersey 1037 pp.

Bazant Z.P. and Oh B.H. (1983): Crack band theory for fracture of concrete. Materials and Structures, RILEM, Vol. 16, No 93, May-June 1983, pp. 155-177.

Bonacci J. and Pantazopoulou S. (1993): Parametric Investigation of Joint Mechanics. ACI Structural Journal, V. 90, No. 1, Jan.-Feb. 1993, pp. 61-71.

Boverket (1994): Boverkets handbok för Betongkonstruktioner BBK 94, Band 1, Konstruktion (Boverket's Handbook for Concrete Structures, BBK 94, Vol. 1, Design. In Swedish). Boverket, Byggavdelningen, Karlskrona, Sweden 185 pp.

BST Byggstandardiseringen (1987), Betongprovning med Svensk Standard, BST handbok 12, (Concrete Testing according to Swedish Standard, BST Handbook 12. In Swedish). SIS - standardiseringskommisionen i Sverige och Svensk Byggtjänst, 272 pp.

CEB (1983): Bond Action and Bond Behaviour of Reinforcement, CEB Bulletin d'Information 151, 153 pp.

CEB (1993): CEB-FIP Model Code 1990, Design Code. Thomas Telford, Lausanne, Switzerland, 437 pp.

Chen W. F. (1982): Plasticity in Reinforced Concrete. McGraw-Hill, USA, 474 pp.

Cheung P. C., Paulay T., Park R. (1993): Behaviour of beam-column joints in seismically loaded RC frames. The Structural Engineer, Vol. 71, No. 8, 20 April 1993, pp. 129-138.

Claeson C., Gylltoft K. (1996): Slender High-Strength Concrete Columns Subjected to Eccentric Loading. Submitted for publication in Journal of Structural Engineering.

Collins M. P. and Mitchell D. (1991): Prestressed Concrete Structures. Prentice Hall, Englewood Cliffs, New Jersey, pp. 766.

Elfgren L., editor (1989): Fracture Mechanics of Concrete Structures, From Theory to Applications. Report of the technical committee 90-FMA Fracture Mechanics to Concrete - Application, RILEM. Chapman and Hall, London, 407 pp.

Eligehausen R., Popov E.G., Bertero V.V. (1983): Local Bond Stress-slip Relationships of Deformed Bars under Generalized Excitations. Report No. UCB/EERC-83/23, October 1983, University of California, Berkeley, California, 161 pp.

Engström B. (1992): Ductility of Tie Connections in Precast Structures. Division of Concrete Structures, Chalmers University of Technology, Publication 92:1, Göteborg, 452 pp.

Gambarova P. G. (1989): Steel-to-concrete bond after concrete splitting: test results. Materials and Structures, 1989, 22, pp. 35-47.

Gylltoft K. (1983): Fracture Mechanics Models for Fatigue in Concrete Structures. Division of Structural Engineering, Luleå University of Technology, Doctoral Thesis 1983:25D, 210 pp.

Hanson W. and Connor W. (1967): Seismic Resistance of Reinforced Concrete Beam-Column Joints. ASCE Journal of the Structural Divison 93(5), pp. 533-560.

Hillerborg A., Modéer M. and Petersson P-E. (1976): Analysis of Crack Formation and Crack Growth in Concrete by means of Fracture Mechanics and Finite Elements. Cement and Concrete Research, Vol. 6, No. 6, Nov. 1976, pp. 773-782.

Johansson M. (1995): New Reinforcement Detailing in Frame Corners in Civil Defence Shelters - Experiments and Fracture Mechanics Analyses, Chalmers University of Technology, Division of Concrete Structures, Report 95:2, Göteborg, 70 pp.

Johansson M. (1996): Non-linear Finite Element Analyses of Frame Corners in Civil Defence Shelters. Chalmers University of Technology, Division of Concrete Structures, Report 96:3, Göteborg, 70 pp.

Kwak H-G. and Filippou F. C. (1990): Finite Element Analysis of Reinforced Concrete Structures under Monotonic Loads. Department of Civil Engineering, University of California Berkeley, California, Report No. UCB/SEMM-90/14, 113 pp.

Lundgren K. and Plos M. (1996): Splicing of Reinforcement in Frame Corners: Finite Element Analyses. Chalmers University of Technology, Division of Concrete Structures, Report 96:2, Göteborg, 13 pp.

Luo Y.H., Durrani A.J., Bai S., Yuan J. (1994): Study of Reinforcing Detail of Tension Bars in Frame Corner Connections. ACI Structural Journal, V. 91, No. 4, pp. 486-496.

Lutz L. A., Gergely P. (1967): Mechanics of Bond and Slip of Deformed Bars in Concrete. ACI Journal, Nov. 1967, pp. 711-721.

Magnusson J. (1997): Licentiate Thesis to be published in 1997. Chalmers University of Technology, Division of Concrete Structures, Göteborg.

Mayfield B., Kong F-K. Bennison A. (1971): Corner Joint Details in Structural Lightweight Concrete. ACI Journal, May 1971, pp. 366-372.

Mayfield B., Kong F-K. Bennison A. (1972): Strength and Stiffness of Lightweight Concrete Corners. ACI Journal, July 1972, pp. 420-427.

Nilsson I. H. E. (1973): Reinforced concrete corners and joints subjected to bending moment. National Swedish Institute for Building Research, Document D7:1973, 249 pp.

Nilsson I. H. E. and Losberg A. (1976): Reinforced Concrete Corners and Joints Subjected to Bending Moment. ASCE Journal of the Structural Division, 102(6), pp. 1229-1254.

Noghabai K. (1995): Splitting of Concrete in the Anchoring Zone of Deformed Bars: A Fracture Mechanics Approach to Bond. Division of Structural Engineering, Luleå University of Technology, Licentiate Thesis 1995:26L, 170 pp.

Paulay T., Park P. Priestley M. J. N. (1978): Reinforced Concrete Beam-Column Joints Under Seismic Actions. ACI Journal, Proceedings V. 75, No. 11, Nov., pp. 585-593.

Plos M. (1994a): Ny armeringsskarv för ramhörn i skyddsrum (New Reinforcement Splice for Frame Corners in Civil Defence Shelters. In Swedish). Division of Concrete Structures, Chalmers University of Technology, Report 94:2, 27 pp.

Plos M. (1994b): Splicing of Reinforcement in Frame Corners -Experimental Studies. Nordic Concrete Research, Publ. no. 14, The Nordic Concrete Federation, pp 103-121.

Plos M. (1995): Application of Fracture Mechanics to Concrete Bridges - Finite Element Analyses and Experiments. Division of Concrete Structures, Chalmers University of Technology, Publication 95:3, Göteborg, 127 pp.

Restrepo I., Park R., Buchanon A. H. (1995): Test on Connections of Earthquake Resisting Precast Reinforced Concrete Perimeter Frames of Buildings. PCI Journal, July-Aug. 1995., pp. 44-61.

RILEM 50-FMC (1985): Determination of the Fracture Energy of Mortar and Concrete by Means of Three-point Bend Tests on Notched Beams. Materials and Structures, Vol. 18, pp. 285-290.

Robertson I. N. and Durrani A. J. (1992): Gravity Load Effect on Seismic Behavior of Interior Slab-Column Connections. ACI Structural Journal, V. 89, No. 1, Jan.-Feb., pp. 37-45.

Rots J.G. (1988): Computational Modelling of Concrete Fracture. Department of Civil Engineering, Delft University of Technology, pp. 132.

Skettrup E., Strabo J., Andersen N. H. (1984): Concrete Frame Corners. ACI Journal, Nov.-Dec. 1984, pp. 587-593.

Swann R. A., (1969): Flexural Strength of Corners of Reinforced Concrete Portal Frames. Technical Report TRA 434, Cement and Concrete Association, London, Nov. 1969, 14 pp.

Swedish Rescue Service Board (1994): Shelter Regulations, SR - English edition. Statens Räddningsverk, Publication B54-168/94, 94 pp.

Tepfers R. (1973): A Theory of Bond Applied to Overlapped Tensile Reinforcement Splices for Deformed Bars. Division of Concrete Structures, Chalmers University of Technology, Publication 73:2, Göteborg, 328 pp.

TNO (1993): DIANA-5.1. TNO Building and Construction Research - Department of Computational Mechanics, P.O. Box 49, 2600 AA Delft, The Netherlands.

TNO (1996): DIANA-6.1. TNO Building and Construction Research - Department of Engineering Mechanics and Information Technology, P.O. Box 49, 2600 AA Delft, The Netherlands.

Tsonos A. G., Tegos I. A., Penelis G. Gr. (1992): Seismic Resistance of Type 2 Exterior Beam-Column Joints Reinforced with Inclined Bars. ACI Structural Journal, V. 89, No. 1, Jan.-Feb. 1992, pp. 3-12.

Yuan R. L., McLelland G. R., Chen, W. F. (1982): Experiments on Closing Reinforced Concrete Corners. ASCE Journal of the Structural Division, 108(4), pp. 771-779.

Zouzou A. and Haldane D. (1993): Detailing reinforced concrete closing corner joints for ductility. Proceedings of the Institution of Civil Engineers, Structures and Buildings, Feb. 1993, Vol. 99, No. 1, pp. 43-48.

Öberg S. (1976): Armerade balkars rotationskapacitet (Rotational Capacity of Reinforced Concrete Beams. In Swedish.), Division of Concrete Structures, University of Technology, Report 76:7, 54 pp.

APPENDIX A Drawings of the Test Specimens in the Second Test Series

The dimensions of the frame corner specimens are shown in Figure A-1. The amount and position of the reinforcement bars are shown in Figures A-2 and A-3.

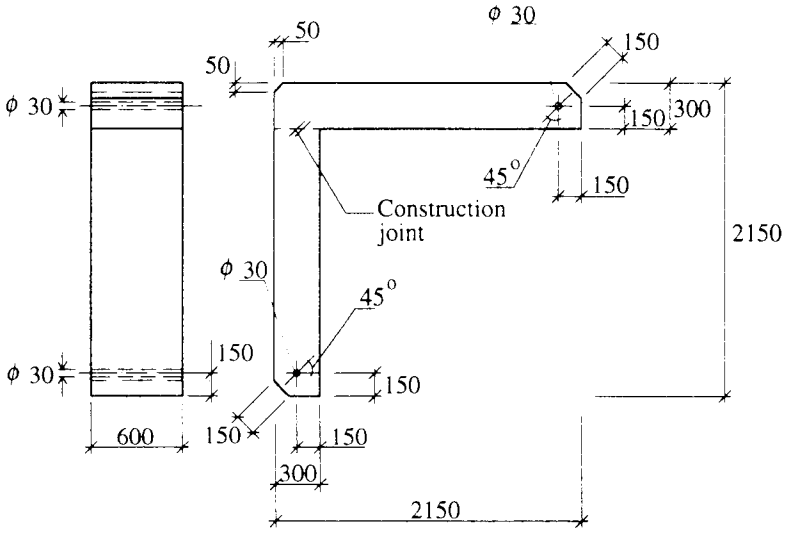

Figure A-1 The dimensions of the test specimens.

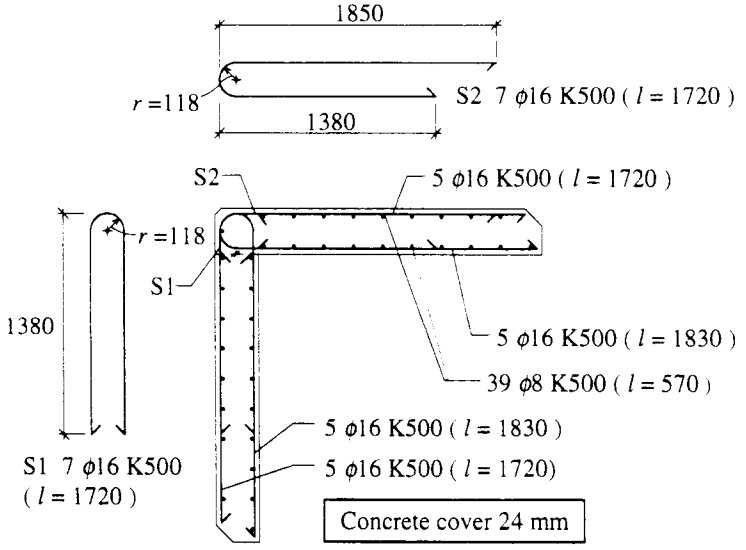

Figure A-2 Reinforcement bars used in specimens RV5 and RV6.

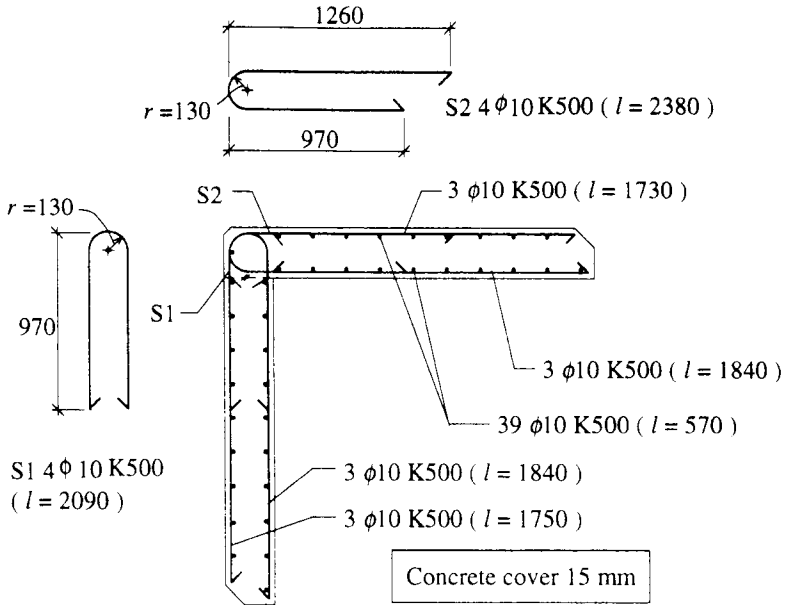

Figure A-2 Reinforcement bars used in specimens RV7 and RV8.

APPENDIX B Concrete in Compression in the FE Analyses

The response of the concrete in compression was modelled by a Drucker-Prager plasticity model. The formulation of the Drucker-Prager yield surface is given by

$$f(\sigma,\kappa) = \sqrt{\frac{1}{2}\sigma^T P\sigma} + \alpha_f \pi^T \sigma - \beta c(\kappa) \tag{B1}$$

where σ is the stress matrix. The projection matrix P and the projection vector π are given by

$$P = \begin{bmatrix} 2 & -1 & -1 & 0 & 0 & 0 \\ -1 & 2 & -1 & 0 & 0 & 0 \\ -1 & -1 & 2 & 0 & 0 & 0 \\ 0 & 0 & 0 & 6 & 0 & 0 \\ 0 & 0 & 0 & 0 & 6 & 0 \\ 0 & 0 & 0 & 0 & 0 & 6 \end{bmatrix} \quad \text{and} \quad \pi = \begin{bmatrix} 1 \\ 1 \\ 1 \\ 0 \\ 0 \\ 0 \end{bmatrix} \tag{B2}$$

The scalar quantities α_f and β are given by

$$\alpha_f = \frac{2\sin\phi(\kappa)}{3-\sin\phi(\kappa)} \quad \text{and} \quad \beta = \frac{6\cos\phi_0}{3-\sin\phi_0} \tag{B3}$$

where $\phi(\kappa)$ is the angle of internal friction as a function of a hardening parameter, κ and ϕ_0 is the initial angle of internal friction. The hardening of the compressed concrete is described by a relation between the cohesion and a hardening parameter. The cohesion, c, is calculated as

$$c = f_{c,cyl}(\varepsilon^p_{uniaxial})\frac{1-\alpha_f}{\beta} \tag{B4}$$

Here, $f_{c,cyl}(\varepsilon^{p}{}_{uniaxial})$ is the compressive strength as a function of the plastic strain in the direction of the uniaxial stress, evaluated from standard tests on cylinders. In the analyses the angle of internal friction was constant; thus, $\phi(\kappa) = \phi_0 = \phi$ and the expression in equation (B4) can be written as

$$c = f_{c,cyl}(\varepsilon^p_{uniaxial})\frac{1-\sin\phi}{2\cos\phi} \tag{B5}$$

The hardening parameter κ is defined as

$$\kappa = -\frac{\sqrt{1+2\alpha_g^2}}{1-\alpha_g}\varepsilon^p_{uniaxial} \tag{B6}$$

where

$$\alpha_g = \frac{2\sin\psi(\kappa)}{3-\sin\psi(\kappa)} \tag{B7}$$

$\varepsilon^p_{uniaxial}$ is the plastic strain in the direction of the uniaxial stress and ψ is the dilatancy angle. In the analyses, associated plasticity was assumed; thus, the dilatancy angle was set equal to the angle of internal friction, i.e. $\psi = \phi$.

According to Chen (1982), the compressive strength of concrete is increased by approximately 16 % when the concrete is subjected to an equal biaxial compression stress state ($\sigma_2 / \sigma_1 = 1$); the corresponding strain at maximum stress is increased by approximately 10 %. Thus, a more ductile stress-strain relation is obtained in an equal biaxial compression state than in a uniaxial stress state, see Figure B-1. However, with the Drucker-Prager plasticity model used in DIANA, it is not possible to obtain such an increase of the ductile behaviour in a biaxial compression state. Instead, contrary to what is expected, the result is a more brittle behaviour with a substantial decrease in the strain at maximum stress. According to Chen, the ratio between the plastic strains (at maximum stress), obtained in an equal biaxial compression state and a uniaxial compression state, should be approximately 1.1. However, it can be shown that with the plasticity model used in DIANA this ratio can at most reach a value of 0.5 (obtained when ψ = 0°). Consequently, when using this material model for compressed concrete, a more brittle behaviour of concrete in compression is obtained for all stress states other than the pure uniaxial one.

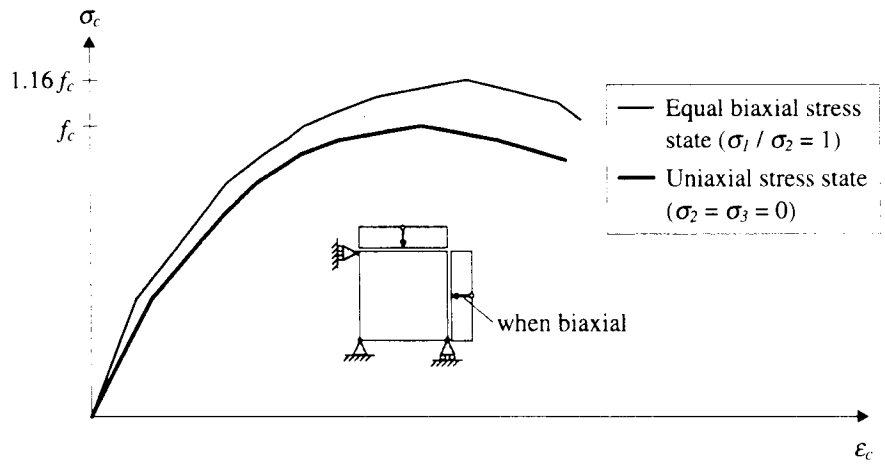

Figure B-1 The difference in the stress-strain relations for concrete in uniaxial and equal biaxial compression states, Chen (1982).

The cohesion-hardening parameter relation used in the FE analyses is determined to correspond with the stress-strain relation from a uniaxial test, see equations (B4) and (B6). The values of the cohesion and the hardening parameter both depend on the angle of internal friction, ϕ. Thus, ϕ can be set to an arbitrary value and still give a stress-strain relation that

corresponds to that from the uniaxial test; however, the choice of ϕ also affects the stress-strain relation in the other stress states. To obtain an increase in compressive strength in an equal biaxial compression state, corresponding to that suggested by Chen (16 %), the angle of internal friction, ϕ, should be set to approximately 10°. However, according to recommendations in the DIANA manual, TNO (1993, 1996), the angle of internal friction was approximated to be 30° in the FE analyses. This resulted in a 200 % increase of the compressive strength at an equal biaxial compression state compared to that in an uniaxial stress state. Further, due to a misunderstanding, the hardening parameter κ was set to be equivalent to the plastic strain $\varepsilon^{p}_{uniaxial}$ when it should have been $\kappa = 1.91\varepsilon^{p}_{uniaxial}$ according to equation (B6); thus, the softening of the concrete in compression occurred at a lower strain also for the uniaxial stress state. To examine the effect of these incorrect material parameters (i.e. $\phi = 30°$ and $\kappa = \varepsilon^{p}_{uniaxial}$), an analysis of a frame corner specimen using more accurate material parameters ($\phi = 10°$, $\kappa = 1.16\varepsilon^{p}_{uniaxial}$) was carried out, see Section 4.5.1. The stress-strain relations for this analysis and for the concrete used in the other FE analyses are compared for uniaxial and equal biaxial compression states, see Figure B-2.

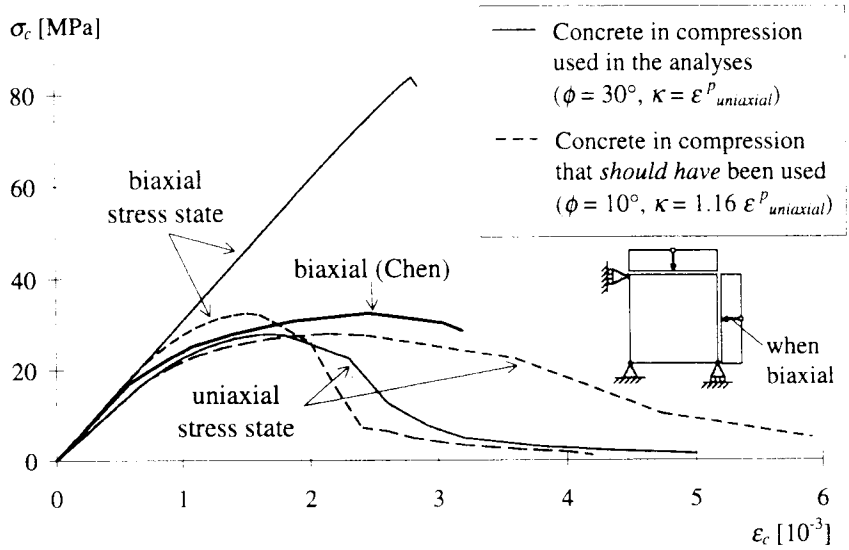

Figure B-2 The difference in the stress-strain relations for concrete used in the FE analyses when it is subjected to different compression states. The corresponding stress-strain relation according to Chen (1982) is shown for comparison.

Tryckt & Bunden
Vasastadens Bokbinderi AB
1996